

**Stratum corneum models as pharmaceutical formulations and
diastereomeric CER[AP] investigated in 2D and 3D model systems**

Dissertation

zur Erlangung des

Doktorgrades der Naturwissenschaften (Dr. rer. nat.)

der

Naturwissenschaftlichen Fakultät I – Biowissenschaften –

der Martin-Luther-Universität

Halle-Wittenberg,

vorgelegt

von Herr Fabio Strati

Gutachter:

Prof. Dr. Reinhard Neubert

Prof. Dr. Gerald Brezesinski

Prof. Dr. Emanuel Schneck

Öffentlich verteidigt in Halle (Saale) am 20.07.2022

Rechtserklärung

Ich erkläre an Eides statt, dass ich die Arbeit selbstständig und ohne fremde Hilfe verfasst, keine anderen als die von mir angegebenen Quellen und Hilfsmittel benutzt und die den benutzten Werken wörtlich oder inhaltlich entnommenen Stellen als solche kenntlich gemacht habe.

Weiterhin erkläre ich, die Angaben wahrheitsgemäß gemacht und die wissenschaftliche Arbeit an keiner anderen wissenschaftlichen Einrichtung zur Erlangung eines akademischen Grades eingereicht zu haben.

Declaration of interest

I declare under oath that this thesis is my own work entirely and has been written without any help from other people. I used only the sources mentioned and included all the citations correctly both in word or content.

Further, I declare that all information given is accurate and complete. The thesis has not been used previously at this or any other university in order to achieve an academic degree.

Halle (Saale), 03.01.2022

Fabio Strati

Table of contents

| | |
|---|----|
| 1. Introduction | 13 |
| 1.1. Skin and epidermis, structure and function..... | 13 |
| 1.2 The stratum corneum | 15 |
| 1.2.1 Origin of the SC lipids | 15 |
| 1.2.2 Lipids composition and role..... | 16 |
| 1.2.3 Lateral organization of SC lipid matrix | 18 |
| 1.2.4 CERs polymorphism | 19 |
| 1.2.5 Molecular models..... | 20 |
| 1.3 Barrier function and permeation routes..... | 23 |
| 1.3.1 Penetration routes | 23 |
| 1.3.2 Penetration enhancers | 23 |
| 1.4 SC barrier disruption and repair strategies..... | 25 |
| 1.5 Motivation and scope of this work | 26 |
| 2. Basic principles of the techniques employed | 28 |
| 2.1 Langmuir monolayers | 28 |
| 2.2 IR spectroscopy | 29 |
| 2.2.1 Fourier-transform infrared spectroscopy..... | 29 |
| 2.2.2 IRRAS | 30 |
| 2.3 X-ray scattering methods..... | 31 |
| 2.3.1 Grazing incidence X-ray scattering..... | 32 |
| 2.3.2 Total Reflectance X-ray fluorescence | 34 |
| 2.3.3 Small- and Wide- angle X-ray scattering | 34 |
| 2.4 Microscopy techniques | 35 |
| 2.4.1 Epifluorescence microscopy..... | 35 |
| 2.4.2 Transmission electron microscopy | 36 |
| 2.5 Vesicle characterization | 37 |
| 2.5.1 Dynamic light scattering | 37 |
| 2.5.2 Z-potential..... | 38 |
| 2.6 Interaction studies | 39 |
| 2.6.1 Subphase injection..... | 39 |
| 2.6.2 AFM..... | 39 |
| 2.6.3 QCM-D | 40 |
| 3. Materials | 41 |
| 4. Cumulative part | 43 |
| 4.1 Itemization of own contribution..... | 44 |

| | | |
|-----------|---|------------|
| 4.2 | Publication I..... | 45 |
| 4.2.1 | Introduction..... | 45 |
| 4.2.2 | Experimental section..... | 47 |
| 4.2.3 | Results and Discussion..... | 50 |
| 4.2.4 | Conclusion..... | 56 |
| 4.3 | Publication II..... | 58 |
| 4.3.1 | Introduction..... | 58 |
| 4.3.2 | Experimental section..... | 60 |
| 4.3.3 | Results and Discussion..... | 62 |
| 4.3.4 | Conclusion..... | 71 |
| 4.3.5 | Supporting information..... | 73 |
| 4.4 | Publication III..... | 79 |
| | Cerosomes as skin repairing agent: Mode of action studies with a model stratum corneum layer at liquid/air and liquid/solid interfaces..... | 79 |
| 4.4.1 | Introduction..... | 79 |
| 4.4.2 | Experimental section..... | 81 |
| 4.4.3 | Results and discussion..... | 84 |
| 4.4.4 | Conclusion..... | 95 |
| 4.4.5 | Supporting information..... | 96 |
| 5. | General discussion and future perspectives..... | 105 |
| 5.1 | Quaternary SC model characterization..... | 105 |
| 5.2 | Hydrogen bonding network and CERs polymorphism..... | 107 |
| 5.3 | NIS and structure activity relationship for penetration enhancing..... | 110 |
| 5.4 | Future work..... | 111 |
| 6. | Conclusion and final remarks..... | 113 |
| 7. | Appendices..... | 115 |
| 8. | Bibliography..... | 122 |

List of figures

| | |
|---|----|
| Figure 1. Overview of skin layers | 13 |
| Figure 2. General structure of the epidermis and upward differentiation | 14 |
| Figure 3. Schematic representation of skin structure and lipid organization in stratum corneum. | 16 |
| Figure 4. Chemical structure of the main sphingoid base and of the fatty acid chains..... | 17 |
| Figure 5. Schematic ceramide conformations in multilayers | 19 |
| Figure 6. Schematic representations of different lipid matrix organisation..... | 21 |
| Figure 7. The unified model of the native SPP | 22 |
| Figure 8. Penetration pathways of drugs through the SC | 24 |
| Figure 9. a) Schematic representation of Langmuir monolayer setup and b) isotherm of a monolayer..... | 29 |
| Figure 10. a) Schematic representation of FTIR and b) IRRAS spectroscopy..... | 30 |
| Figure 11. Representation of Bragg's law | 31 |
| Figure 12. a) Geometry of GIXD setup and b) schematic representation of a SAXS/WAXS setup | 32 |
| Figure 13. Diagram of experimental setup for fluorescence microscopy with upright geometry with monolayer illuminated from above | 36 |
| Figure 14. Schematic representation of a transmission electron microscope | 37 |
| Figure 15. Schematic representation of DLS apparatus | 38 |
| Figure 16. Modified Langmuir setup used for penetration studies..... | 48 |
| Figure 17. Surface pressure-area isotherms of the SC model system spread at 25 and 35°C | 50 |
| Figure 18. Injection of increasing NIS concentration underneath a pre-formed SC monolayer at a surface pressure of 20 mN/m | 51 |
| Figure 19. Injection of constant NIS concentration underneath SC model monolayers with increasing initial surface pressure | 52 |
| Figure 20. a) Part (CH_2 symmetric and asymmetric bands as well as the -OH band) of IRRAS spectra of the SC model system at different surface pressures and b) wavenumbers of CH_2 asymmetric stretching vibration at different surface pressures..... | 53 |
| Figure 21. a) IRRAS spectra of the SC model system plus the studied NIS and b) wavenumber of CH_2 asymmetric stretching vibration of the different systems..... | 54 |
| Figure 22. Epifluorescence micrographs of SC monolayer at increasing surface pressure plus micrographs of SC + NIS systems | 55 |
| Figure 23. a) Schematic representation of SC monolayer with presence of defected regions, and b) adsorption of surfactants monomers with local disordering of SC lipids..... | 56 |
| Figure 24. Chemical structure of CER[AP] | 59 |

| | |
|---|-----|
| Figure 25. Contour plots of the X-ray intensities of D-CER[AP], L-CER[AP] and D/L-CER[AP] with symmetric chains (C18:C18)..... | 62 |
| Figure 26. Contour plots of the X-ray intensities of D-CER[AP], L-CER[AP] and D/L-CER[AP] with asymmetric chains (C24:C18)..... | 64 |
| Figure 27. Schematic representation of chain ordering of symmetric and asymmetric L-CER[AP] in monolayers and partial fluidization of the longer chain due to chain mismatch.... | 67 |
| Figure 28. Schematic representation of fully extended and hairpin configuration of D-CER[AP], as well V-shape and hairpin configuration with tilted chains of L-CER[AP] | 68 |
| Figure 29. Small-angle X-ray scattering profiles of D/L-CER[AP], L- CER[AP] and D- CER[AP] with asymmetric chains (C24:C18)..... | 69 |
| Figure 30. WAXS profile and corresponding fitting of D-CER[AP] and L-CER[AP] (24:0, 18:0). | 70 |
| Figure 31. FTIR profiles of amide region with CH ₂ scissoring regis..... | 71 |
| Figure 32. Chemical structure of human CERs and possible chain and head modifications. | 80 |
| Figure 33. a) Contour plot of the scattered X-ray intensity of model SC monolayer and b) fitting of Bragg peaks by Lorentzian functions..... | 86 |
| Figure 34. Stability analysis of vesicle formulations presented as polydispersity index versus time. | 88 |
| Figure 35. TEM images by negative staining of Cerosome, Cerosome + S75-3, P100-3 and S75-3..... | 90 |
| Figure 36. a) Maximum variation of surface pressure, $\Delta\Pi$, from the initial surface pressure value of 20 mN/m after injection of vesicle formulations and b) $\Delta\Pi$ versus time kinetics of adsorption of liposomes. | 91 |
| Figure 37. Schematic representation of cerosome injection underneath a pre-formed SC model monolayer and presentation of the interaction types with vesicle adsorption driven by hydrogen bonding forces between CERs | 92 |
| Figure 38. AFM scans of SC model monolayer transferred via LB method onto mica support, SC model monolayer after injection of cerosomes, SC model monolayer after injection of cerosome + S75-3 formulation, and SC model monolayer after injection of S75-3 liposomal formulation..... | 94 |
| Figure 39. On the left structure of the proposed quaternary model bilayer arrangement with lipids arranging in an orthorhombic lattice and proposed arrangement of CER[NP] in a V-shape configuration with 39° chain tilt..... | 105 |
| Figure 40. Molecular structure of used lipids in publication III and representation of hydrogen bond donor groups and bond acceptor groups | 109 |
| Figure 41. Representation of a PAMPA system | 112 |

List of tables

| | |
|---|----|
| Table 1. List of publication and specification of the percentage of own contribution..... | 44 |
| Table 2. The variation of surface pressure ($\Delta\Pi$) after injection of a defined NIS solution as a function of increasing initial surface pressure of the SC monolayer | 57 |
| Table 3. Structural parameters extracted from GIXD data of the different forms of CER[AP] | 65 |
| Table 4. Structural parameters extracted from GIXD data of a SC model monolayer..... | 85 |
| Table 5. Compositions of the tested extruded liposomal formulations..... | 87 |

List of abbreviations**Substances**

| | |
|---------|---|
| CER[AP] | Ceramide alpha-hydroxy phytosphingosine |
| CER[AS] | Ceramide alpha-hydroxy sphingosine |
| CER[NP] | Ceramide non-hydroxy phytosphingosine |
| CER[NS] | Ceramide non-hydroxy sphingosine |
| Chol | Cholesterol |
| LA | Lignoceric acid |
| PC | Phosphatidylcholine |
| PL80 | Polysorbate 80 |
| SA | Stearic acid |
| SL | Sucrose monolaurate |

Methods

| | |
|-----------|--|
| AFM | Atomic force microscopy |
| DLS | Dynamic light scattering |
| DSC | Differential scanning calorimetry |
| GIXD | Grazing incidence X-ray diffraction |
| FTIR | Fourier-transformation infrared |
| IRRAS | Infrared reflectance absorbance spectroscopy |
| QCM-D | Quartz crystal microbalance with dissipation |
| SAXS/WAXS | Small/Wide angle X-ray scattering |
| TEM | Transmission electron microscopy |
| TRXF | Total reflectance X-ray fluorescence |
| XRD | Powder X-ray diffraction |

Others

| | |
|----|-----------------|
| 2D | Two-dimensional |
|----|-----------------|

| | |
|-----------------|---|
| 3D | Three dimensional |
| A ₀ | Cross sectional area |
| A _{xy} | In-plane lattice area of one chain |
| AD | Atopic dermatitis |
| C _c | Characteristic curvature |
| CER | Ceramide |
| CMC | Critical micellar concentration |
| d | Lamellar repeat distance |
| FE | Fully extended |
| FFA | Free fatty acid |
| Fwhm | Full-width half-maximum |
| G | Gas |
| Hb | Hydrogen bond |
| HbN | Hydrogen bonding network |
| IR | Infrared |
| LB | Langmuir Blodgett |
| LC | Liquid condensed |
| LE | Liquid expanded |
| LM | Lipid matrix |
| LPP | Long periodicity phase |
| LS | Langmuir Schaefer |
| MIP | Maximal insertion pressure |
| NIS | Non-ionic surfactant |
| PAMPA | Parallel artificial membrane permeability assay |
| PE | Penetration enhancer |
| PL | Phospholipid |
| S | Solid |
| SAR | Structure activity relationship |
| SB | Stratum basale |
| SC | Stratum corneum |
| SG | Stratum granulosum |
| SP | Surface pressure |
| SPP | Short periodicity phase |
| SS | Stratum Spinosum |

| | |
|------|---------------------------|
| t | Tilt |
| TEWL | Transepidermal water loss |
| Wt% | Weight percent |

Symbols

| | |
|-----------|----------------------|
| λ | Wavelength |
| ν | Stretching vibration |
| π | Surface pressure |
| γ | Surface tension |
| ζ | Correlation length |

List of equations

| | | |
|--------------|---|----|
| Equation 1: | $\pi = \gamma_{water} - \gamma_{monolayer}$ | 28 |
| Equation 2 : | $K = \frac{1}{c} = -A \left(\frac{d\pi}{dA} \right)_T$ | 29 |
| Equation 3: | $E = h\nu$ | 31 |
| Equation 4: | $n\lambda = 2d\sin\theta$ | 32 |
| Equation 5: | $q_{xy} \cong (4\pi/\lambda) \times \sin 2\theta_{xy}/2$ | 33 |
| Equation 6: | $q_z \cong (2\pi/\lambda) \times \sin \alpha_f$ | 33 |
| Equation 7: | $L_z = 0.9/(2\pi/fwhm(q_z))$ | 33 |
| Equation 8: | $L_{xy} = 0.9/(2\pi/fwhm(q_{xy}))$ | 33 |
| Equation 9: | $fwhm_{xy}^{cor} = \sqrt{(fwhm_{xy}^{meas2} - fwhm_{xy}^{res2})}$, | 33 |
| Equation 10: | $I_f = b_i \int I_{ex} (z) c (z) dz$ | 34 |
| Equation 11: | $q = (4\pi/\lambda) \sin \theta$ | 34 |
| Equation 12: | $d = 2\pi/q = 1/s$ | 35 |
| Equation 13: | $D = KbT/6\pi\eta t$ | 38 |
| Equation 14: | $P_w = 2Dq^2/\pi\omega^2 + (2Dq^2)$ | 38 |
| Equation 15: | $U_e = V/E$ | 39 |
| Equation 16: | $U_e = 2\epsilon z f(\kappa\alpha)/3\eta$ | 39 |
| Equation 17: | $F = -kz$ | 40 |
| Equation 18: | $\Delta m = -\Delta F n C$ | 40 |

Abstract

The uppermost layer of the skin, the stratum corneum (SC), is the first human barrier against chemical, thermic and biological stresses. It is composed of a brick and mortar system where the bricks consist of dead corneocytes and the mortar of a dense and extremely lipophilic lipid matrix. In particular is the lipid matrix that confers the typical physical chemical properties responsible for the protection role. The main lipid species present in the matrix are ceramides, free fatty acids and cholesterol, and it has been observed that the ceramides play a central role in conferring the lipid matrix its peculiar characteristics. The ceramides consist of a sphingoid moiety connected through an amide bond with a fatty acid moiety. Modifications in the fatty acid and sphingosine moieties generate different subclasses for a total of 18 subclasses evidenced in the human SC. As well the alkyl chain length of these moieties can change. An alteration of the lipid matrix composition can cause acute or chronic pathologies due to the alteration of the SC barrier properties. Because of its relevant functions, the SC is studied for characterizing its precise molecular structure and as well for the delivery of dermal and transdermal formulations.

In this work, a simple SC *in-vitro* model consisting of CER[NP]:D-CER[AP]:Cholesterol:Lignoceric acid (0.66:0.33:0.7:1 in molar ratio) was developed and characterized via Langmuir monolayers by the application of relevant biophysical methods such as: X-ray scattering based techniques, infrared spectroscopy, atomic force microscopy and others. The selected lipids presented the fatty acid moiety with a C24 chain length, fundamental feature since in the SC most of the lipids present long chains (between C20 and C26). The characterized monolayer model was used for screening the potential application of non-ionic surfactants as penetration enhancers. In addition, stratum corneum liposomes, i.e. cerosomes, have been developed and characterized in order to define the mode of action by which these formulations enact their observed skin repairing effect using as model the tested SC monolayer.

In parallel to these studies, a detailed physical-chemical analysis of CER[AP] was devised. CER[AP] can be produced synthetically in its D(2R)- and L(2S) forms. Although the native form in the skin is the D-form, CER[AP] is often used for the development of *in-vitro* models in its diastereomer mixture. By the use of X-ray scattering based methods in mono- and multi-layer systems, the properties of the two diastereomers and of the 1:1 mixture have been we defined, studying in parallel the effect of chain symmetry between the fatty acid and sphingosine moieties.

Zusammenfassung

Die oberste Schicht der Haut, das Stratum corneum (SC), ist die erste menschliche Barriere gegen chemische, thermische und biologische Belastungen. Sie besteht aus einem System

aus Ziegeln und Mörtel, wobei die Ziegel aus abgestorbenen Korneozyten und der Mörtel aus einer dichten und extrem lipophilen Lipidmatrix bestehen. Es ist vor allem die Lipidmatrix, die die typischen physikalisch-chemischen Eigenschaften verleiht, die für die Schutzfunktion verantwortlich sind. Die wichtigsten Lipidarten in der Matrix sind Ceramide, freie Fettsäuren und Cholesterin, und es wurde festgestellt, dass Ceramide eine zentrale Rolle dabei spielen, der Lipidmatrix ihre besonderen Eigenschaften zu verleihen. Die Ceramide bestehen aus einer Sphingoideinheit, die über eine Amidbindung mit einer Fettsäureeinheit verbunden ist. Modifikationen in den Fettsäure- und Sphingosinanteilen führen zu verschiedenen Unterklassen, insgesamt 18 Unterklassen, die in der menschlichen SC nachgewiesen wurden. Auch die Alkylkettenlänge dieser Anteile kann sich ändern. Eine Veränderung der Zusammensetzung der Lipidmatrix kann akute oder chronische Krankheiten verursachen, die auf eine Veränderung der Barriereigenschaften des SC zurückzuführen sind. Aufgrund ihrer wichtigen Funktionen wird das SC untersucht, um seine genaue molekulare Struktur zu charakterisieren und um es für die Verabreichung von dermalen und transdermalen Formulierungen zu nutzen.

In dieser Arbeit wurde ein einfaches *in-vitro* SC-Modell bestehend aus CER[NP]:D-CER[AP]:Cholesterin:Lignocerinsäure (0,66:0,33:0,7:1 im molaren Verhältnis) entwickelt und mittels Langmuir-Monoschichten unter Anwendung relevanter biophysikalischer Methoden wie Röntgenstreuung, Infrarotspektroskopie, Rasterkraftmikroskopie und anderer charakterisiert. Die ausgewählten Lipide wiesen eine Fettsäureeinheit mit einer Kettenlänge von C24 auf, ein grundlegendes Merkmal, da die meisten Lipide im SC lange Ketten (zwischen C20 und C26) aufweisen. Das charakterisierte Monoschicht-Modell wurde für das Screening der potenziellen Anwendung von nichtionischen Tensiden als Penetrationsverstärker verwendet. Darüber hinaus wurden Stratum-Corneum-Liposomen, d. h. Cerosomen, entwickelt und charakterisiert, um die Wirkungsweise zu definieren, durch die diese Formulierungen ihre beobachtete hautreparierende Wirkung entfalten, wobei die getestete SC-Monoschicht als Modell diente. Parallel zu diesen Studien wurde eine detaillierte physikalisch-chemische Analyse von CER[AP] durchgeführt. CER[AP] kann synthetisch in seiner D(2R)- und L(2S)-Form hergestellt werden. Obwohl die native Form in der Haut die D-Form ist, wird CER[AP] für die Entwicklung von *in-vitro* Modellen häufig in seiner Diastereomerenmischung verwendet. Durch den Einsatz von Röntgenstromethoden in Mono- und Mehrschichtsystemen wurden die Eigenschaften der beiden Diastereomere und des 1:1-Gemischs bestimmt und parallel dazu die Auswirkungen der Kettensymmetrie zwischen der Fettsäure- und der Sphingosineinheit untersucht.

1. Introduction

1.1 Skin and epidermis, structure and function

Human skin (Figure 1) with an average surface area of 1.5-2 m² is the second largest organ of the human body [1]. Because of its direct exposition to the external environment, the skin provides protection against external agents such as bacteria and chemical xenobiotics, it protects against heat, mechanical and physical (UV-radiation) stresses. It as well possesses different types of receptors making the skin the largest sensory organ helping to differentiate touch, temperature and pain signals. The skin also regulates the body's water retention, also called transepidermal water loss (TEWL), by inhibiting the loss of water and by secreting solutes and/or water via sweating glands [2]. Finally, the skin fulfils a metabolic and endocrine role by synthesising vitamin D which has hormone like functions. Therefore, the skin has evolved as a complex organ capable of interacting with the immune system, muscles, and the brain [3].

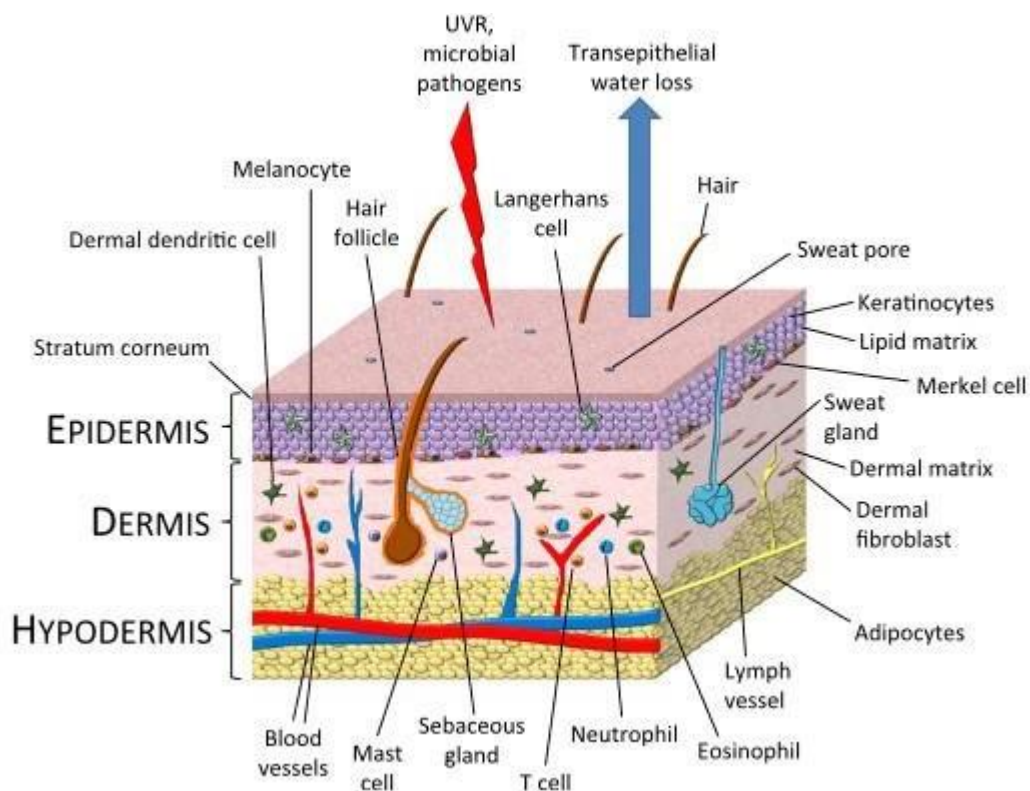


Figure 1. Overview of the skin layers and main function of the external layer, image adapted from [4].

The skin is divided in three layers (Figure 1): the hypodermis which is the site of fat cells regulating the energy metabolism having a role in thermoregulation, the dermis which is the site of the big majority of sensory nerves in the skin containing large blood vessels which transport oxygen and important metabolites necessary for keeping the homeostasis of the skin,

and finally the epidermis which has the protection role by continuously being regenerated starting from the upper layers of the dermis.

The epidermis is a continuously renewing epithelium and it is the only compartment of the skin where no blood vessels are present, and the main cellular type found is the one of keratinocyte. The epidermis presents one of the highest turnover rates in the mammalian body and its homeostasis is achieved by a balance of cell proliferation from basal layers and cell loss through terminal differentiation. The epidermis itself is divided in four main compartments, each one of them involved in the differentiation and migration of keratinocytes from basal layers process which is also referred as *cornification*. Here the proliferation, differentiation and death of keratinocytes occur sequentially and each process is regulated by the expression of specific genes and proteins (Figure 2) [5].

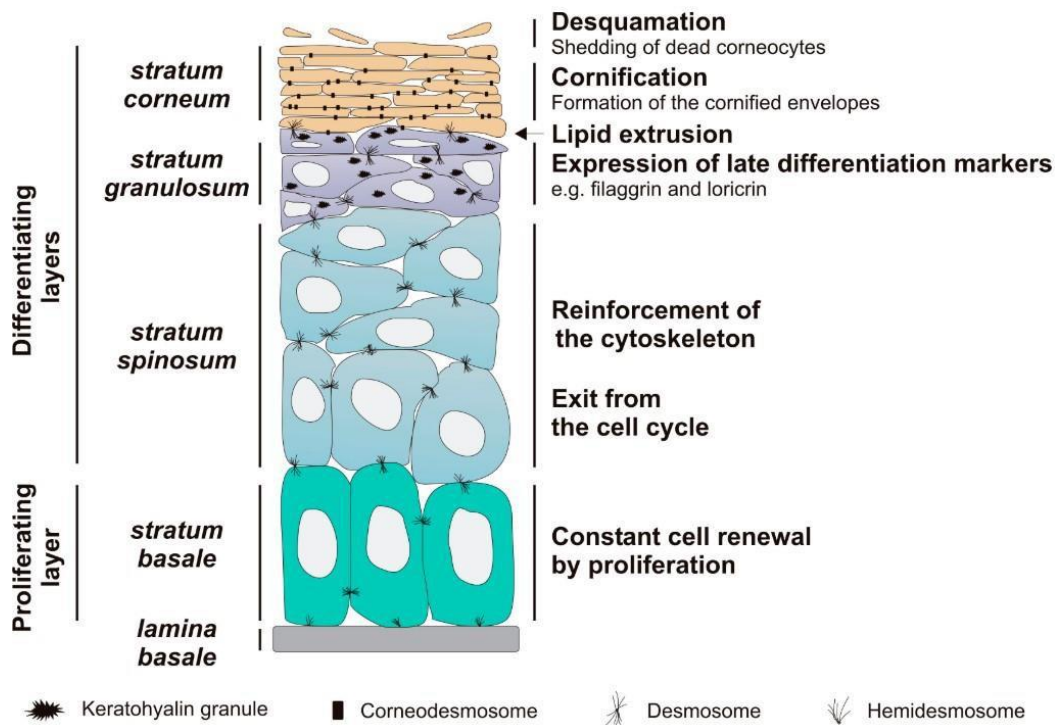


Figure 2. General structure of the epidermis and description of the upward differentiation of keratinocytes. Image adapted from [6].

The cornification process begins from the stratum basal (SB), lowest layer of the epidermis, where keratinocytes are excreted from the lamina basal, final layer between dermis and epidermis. In here, the keratinocytes are detached from the basement membrane and the cornification process starts differentiating while migrating in upper layers. Once keratinocytes are detached from the SB they start to migrate into the stratum spinosum (SS) modifying their gene expression, losing the mitotic activity and replenishing the dead and non-dividing cells. Here, the cells start synthesizing proteins and enzymes necessary for the cornification such as keratin and keratin filaments which contribute for the formation of desmosomes which holds

the different cells together. The cells start to form Odland bodies which are enclosed membrane granules containing hydrolytic enzymes, lipids and proteins necessary for the following cornification steps and formation of a dense lipid matrix. From the SS the keratinocytes continue to migrate upward in the stratum granulosum (SG) where they acquire keratohyalin granules which contain profilaggrin, precursor of the protein filaggrin. Filaggrin has the role to aggregate the keratin filaments into tight bundles that promotes the collapse of the cells in flattened shape cells creating the corneocyte which finally migrate in the stratum corneum (SC) and completing the cornification process. The corneocytes in the SC consist of keratin filaments embedded in a filaggrin matrix surrounded by insoluble cornified envelop produced by the release of the content from the Odland bodies. The cornified envelop of each corneocyte is tightly attached to neighbour cornified envelopes via corneodesmosomes, modified desmosomal structures, which in the latest layer of the SC are proteolytically depredated in order to allow the final desquamation of the corneocytes from the skin. Together with the formation of corneocytes, the content of the lamellar granules previously formed in the SG is released. The expelled glycolized lipids are hydrolysed by enzymes in the SC and this process, which alters the polar lipids to non-polar ones, is essential to constitute the intercellular lipid matrix of the SC.

1.2 The stratum corneum

The SC is the last and uppermost layer of the skin. When the SC was studied for the first time using a light microscope [7,8], it was observed that the organization of the SC could be summarized by a "brick and mortar" system (Figure 3) where 15-30 layers of corneocytes with a thickness of 9-13 μm are surrounded by a dense lipid matrix (LM). The corneocytes are filled with water and microfibrillar keratin that is surrounded by a cornified envelope consisting of a densely crosslinked layer of proteins (filaggrin, loricrin and involucrin) [9]. Moreover, a monolayer of non-polar lipids (gamma-hydroxylated ceramides (CER) and free fatty acid (FFA)) is esterified to the cornified envelope forming the so called lipid envelope. The lipid envelope together with the cornified envelope minimize the uptake of substances into the corneocytes and allow the proper formation of the LM [10,11].

Two layers can be distinguished inside the SC. First, the stratum compactum is stabilized by corneodesmosomes between the cells, which confer structural stability to the SC. Second, the stratum disjunctum where the degradation of corneodesmosomes allows the process of corneocyte desquamation completing the cornification process.

1.2.1 Origin of the SC lipids

Human LM consists of a mixture of CERs, cholesterol (Chol), FFA and by a small percentage of cholesterol sulphate and cholesterol esters [12–14]. The lipids are originally synthesised

and stored in the Odland bodies and extruded into the extracellular space in the upper granular layer during cornification [15,16]. This lamellar bodies consist mainly of glycosphingolipids, Chol and phospholipids (PL) which once extruded are enzymatically converted into lipophilic product and assembled in order to surround the corneocytes and form the lipid matrix. The PLs are catabolized to FFA and the glycosphingolipids are converted to CERs [17].

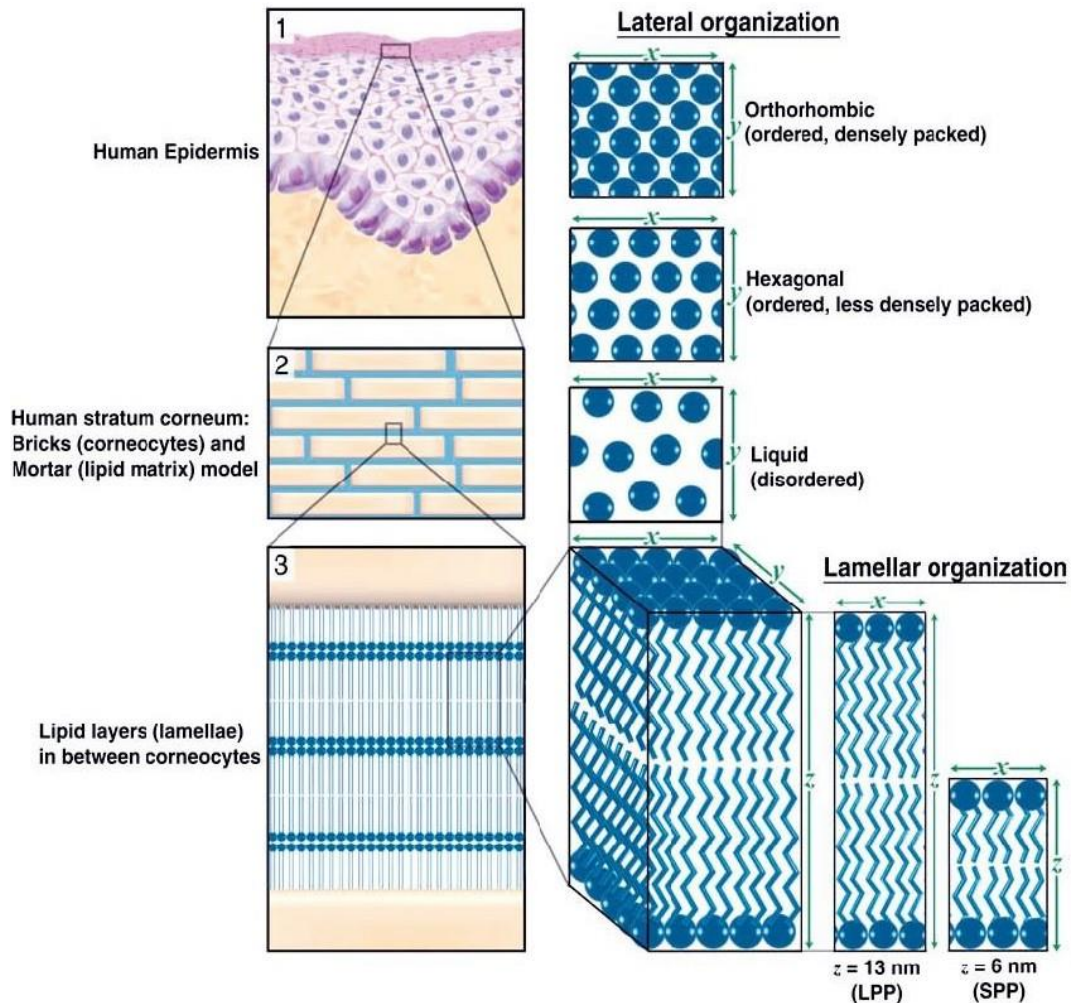


Figure 3. (1) Representation of human skin. (2) Schematic representation of the SC and representation of the brick and mortar system where the bricks are represented by dead corneocytes and the mortar is the dense lipid matrix. (3) The lipids in the matrix are arranged in lamellae each presenting a distinctive repeating distance (d), in particular the long periodicity phase (LPP) ($d \sim 13 \text{ nm}$) and the short periodicity phase (SPP) ($d \sim 6 \text{ nm}$) are shown. In the lipid matrix, three types of lateral organization have been observed. The dense and less permeable orthorhombic phase, the less dense and ordered hexagonal phase and the disordered and permeable liquid phase. Image adapted from [18].

1.2.2 Lipids composition and role

As previously mentioned, the SC lipid matrix is constituted by a mix of 46 wt% CERs, 27 wt% Chol and 27 wt% FFA [12,19,20]. The homeostasis of the SC and in particular of its lipid composition is fundamental for keeping and maintaining the barrier properties of the skin, and each lipid alone and collectively presents important roles.

Chol is a hydrophobic molecule which possesses a very small hydrophilic group. In the SC, it is reported to regulate the chain mobility of the lipids present in a gel state and to decrease their mobility when present in the liquid-crystalline state [21]. This leads to a higher lateral area of the SC lipids, thus lowering chain ordering which improves the intermixing of the lipids [22]. This process increases compressibility and mechanical stability of the LM and provides fluidity below and rigidity above the phase transition temperature [23]. Together with Chol, small fractions of cholesterol sulphate and cholesterol ester are found as components of the SC. The cholesterol sulphate plays an important role in the cell cohesion helping the desquamation process of the corneocytes [24,25]. The cholesterol esters may serve to prevent the fluidification effect if residual unsaturated fatty acids on intercellular membrane domains [26].

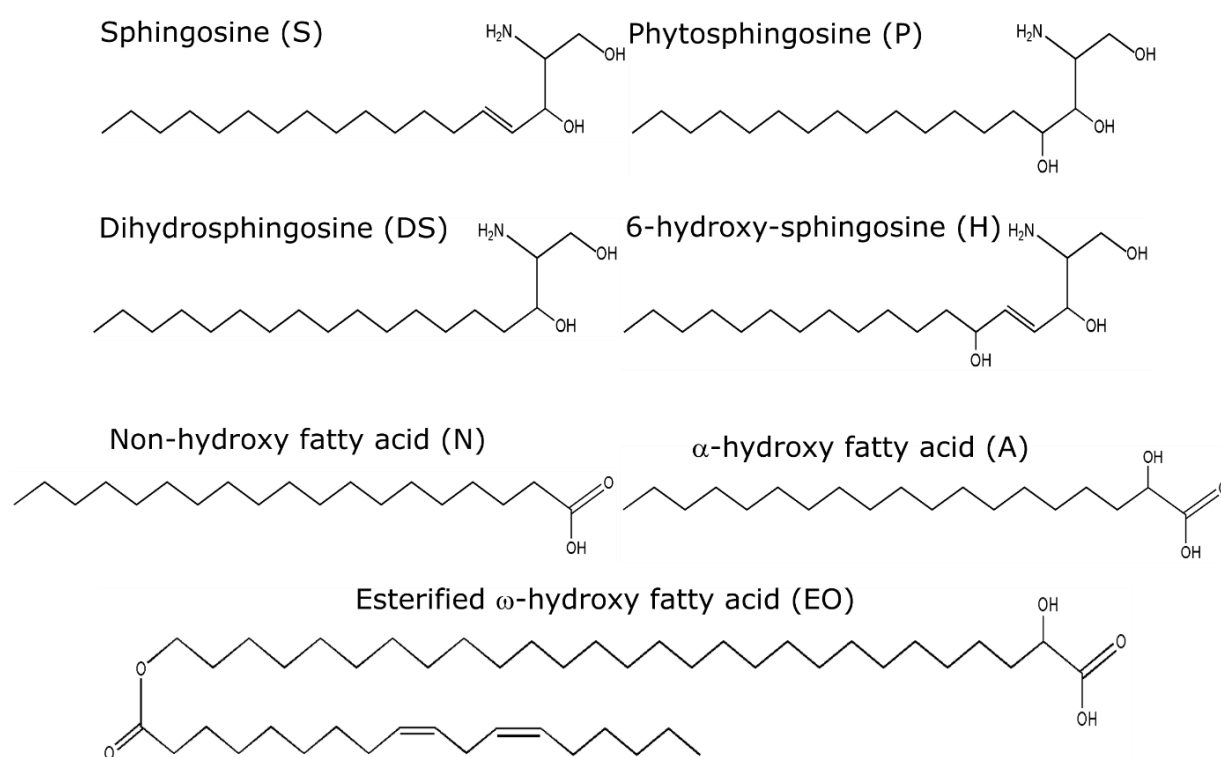


Figure 4. Chemical structure of the main sphingoid base and of the fatty acid chains.

The free fatty acids of the SC consist mainly of saturated chains which can have length between C14-C30 with a prevalence of C24\26 and C16\18 alkyl chains [19,27]. The FFA present an important role for the barrier property of the lipid matrix, and together with cholesterol sulphate represent the only ionisable lipid having an important role for the organization in bilayers of the LM [28]. Moreover, it was reported that in chronic model of essential fatty acid deficient mice brought to a disturbed permeability barrier with increased TEWL [29].

The dominant class of lipids in the SC is the one of the CERs which are constituting almost 50 % of the lipid weight. CERs are fundamental molecules with many properties, in the SC these

establish and keep the barrier properties and present a role in the LM for the association of membrane proteins. In other body compartments, they have physiological roles in signal transduction and cell regulation relevant to apoptosis, cell growth arrest, differentiation, senescence, and immune responses [30–33]. CERs consist of a sphingoid moiety which is covalently bound by an amide to a fatty acid moiety. The current classification of CERs was created by Motta [34] and then expanded by Robson, Masukawa and Rabionet [12,35,36], CERs can be classified based on the presence of specific groups in the sphingoid and fatty acid moieties. Currently, four sphingoid moieties are known to exist with variations in the head group region at position C4 and C6. Different groups are distinguished with the use of a letter such as (S) for sphingosine with a single double bond in position C4-5, (P) phytosphingosine with saturated chain and hydroxy group in position C6, (H) for 6-hydroxy-sphingosine with hydroxy group in C6 and double bond in C4-5 and (DS) dihydrosphingosine without any modification. Different groups are also present in the fatty acid chains, the letter (A) indicates the presence of alpha-hydroxyl group towards the carbonyl group, the (N) state for non-hydroxy and (O) indicates ω -OH fatty acids, a class which usually presents ester linkages forming a new class indicated as (EO). In total 18 subclasses of CERs have been confirmed in different studies were samples of human epidermis have been analysed with analytical techniques such as LC/MS, TLC, MS/MS and NMR [12,20,34–38]. Not only the fatty acid and sphingoid moieties can vary but also the chain length varies in the SC lipid matrix. The sphingoid moiety can exist between C14 and C20 [39] while different studies based on LC/MS showed that the length of the fatty acid moiety can vary in a range of C12 to C36 with majority of the chains found between C24 and C26 [40–42]. All these different ranges of chain lengths and CERs classes allow the presence in the LM of more than 1000 of different CERs in the human SC [20].

1.2.3 Lateral organization of SC lipid matrix

The SC lipid matrix is the most important structure regarding the permeability properties of the skin. Thanks to its peculiar composition, it represents an extreme hydrophobic environment where the lipids exhibit ordered and densely packed lateral structures. As beforehand mentioned, the CERs with two relatively long alkyl chains in all-trans conformation and a small head group are the main determining factor for the organization of the LM [43]. Three types of lateral packing have been observed (Figure 3), orthorhombic, hexagonal and liquid [44–48]. The prevalent packing of skin lipids is the orthorhombic subcell, characterized by densely packed lipids with small rotational freedom and unevenly distributed lipids, which confers very low permeability to the SC. The hexagonal subcell presents higher order with the lipids in a gel state with medium permeability. Finally, the liquid subcell, where the lipids are present in a disordered state, presenting high permeability [18]. The presence of specific classes of CERs

is fundamental for stabilizing and forming specific types of subcells. For instance, the class of the phytosphingosine has been proved to create intermolecular hydrogen bonding network (HbN) and to favour the stabilization of the orthorhombic subcells [49].

Not only different subcells are observed but also different arrangements of the CERs alkyl chains are possible. The three arrangements known (Figure 5) are the hairpin conformation, where the two chains are parallel to one another forming a 0° angle [50], the fully extended (FE) conformation, with the two chains pointing in opposite direction creating an angle of 180° [51], and last the so called V-shape conformation, where the chains angle can range between 0 and 180° [52]. The most likely conformations existing in the LM are the fully extended and the hairpin. The V-shape conformation was observed in studies with either single CERs [53] or in simple models of the SC [54].

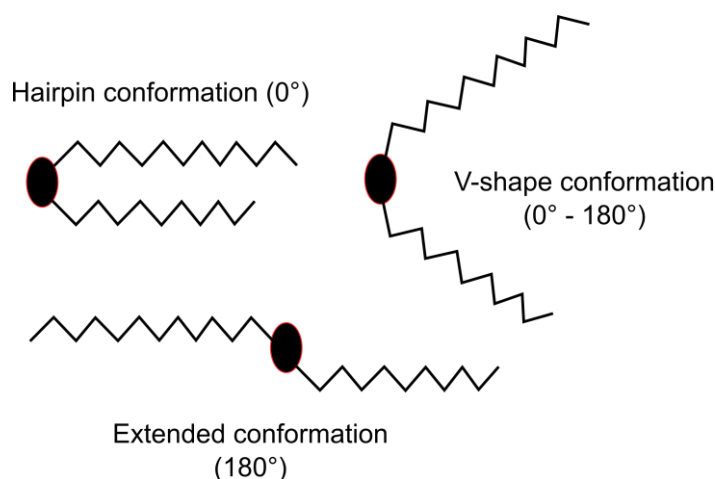


Figure 5. Schematic of the possible conformations of ceramides in a multilayer organization, the $^\circ$ is referred to the angles between the two chains.

1.2.4 CERs polymorphism

CERs in comparison to other lipids present very peculiar physical-chemical properties which are responsible for creating a tight and impermeable LM. CERs possess two chains originating from a fatty acid and a sphingosine moiety, modifications in the head group or in the chains lead to the creation of different subclasses, each class presenting unique characteristics, moreover, in comparison to other lipids such as PLs, they possess very small head groups.

Studies with simplified models of SC or single CERs showed that the CERs are polymorphic compounds. In a neutron diffraction study made by Kiselev et al. was shown how the amount of water present in a SC *in-vitro* multilayer system can lead to a transition of the CERs alkyl chains from a FE to a hairpin configuration [55]. The presence of excess water has the effect to stabilize a configuration where the head group is directly exposed to the water rather than the alkyl chains. Another work from Dahlen and Pacher [53] based on X-ray scattering studies of the single CER[NP], showed how this CER possesses alone at least six different solid

phases, five of them where the chains are present in V-shape conformation with different possible angles, and a single configuration where the molecule presents a hairpin configuration. Most of the polymorphic phenomena related to CERs are connected with the ability of such molecules to create intermolecular HbN. In thermotropic, IR, molecular dynamics and X-ray scattering experiments was shown that the CER subclasses created intermolecular HbN which from a biological point of view are fundamental for the creation and stabilization of the orthorhombic lateral organization in the SC lipid matrix [23,49].

1.2.5 Molecular models

The LM surrounds the corneocytes in the SC and it is reported to be responsible for the permeability and barrier properties of the SC itself. The exact structure of LM has been not yet completely clarified and since its discovery is still an important research topic.

Since the discovery in the early 70s that the SC extracellular space is filled with lipids [56], a lot of progress has been made regarding the characterization and description of the LM organization. One of the first pioneer works dates back to the 1985 where an electron microscopy study from Madison et al. [57] using mice SC stained with RuO₄, allowed to visualize for the first time the ~ 13 nm broad-narrow-broad based sequences proving the complex organization of the LM. Few years later, Swartzendruber et al. [58] again visualized the same pattern postulating the presence of a *stacked monolayer model* where stacked monolayers of FE CERs were present with interdigitation of the alkyl chains which formed planar multilamellar layers.

In the following years, Forslind et al. in 1994 postulated a new model which created great debate in the scientific skin community [59]. This model, called *domain mosaic model* (Figure 6a), was based on the observations of Potts et al. where the coexistence of dense orthorhombic domains and liquid-like gauche conformers was observed [60]. In this model, the LM is organized in two main domains, a first domain where the lipids are organized in bilayers of crystalline-gel lipids responsible for the typical permeability and mechanical properties of the SC, and a second domain where the lamellae are embedded into a continuous liquid matrix also referred as *grain border* domain. Such grains or pores would permit a certain degree of water permeation allowing the lower layers of the skin to remain hydrated, nevertheless, keeping the typical physical-chemical protection properties [59].

In 2001, Norlen contradicted the domain mosaic model with the idea that the presence of liquid domains would allow not only water but also xenobiotics to permeate through these grains, permeation of xenobiotics in healthy skin was not observed [22]. Instead, a new model defined as *single gel phase* (Figure 6b) was proposed. In this model, Norlen proposed that the LM is organized in a single coherent lamellar phase with layers of heterogeneously distributed lipid composition and chain length. In this model, the coexistence of orthorhombic and hexagonal

lateral structures, stabilised by the presence of large amounts of Chol with the CERs that can order both in a hairpin or FE conformation, is proposed. This structure would justify simultaneously a broad phase transition range and a stabilized gel phase. The proposed single layer possesses low water content, low permeability and high mechanical resistance.

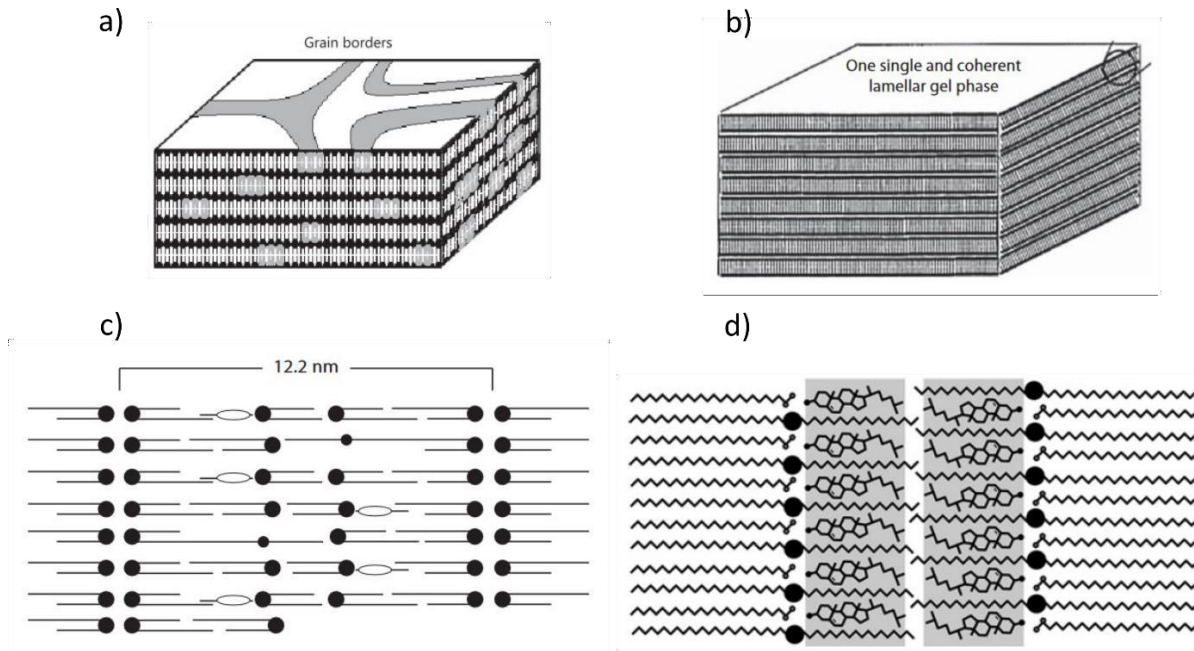


Figure 6. Schematic representations of the discussed LM organizations: a) domain mosaic model representation (adapted from [59]), b) single gel phase model (adapted from [22]), c) sandwich model (adapted from [61]) and d) asymmetric model (adapted from [51]).

After the discovery of the broad sequence in the work of Madison [57], Bouwstra et al. introduced the *sandwich model* (Figure 6c) to justify the presence of such long sequence in the LM [61]. This model was based on the results of X-ray diffraction studies on isolated human skin which allowed the observation of perpendicular arrangement of lipids and to observe the repeating distance of different lamellar domains [62,63]. This model reinterpreted the broad-narrow-broad sequence considering the coexistence of gel and liquid domains present in a trilayer arrangement which creates a lipid sandwich. In this work, two phases, a short 6 nm sequence referred as SPP and a long 13 nm referred as LPP, were observed. In this model, the fluid phase is mainly present in the narrow layer located in the centre of the LPP, where mainly unsaturated linoleic acid, CER[AS] and Chol are present. The lipid packing in this central layer gradually changes into more densely packed lipid layers on both sides of the central layer. Later on it was found that the presence of long chain CERs such as CER[EOS] is fundamental for the formation of the LPP and for the central narrow layer [44]. The sandwich model is one of the most described and used models of the LM, however, may present a limitation connected to the relative low amount of long gamma-OH CERs (10 %) which would hardly explain the presence of such LPP domain over the whole thickness of the SC [12,64].

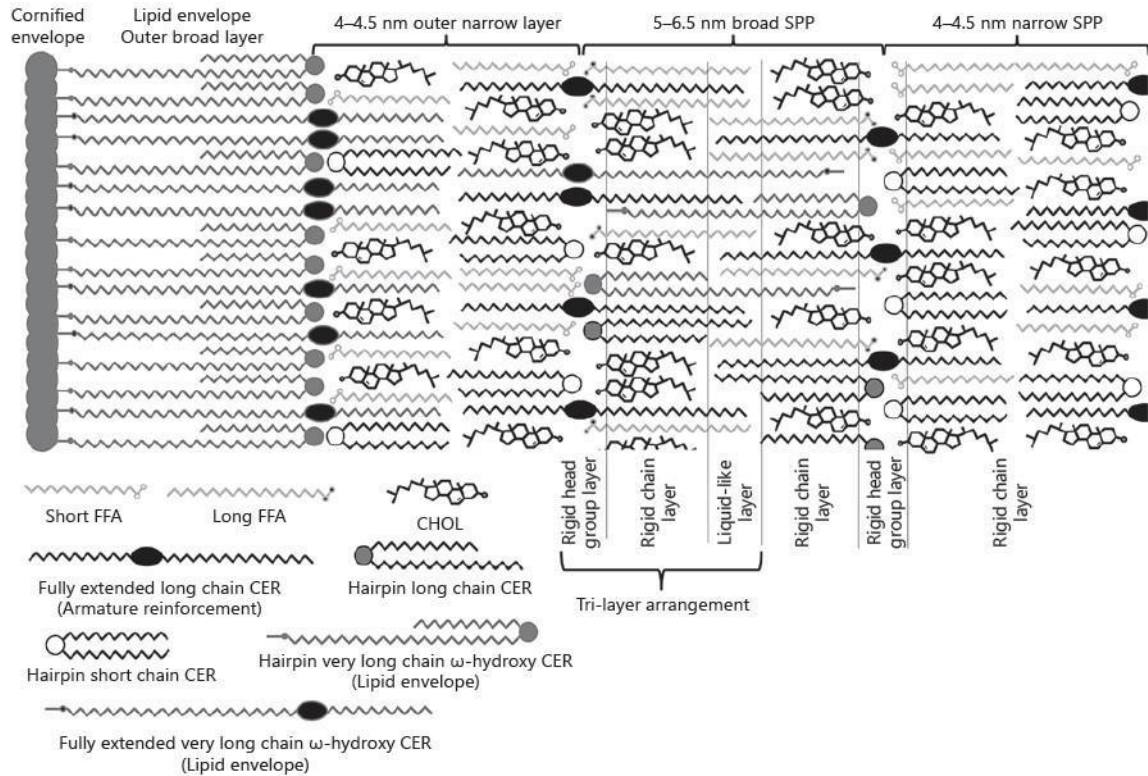


Figure 7. The unified model of the native SPP (exact proportions of fully extended and hairpin-folded CER are unknown, no broad-broad arrangements shown) according to [64].

With the development of microscopy techniques, the group of Norlen was able to visualize in detail the LM organization in 2012 by using cryo-electron-microscopy on vitreous skin sections combined with atomistic 3D cryo-EM model simulations. They visualized again an organization that is closely connected to the bilayer organization found by Madison in 1987 with the typical broad-narrow-broad sequence. In their model, instead of a bilayer arrangement based on the influence of very long gamma-OH CERs, the bilayers were formed by CERs with long chains in a fully extended configuration. A new arrangement of asymmetric (from here *asymmetric model*) repeating unit with length of 11 nm consisting of a narrow unit (4-4.5 nm) plus a broad unit (5-6.5 nm) was observed (Figure 6d). In these bands, the lipid layers are in full-extended conformation but stacked in an alternate fashion as bilayers rather than stacked monolayers [65]. It was also assumed that in this configuration the Chol molecules have to be associated with the sphingoid moiety of CERs and the FFAs are associated to the fatty acid chains which are longer therefore creating asymmetry in the model [51].

The organization of the LM is still today a topic of great discussion. Since the release of the first pioneer work, new studies are published adding new perspectives about LM organization. In 2020, Schmitt and Neubert analysed in a review the past and recent progresses of the LM. An organization of the LM, which tries to unify the different findings regarding the LM organization (Figure 7), has been proposed [64]. In this model, the coexistence of 3 main domains is described. Lipids that have a short symmetric chain get concentrated in a narrow

domain with shorter lamellae arrangement (4-4.5 nm). The long lipids/chains would get concentrated in 5-6 nm broad lamellae forming a broad-narrow repeating unit which justifies the presence of the ~ 11 nm broad-narrow pattern visualized in the asymmetry (splayed) bilayer model. In this model is not clarified in which conformations the CERs chain are present. The inner liquid like layer of the 5-6.5 nm broad SPP can be used by the lipophilic molecules to penetrate the SC due to lateral diffusion.

1.3 Barrier function and permeation routes

1.3.1 Penetration routes

The SC constitutes only a small portion of the entire skin composition and yet is the main tissue regulating its barrier properties. Although the SC possesses this protection role, dermal and as well trans-dermal drug delivery has been extensively investigated with the objective to deliver at a constant rate drugs into the systemic circulation. The theoretical advantages of using the skin as administration route are multiple: avoidance of first hepatic passage effect, painless administration, high compliance, readily accessible surface area. Hair follicles, sweat and sebaceous glands of the skin can be used for the absorption of hydrophilic and high molecular weight molecules and can retain these molecules (reservoir effect) up to 10 days [66], however, since they occupy less than 0.1 % of the skin surface, the delivery is not sustained over time. These characteristics and the fact that the SC is a natural barrier against the permeation of xenobiotics, make the transdermal drug delivery extremely complicated.

The pathways across which metabolites can diffuse intact SC are an intercellular and an intracellular route (Figure 8). In both cases, the permeant must diffuse through the intercellular lipid matrix [67]. In the first route, the metabolites must cross only the hydrophobic LM, while in the second one the metabolites diffuse also via the corneocytes. In general, molecules, which diffuse more easily through the LM, have specific physical-chemical properties such as low molecular weight and high hydrophobicity. Molecules with high molecular weight and/or hydrophilic properties cannot diffuse via any of these routes [68,69].

1.3.2 Penetration enhancers

In order to facilitate transdermal drug delivery, different strategies based on physical and/or chemical methods can be applied. Within the physical methods, different technologies such as microneedles, electroporation, iontophoresis and thermal poration can be used. The main advantage of these methods is an increased transport of active metabolites through the skin coupled with a sustained delivery over time, however, each presents individual disadvantages that will not be here discussed, for detailed studies refer to [68,70,71].

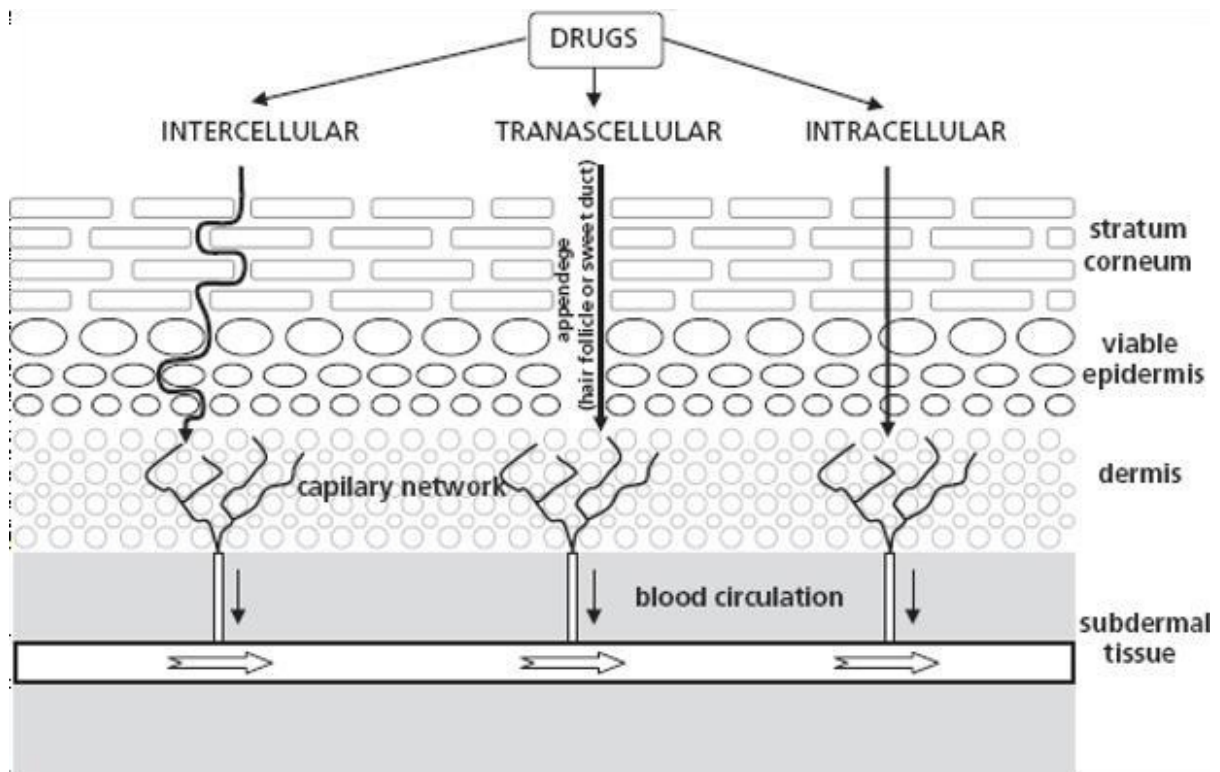


Figure 8. Penetration pathways of drugs through the SC, adapted from [72].

In this work, we are interested in chemical penetration enhancers (PE). Chemical enhancing methods are based on the use of different compounds which have the role to facilitate the permeation of metabolites through the intercellular LM allowing to reach deep skin layers. The rational selection of chemical enhancer should be based on the presence of specific properties: non-toxic, non-irritating, work rapidly, activity and duration should be both predictable and reproducible, should have no pharmacological activity within the body and should work unidirectional [73]. The mechanisms of action by which PEs act are very complex and are different depending on the class used. They can exert their influence on the SC by several manners, by extracting lipids from the skin, creating defects which work as diffusion pathways, by increased drug solubility in the skin, disruption of the highly ordered lipid matrix causing the fluidization of the lipids or disruption of the skin water structure [73]. Different molecules can be used as PEs, for instance water can be used as PE. By occluding the skin and avoiding transepidermal water loss, the water amount in the SC is increased enhancing the permeation of hydrophilic drugs. Skin occlusion demonstrated to be highly effective, nevertheless, it presents high risk in causing skin irritation and/or local infections [74].

Classical PEs are surfactants. Surfactants are amphiphilic molecules that can be classified according to the nature of the head group as cationic, anionic, non-ionic, and zwitterionic. In general, charged surfactants have a stronger effect on enhancing the permeation of drugs in comparison to zwitterionic and non-ionic ones [75], however, charged surfactants also present higher potential of causing skin irritation [76]. Most studies evaluating enhancement activity

have focused on the use of anionic and non-ionic surfactants (NIS). Anionic materials cause the uncoiling of keratin filaments separating the protein matrix and allowing a higher exposition to water in the skin [77]. However, they tend to permeate relatively poorly through the SC, but permeation increases with application time [73]. NIS are promising chemical enhancers thanks to their relatively low skin toxicity. Different studies showed that their mechanism of action can consist in a fluidizing and extracting effect on SC lipids, and/or by interacting and binding keratin filaments causing the disruption of corneocytes [78,79]. Nevertheless, these types of chemical enhancers don't find extensive use in pharmaceutical technology and currently are mainly used in cosmetic technology for their solubilisation properties.

1.4 SC barrier disruption and repair strategies

Another important research topic in the skin field regards the restoration of the SC barrier after being damaged by external and/or internal factors. Periodical exposure to external factors such as cleansing and sanitation products, environmental pollutants and some pharmaceutical ingredients may affect negatively the composition and organization of SC lipids [48]. The degree of barrier disruption is dependent on the nature of the chemical and on the time of exposure. Some of these chemicals may act as a contact allergen causing allergic reaction with development of dermatitis [80].

An alteration of the natural composition of SC lipids can occur also from internal factors. Genetic predisposition, mental state and age can be key factors that affect SC composition [48]. The pathogenesis of different skin diseases derives from the up/down regulation of specific enzymes that have fundamental roles in the synthesis of SC lipids. The depletion and/or alteration of lipid composition can cause skin dryness and barrier disruption. As result of this process TEWL is increased and different xenobiotics can more easily permeate causing inflammations [81–83].

Two of the most common skin diseases are atopic dermatitis (AD) and psoriasis [34,84,85]. AD is a chronic inflammatory disease associated with a modified composition of CERs in particular of CER[NP] and CER[EOS]. Their decreased levels were associated with high expression of sphingomyelin/glucosylceramide deacylase enzymes which cleave the N-acyl linkage of both sphingomyelin and of glucosylceramides destroying ceramides and causing barrier abnormalities [84].

Psoriasis is a systemic chronic inflammatory disease with impaired skin function. Similarly to AD, the CERs profile in psoriatic skin is altered. Not everything is yet understood about the pathophysiology of psoriasis although the impaired barrier function could also be related to the abnormal expression of enzymes involved in the synthesis and degradation of CERs.

The clinical strategies to treat diseased skin depend on the severity and on the pathophysiology of the disease. The basic management for mild disrupted skin is by topically

treating it with anti-inflammatory drugs, such as corticosteroids, in order to reduce irritation and local inflammations [86,87]. The long-term administration of corticosteroids can be associated with a variety of side effects including high blood pressure, headache and muscle weakness. An alternative to conventional treatments in light and mild skin conditions involves supplying the damaged skin with CERs based formulation. Studies have shown that the application of formulations containing SC lipids in the proper ratio facilitates the process of barrier recovery reducing the TEWL, enhancing skin hydration, decreasing bacterial colonization and improving skin barrier function reducing the need for corticosteroids use [88]. Traditional formulations as ointments or creams suffer of disadvantages connected to poor adsorption and patient's discomfort due to greasiness and stickiness of the product. On the other hand, new formulations based on mimicking the SC structure appear to be more effective. *In-vitro* studies with damaged skin models showed that the application of formulations based on SC lipids vesicle was able to reduce the permeation of indomethacin [89] proving the potential of the application of SC lipids based formulation as skin repairing agents.

1.5 Motivation and scope of this work

In scientific literature every year are published hundreds of publications regarding the effective use of pharmaceutical formulation for restoring the skin barrier property and as well to show the effective penetration of drugs through the SC, however, very few of these works showed the mode of action by which these formulations acted their specific mechanism. Objective of this work was to create and develop a simple and reliable SC monolayer model system and to study on it the mode of action by which pharmaceutical excipients and formulations affects its lipid organization.

The quaternary SC model was originally conceived by Schmitt [90] and here was further characterized via mono- and multi- layer systems in order to study the lateral (in-plane) and lamellar (long range order) organization of the lipids. The composition of the model was based on a 0.66:0.33:0.7:1 mixture of CER[NP]:D-CER[AP]:Chol:LA with CERs presenting a C24 fatty acid chain and C18 sphingosine moiety. In parallel to the characterization of this model, CER[AP] diastereomers were characterized in detail via X-ray scattering based techniques and FTIR. In detail, a study based on chirality and chain symmetry was performed in order to understand the biological relevance of the natural D(2R)-CER[AP] over the synthetically available L(2S)-form.

The SC model once it was characterized was used for investigating the impact of different pharmaceutical excipients and/or formulations on the organization of the lipids. PEs monomers and micelles have been studied at the liquid-monolayer interface in order to observe the mode of action by which these enact their disordering and fluidisation effect on skin lipids. On the other hand, SC lipid based liposomes i.e. cerosomes, known to act as skin barrier repairing

agents, have been as well studied in order to define the mode of action by which these enact their skin repairing effect. The composition of the cerosome was based on the one of SC monolayer, 0.66:0.33:0.7:1 CER[NP]:D-CER[AP]:Chol:SA with the CERs with symmetric C18 chains. In one formulation, PLs have been added as stabilizers in order to extend long term stability and to reduce the pH of the formulation.

Simple SC models based on Langmuir monolayers were principally investigated. X-ray scattering based techniques, Infrared Reflection-Absorption Spectroscopy (IRRAS), epifluorescence, atomic force microscopy (AFM) and quartz crystal microbalance with dissipation (QCM-D) were used on the monolayers to achieve a detailed study of the model. For the characterization of multilayer systems, Small- and Wide- angle X-ray Scattering (SAXS/WAXS), and Infrared (IR) spectroscopy have been deployed. Finally, the characterization of liposomal formulation has been achieved via Dynamic light scattering (DLS), Z-potential and Transmission Electron Microscopy (TEM).

2. Methods and employed basic principles

2.1 Langmuir monolayers [91]

Langmuir monolayers are models used to study the physical-chemical properties of amphiphiles at the air-water interface. These are versatile systems, different parameters can be controlled simultaneously (ionic strength of water subphase, controlled pH, controlled temperature) and many techniques can be coupled for obtaining information regarding the structure and morphology of the monolayer. Molecules that can be studied via Langmuir monolayers need to be amphiphilic (i.e. lipids), insoluble in water and able to order at the air-water interface. Thanks to the presence of a Whilhelmy plate connected to a sensitive electronic balance and the presence of two lateral barriers, a surface pressure (π) against the area per molecule (A) plot is registered (Figure 9). This plot is also called isotherm since the measurement is performed at constant temperature.

The water at a defined temperature presents a defined surface tension (γ) that changes when an amphiphile is present at the air-water interface. The variation of surface tension is defined as surface pressure (π) and is described as:

Equation 1: $\pi = \gamma_{water} - \gamma_{monolayer}$

The formation of a monolayer at the air-water interface leads to a decrease of the water surface tension (γ_{water}), therefore, an increase in π .

Through an isotherm the phase transitions of a certain compound can be studied. As described in figure 9b, at larger areas per molecule an amphiphile is found in its gas phase (G) where each molecule can freely move at the surface causing no detectable variation of π . Once the barriers start to compress the film, the area per molecule will be reduced and neighbor molecules will start to interact. Here the film passes from a G to a liquid-expanded (LE) phase. The molecules have now less liberty of movement but the chains are still in a disordered or *gauche* conformation. Upon further compression, the amphiphile transits from the LE to the liquid-condensed phase (LC) with molecules much closer together, less liberty of movement and with ordered alkyl chains. At this point, keeping compressing the monolayer it will be reached a point in which molecules cannot be further compressed and as direct consequence a drop in π can be observed representative of the collapse of the monolayer. Finally, phase transitions can be of two types, first-order phase transition characterized by a plateau with constant π , and second-order phase transition characterized by a kink in the isotherms.

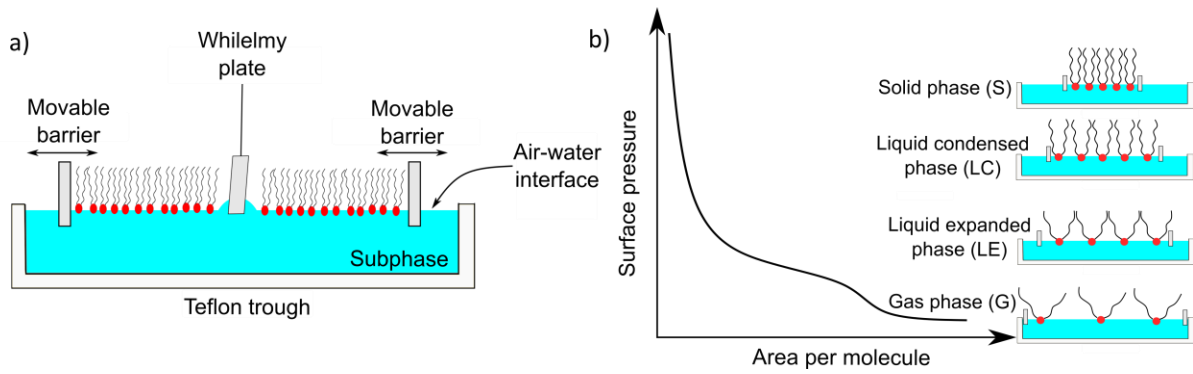


Figure 9. a) Schematic representation of a Langmuir monolayer setup and b) generalized isotherm of a monolayer. The phase states are indicated along the isotherm. Schematic molecular arrangements are shown for gaseous, liquid-expanded, liquid condensed and solid phases.

Another property that can be measured via the isotherm is the so called surface compressional modulus K calculated as:

$$\text{Equation 2 : } K = \frac{1}{c} = -A \left(\frac{d\pi}{dA} \right)_T$$

where C is the compressibility of the monolayer, A is the molecular area, and $\Delta\pi/\Delta A$ is the slope of the isotherm at a defined π . The surface compressional modulus is used to understand at a determined surface pressure how stiff and compressed a monolayer is, the compressibility is different in the sequence $G > LE > LC > S$ [92].

2.2 IR spectroscopy

IR spectroscopy is a well-established analytical field where the interactions of molecule vibrations with electromagnetic vibrations are studied. The wavelength associated with IR ranges from 14000 cm^{-1} to 10 cm^{-1} and the region used to study molecules vibration is comprehended between $4000\text{-}400 \text{ cm}^{-1}$, also defined as mid-IR. The molecule vibration absorbs part of the radiation which is then directed to a detector allowing to analyse an IR-profile. Each wavenumber is characteristic of specific groups in a molecule providing structural and/or interactions information. Not all the molecules are able to absorb such wave, prerequisite is that the dipole momentum of the bond changes during this interaction. IR-spectroscopy can be applied in different type of systems, in particular here IR-based methods were used to characterize lipid monolayers and dry lipid powders.

2.2.1 Fourier-Transform infrared spectroscopy (FTIR) [93]

FTIR is a technique based on IR spectroscopy which allows to get insights on structural properties of solid, liquid or gas. The three major parts are the source, the interferometer and

the detector. The most important part is the interferometer which consists of a beamsplitter which splits the light into two paths with half of the light going to the stationary mirror and the other half going to a moving mirror (Figure 10a). The beams from the moving and stationary mirror are then recombined at the beamsplitter and steered toward the sample. The beam hits then the sample and goes onto a detector where the signal is converted to an interpretable spectrum. The term Fourier-transform origins from the mathematical process necessary to convert the raw data in an easily interpretable spectrum. In this technique, instead of using a monochromatic beam, in a short time span consecutive beams containing light with different frequencies are shined at once on a sample and what is measured is how much of each the beam is absorbed. Afterwards, a computer takes the absorption data and works backwards to infer what the absorption is at each recorded wavelength.

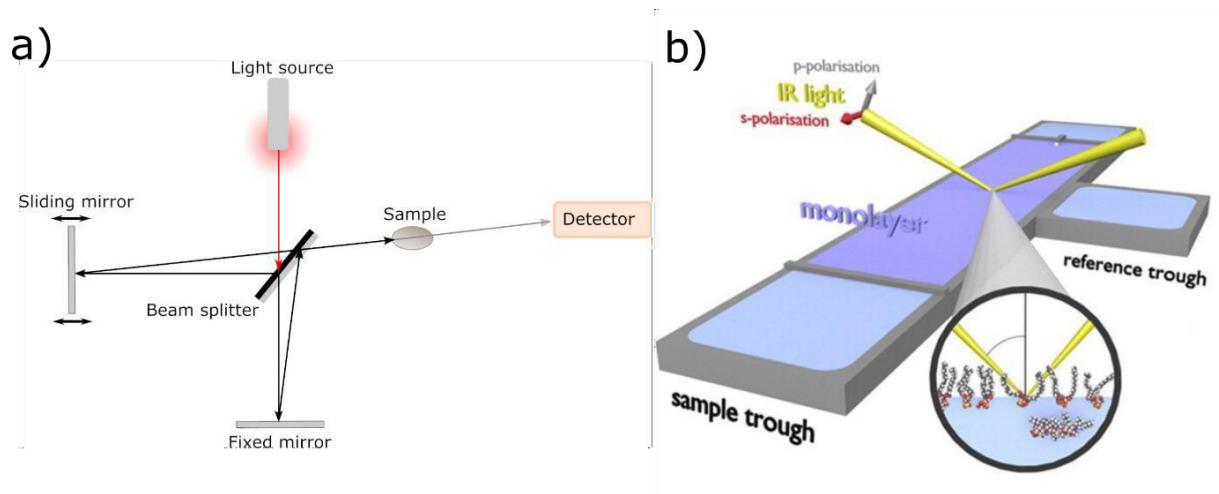


Figure 10. a) Schematic representation of FTIR instrumentation and b) schematic representation of IRRAS spectroscopy taken from [94].

2.2.2 IRRAS [95]

IRRAS is a technique that uses IR light to determine the conformation and orientation of amphiphile chains in a monolayer and to study head group interactions via changes in vibrational frequencies.

In IRRAS experiments the IR light can present a parallel (p-polarization) or perpendicular (s-polarization) polarization to the plane of incidence and is focused on the surface at a defined angle of incidence. The reflected light from the monolayer surface is then detected at the same angle of incidence. The polarization of the light and the angle of incidence are controlled manually via the computer software. The obtained signal represents the sum of all existing molecules with enriched concentration at the interface.

In the setup introduced by Mendelsohn et al. [96], in parallel to the trough containing the monolayer there is a second smaller trough where only the subphase is measured (Figure

10b). This setup allows to subtract the spectral interference from the rotation-vibration bands of the water vapor ($1400\text{-}1800\text{ cm}^{-1}$). The spectrum recorded at the surface reference (R_0) is subtracted from the sample spectrum (R) allowing to eliminate signals coming from the atmosphere and plotted as reflectance-absorbance (RA) vs. wavenumber. The IRRRA spectrum is interpreted by evaluating the intensities generated by molecular vibrations at different wavenumbers.

2.3 X-ray scattering methods [97,98]

X-rays are electromagnetic radiations that can interact with matter giving rise to a multitude of phenomena. Like all electromagnetic radiations, X-rays can be considered as waves or photons. The photon energy is given by:

Equation 3: $E = h\nu$

where h is the Planck's constant and ν is the frequency. Conventionally X-rays are obtained by an electron bombardment of a water-cooled anode that depending on the material, can originate X-rays with different wavelength. For instance, the emission of X-rays from Cu anodes shows a wavelength of 0.1542 nm . In a Synchrotron, charged particles (electrons or positrons) are accelerated to extremely high energy and then make them change direction periodically. The electrons for the storage ring are produced in an electron gun (Linac). These electrons are packed in "bunches" and injected into the synchrotron. Kept by bending magnets, the charged particles travel around the ring, and in the process produce X-rays. The synchrotron light covers a wide and continuous spectrum, from microwaves to hard X-rays, $0.3\text{ nm} > \lambda > 0.02\text{ nm}$. The characteristics of a modern synchrotron radiation are: collimated radiation, high intensity, polarization, continuous spectrum and beams size from $1\text{ }\mu\text{m}$ to 1 nm .

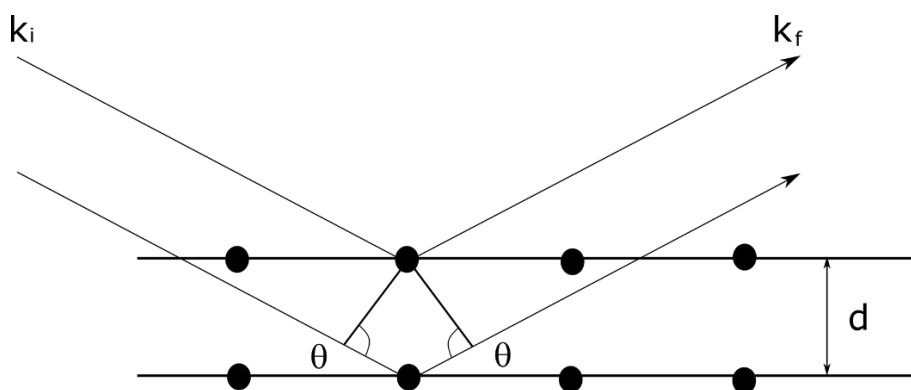


Figure 11. Representation of Bragg's law by an optical analogy to crystallographic planes reflecting X-rays.

Thanks to its small wavelength, X-rays interact with matter through the electrons contained in the atoms, and the scattered radiation allows to analyse the structure of matter. This phenomenon is described as X-ray diffraction that express the fundamental interaction between X-rays and crystals which is based on the Bragg law. The Bragg law or Bragg diffraction is described by:

Equation 4: $n\lambda = 2d \sin \theta$

where n (an integer) is the order of reflection, λ is the wavelength, d is the interplanar spacing and θ is the angle of incidence. It occurs when a radiation is scattered in a mirror-like reflection by a symmetrical arrangement of the system and it undergoes a constructive interference. In the next section, the X-ray methods used for this work are described more in detail.

2.3.1 Grazing incidence X-ray scattering (GIXD) [99]

GIXD is an X-ray scattering technique that allows the precise characterization of molecules lateral structure in condensed monolayers at the soft air-water interface. To obtain a good enough signal to noise ratio, X-rays from a synchrotron source are needed. The method is based on the phenomenon of total reflection. A monochromatic X-ray beam is directed onto the surface of the monolayer at an angle of incidence smaller than the critical angle for total reflection from the medium with lower refractive index. Such angle is for the used X-ray energy $\sim 0.07^\circ$. The incidence angle used in such experiments is $\sim 80\%$ to reduce the penetration depth and therefore the scattering from the background. Since the reflectivity index of matter for high energy X-rays is slightly less than 1, the beam undergoes total reflection and only an evanescent wave travels along the surface of the subphase. The illuminated area has to be big enough to allow enough material in the monolayer to scatter the X-rays and usually is in the order 100 mm^2 .

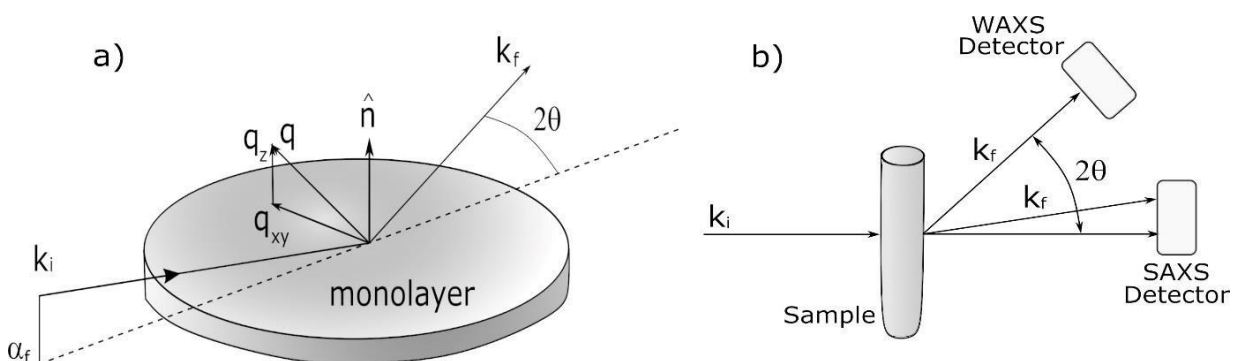


Figure 12. a) Geometry of GIXD, k_i is the incident beam with α_f the incidence angle, k_f is the reflected beam and 2θ is the horizontal scattering angle, b) schematic representation of a SAXS/WAXS setup, the incident beam k_i hits the sample in the sample chamber and the diffracted beam k_f is directed to a detector and depending the scattering angle SAXS or WAXS profile can be measured.

In figure 12a the geometry of the X-ray diffraction under the grazing incidence angle is shown. In GIXD experiment monolayers can be considered as a so called '2D powder' fulfilling the Bragg condition. The diffracted intensity is often monitored by a linear position-sensitive detector from which a horizontal in-plane component q_{xy} (Bragg peak) and vertical out-of-plane component q_z (Bragg rod) of the scattering vector q can be simultaneously measured using the following equations:

$$\text{Equation 5: } q_{xy} \cong \frac{4\pi}{\lambda} \times \sin \frac{2\theta_{xy}}{2}$$

$$\text{Equation 6: } q_z \cong \frac{2\pi}{\lambda} \times \sin \alpha$$

Analyzing the q_{xy} and the q_z positions of the peaks from a certain monolayer lattice allows to obtain important structural information of the amphiphile such as the tilt angle (t), the cross-sectional area (A_0), the area per molecule (A), and the thickness of the monolayer (L_z). In order to fit the peak center of q_{xy} component the Lorentzian function is used while for the q_z component a Gaussian function. From the full-width-half-maximum (fwhm) obtained from the fitting of the Bragg rod is possible to determine the thickness L_z of the diffracting layer by the Scherrer formula:

$$\text{Equation 7: } L_z = 0.9 \left(\frac{2\pi}{fwhm(q_z)} \right)$$

On the other hand, the fwhm obtained from the fitting of the Bragg peak can be used to determine the correlation length ξ , i.e., which gives information about the homogeneity of the monolayer using:

$$\text{Equation 8: } L_{xy} = 0.9 \left(\frac{2\pi}{fwhm(q_{xy})} \right)$$

In order to take into account, the in-plane divergence of the X-ray beam the fwhm of the Lorentian peaks were corrected as follows:

$$\text{Equation 9: } fwhm_{xy}^{cor} = \sqrt{(fwhm_{xy}^{meas})^2 - (fwhm_{xy}^{res})^2}$$

where $fwhm_{xy}^{res} = 0.012 \text{ \AA}^{-1}$

In a GIXD experiments with monolayers, usually the hydrophobic tails are the elements that are creating the periodic structures which give rise to the observed diffraction peaks which

correspond to the distances between neighbouring chains in a monolayer. Depending on the number of Bragg peaks and the relative position of the Bragg rod, different geometries can be observed.

2.3.2 Total reflectance X-ray fluorescence (TRXF) [100]

TRXF is an analytical method for the quantification of ions at the air-water interface. The technique is based on the principal that synchrotron monochromatic X-ray beams at the air/liquid surface are energetic enough to expel tightly held electrons from the inner orbitals of the atom. The removal of an electron in this way makes the electronic structure of the atom unstable, and electrons from higher orbitals jump into the lower orbital to fill the hole. Therefore, energy is released in the form of a photon, the energy of which is equal to the energy difference of the two orbitals involved. This energy depends on the type of element to be detected. Low energy X-rays are absorbed more than high energy photons, however, with low energy X-rays certain elements with low atomic weight cannot be detected. In a TRXF experiments in the simplest case the elements to consider are a charged Langmuir monolayer which is represented by two sublayers, an organic layer with thickness L_1 (the lipid molecules) and the ion-rich layer with thickness L_2 (containing the counter-ions from the subphase). The fluorescence intensity I^f of an element i with a concentration profile $c_i(z)$ can be written as:

$$\text{Equation 10: } I_i^f = b_i \int I_{ex,i}(z) c_i(z) dz$$

where $I_{ex}(z)$ is the exciting X-ray intensity at a distance z from the surface and b_i is a constant. The concentration profile $c_i(z)$ can be evaluated theoretically.

2.3.3 Small- and Wide- angle X-ray scattering (SAXS/WAXS) [101,102]

SAXS and WAXS are complementary scattering techniques that give information regarding the organization of lipids in bulk in particular about the lateral structure of lipids (WAXS) and the long range order of lipids (SAXS). The X-ray beam hits the sample and the diffracted beam is measured by a detector as a function of scattering angle relative to the incident beam (Figure 12b). The scattered intensity is expressed in terms of scattering vector q which represents the modulus of the change in momentum of the scattered radiation and is calculated by:

$$\text{Equation 11: } q = \frac{4\pi}{\lambda} \sin \theta$$

where λ is the wavelength and θ is the scattering angle. The representation of the X-ray scattering vector are peaks. The method is based on the Bragg law which defines the

constructive X-ray waves in the presence of periodic structures scattered from lattice planes separated by an interplanar distance d . The d can be calculated using the Bragg law (Equation 4).

A SAXS profile allows the determination of the symmetry and long range order of a lipid phase. Different SAXS profile patterns can be observed. Regarding lipids, the most common one is the lamellar (L) profile where each lipid bilayer is divided by an adjacent water layer and the SAXS peaks are characterized by an equidistant pattern (1: 2: 3:...). Nevertheless, other types of organizations can be observed like the hexagonal and inverted hexagonal with a pattern expected of 1: $\sqrt{3}$: $\sqrt{4}$: ... Many other types of crystalline phases can be observed.

In order to calculate the repeating distance d (lipid bilayer with adjacent water layer) of each lamellar phase, the Bragg law can be applied using the following equation:

Equation 12:
$$d = \frac{2\pi}{q} = \frac{1}{s}$$

with q being the scattering vector connected with the scattering angle 2θ and s is the reciprocal spacing.

The WAXS pattern complements the SAXS data since it gives information regarding the lateral organization of lipid bilayers (short-range ordering of the lipids). By analyzing the position of each peak, similarly to GIXD in monolayers, the molecular packing of the lipids can be deduced, however, information regarding the out of plane component, therefore the tilt of the chains, cannot be obtained.

2.4 Microscopy techniques

2.4.1 Epifluorescence microscopy [103]

Epifluorescence microscopy is an optical technique that uses fluorescence to generate an image. This method coupled with Langmuir monolayers allows to study in detail the structure and the domains shape formed in a monolayer at the air-water interface (Figure 13). To generate the fluorescent signal, a fluorescent dye is used that is incorporated in the monolayer at low concentration (0.05 %mol) to avoid an influence of the dye on the phase behavior of the monolayer itself. The monolayer is illuminated with a light of specific wavelength which is absorbed by a fluorophore which emits light of longer wavelengths. The emitted wave is much weaker than the illumination light and the use of spectral emission filter are necessary to match the spectral excitation and emission of the used fluorophore. The microscope and the trough are decoupled allowing to mount the trough on a xy translation stage and investigate the entire monolayer.

The micrographs consist of an image where dark and bright areas can be visualized, the darker areas (domains) represent regions with no or few dye molecule while the bright regions consist of areas with large amount of dye molecules. This technique along an isotherm allows to study the formation and modification of monolayer domains along the different phase transitions.

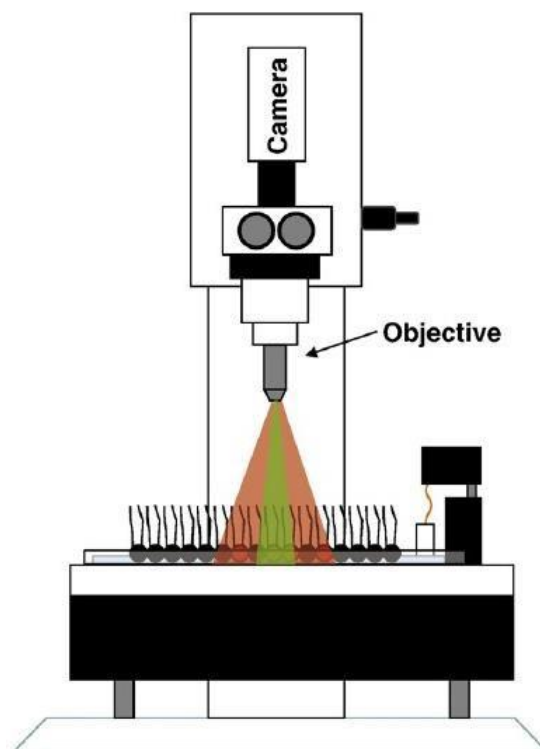


Figure 13. Diagram of experimental setup for fluorescence microscopy with upright geometry with monolayer illuminated from above, taken from [103].

2.4.2 Transmission electron microscopy (TEM) [104]

TEM is a microscopy technique in which a beam of electrons is transmitted through a specimen to form an image. TEM works with the same principal of light microscopy but since electrons have much lower wavelengths, the optimal resolution for TEM images is many orders better than light microscopy.

The electrons are emitted by an electron gun and focused into a small, thin, coherent beam by the use of condenser lens (Figure 14) while vacuum system is used to prevent the interaction of the electron beam with air particles. The beam pass through the specimen and the transmitted electrons are focused via objective lens into a phosphor screen which is going to create an image, also called a micrograph, processed by the coupled camera device CCD. The image created is black and white, the darker areas of the image represent those areas of the sample that fewer electrons are transmitted (higher absorbance from the sample) while the lighter areas of the image represent those areas of the sample that more electrons were transmitted.

A sample prepared for TEM experiment must be thin enough to transmit sufficient electrons to form an image, the specimen should be less than 100 nm thick. Therefore, specific sample preparation is an important aspect of the TEM analysis.

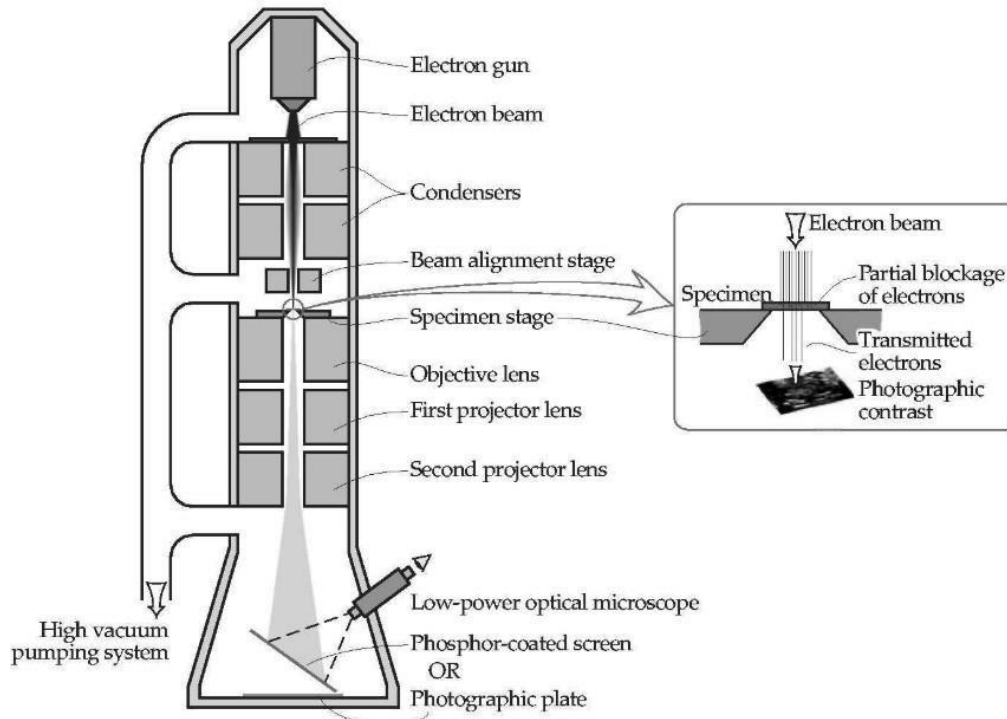


Figure 14. Schematic representation of a transmission electron microscope adapted from [105].

2.5 Vesicle characterization

2.5.1 Dynamic light scattering (DLS) [106]

DLS also known as photon correlation spectroscopy, is a technique that allows the measurement of particle sizes and distribution of different colloidal systems. One of the advantages of the technique is that compared to other sizing techniques such as electron microscopy or size exclusion microscopy, there is no physical disturbance to the system. A laser beam passing through the sample should appear as a bright line which is well defined throughout the entire scattering volume. The scattered light signal is collected with one or two detectors, either at 90° (right angle) or 173° (back angle) (Figure 15). The inclusion of both detectors allows more flexibility in choosing measurement conditions. The measurement is based on the Brownian motion of macromolecules and colloidal particles. Such motion depends on the particle size, the medium viscosity and the temperature. One important assumption is that the vesicles used in this experiment, are spherical particles with a small diameter compared to the molecular dimensions. If it is so, is possible to apply the Stokes-Einstein relation and have a formula that easily gives the diffusion coefficient (D):

Equation 13:
$$D = \frac{K_b T}{6\pi\eta t}$$

where K_b is the Boltzmann constant, T is the temperature in Kelvin, η is the viscosity of the liquid used and t the time. The intensity of light scattering depends on the dimension of each particle. Bigger particles will have a smaller diffusion function than small particles and the variation of scattering intensity will also occur more slowly. The analysis of scattering is carried out by a correlator. This is done through a spectrum analyzer that obtains a power spectrum (P_w) of a signal by using the Lorentzian function:

Equation 14:
$$P(\omega) = \frac{2Dq^2/\pi}{\omega^2 + (2Dq^2)}$$

where q is the scattering wave vector, ω is the frequency shift. The quality of the measurement depends on the power of the laser used and on the aqueous medium which should be free of any dust contaminant. Particles can be dispersed in a variety of liquids. Only liquid refractive index and viscosity are needed to be known for interpreting the measurement result.

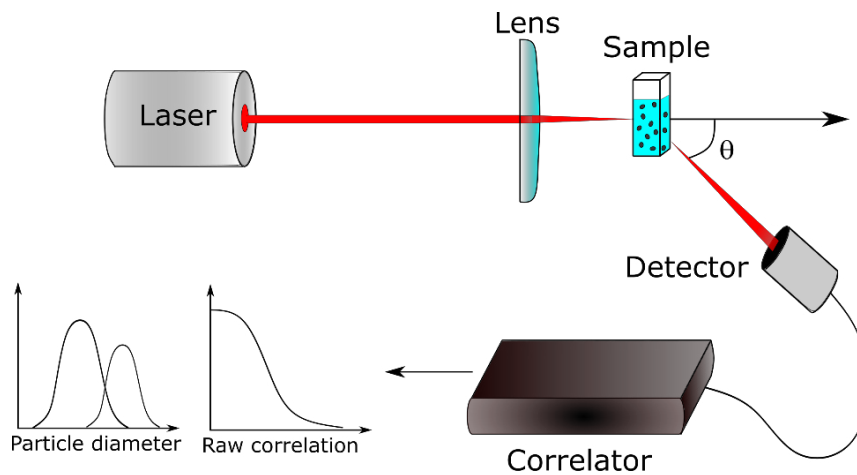


Figure 15. Schematic representation of DLS apparatus.

2.5.2 Z-potential [107]

The term zeta potential refers to the charge of particles at the liquid/surface interface in a specific liquid medium. Every particle in an ionic solution, will have a layer of ions of opposite charge strongly bounded to its surface called the Stern layer. A second diffuse outer layer is present with loosely associated ions. This second layer is balanced by random motion and electrostatic forces. The two layers together form the so called electrical double layer. The electrostatic potential of the slipping plane between the Stern and the diffuse layers is called zeta potential and it is related to the surface charge of the particle. During the measurement

an electrical field is applied across the solution facilitating an electrophoretic movement of the particles, this is measured by laser Doppler velocimetry. The electrophoretic mobility (U_e) of the particles is calculated applying:

Equation 15:
$$U_e = \frac{V}{E}$$

where V is the particle velocity ($\mu\text{m/s}$) and E is the electric field strength (Volt/cm). The Z-potential is then calculated from the obtained electrophoretic mobility by the Henry's equation:

Equation 16:
$$U_e = \frac{2\epsilon z f(\kappa a)}{3\eta}$$

where ϵ is the dielectric constant, η is the absolute zero-shear viscosity of the medium, $f(\kappa a)$ is the Henry function, and κa is a measure of the ratio of the particle. Particles with a zeta potential between -10 and $+10$ mV are considered approximately neutral and unstable, while nanoparticles with zeta potentials greater than $+30$ mV or lower than -30 mV are considered strongly cationic or anionic and thus form more stable dispersions.

2.6 Interaction studies

2.6.1 Subphase injection

Langmuir monolayers at the air-water interface allow to study the properties of an amphiphilic monolayer and as well the interaction between the monolayer and a certain surface active system. In the subphase injection method, a surface-active compound is injected underneath a pre-formed monolayer, and the variation in surface pressure ($\Delta\Pi$) against time (t) is measured allowing to analyze the kinetic of interaction and the affinity between the two systems.

In our setup, a modified Langmuir trough consisting of a PFA (perfluorether) petri dish and a Wilhelmy balance connected to a sensitive electronic balance is used. The petri dish had a diameter of 5.5 cm and a depth of 0.5 cm with an area of 23.8 cm². In order to inject the surface active system underneath the pre-formed monolayer, a syringe with the needle inserted vertically through the monolayer was used to minimize membrane perturbations (Figure 16).

2.6.2 AFM [108]

Atomic force microscopy (AFM) is a powerful and multifunctional imaging method that allows to characterize extremely tiny samples such as individual molecules and as well more complex ones such as living cells. The technique counters a surface by controlling a conglomerate of

forces acting between a probe mounted on a cantilever and the surface, these forces are then measured as the deflection of the lever knowing the stiffness of the cantilever. For measuring the force generated, the Hooke's law is used:

Equation 17: $F = -kz$

where F is the force, k is the stiffness of the lever and z is the distance the lever is bent. Different operating modes can be used such as the classical contact mode or dynamic mode, which, however, present limitation connected to the possibility to directly damage the sample and/or not being able to control vertical forces of soft and sticky samples.

To overcome such problems, in this work the quantitative image mode was used which is a curve based imaging mode that allows to avoid sample damaging by reaching peak forces down to 10 pN.

2.6.3 QCM-D

Quartz crystal microbalance with dissipation monitoring is a highly versatile and sensible technique to study processes occurring at the surfaces or within thin films. QCM-D can be used to monitor processes in real time by measuring changes in frequency and dissipation of the system adsorbed on a piezoelectric quartz sensor. By applying an alternated electric field on a quartz sensor mechanical oscillation of characteristic frequency are observed. When a change of mass occurs at the surface of the system, a frequency shift (ΔF) is measured. Simultaneously, the viscoelastic properties of the film adsorbed to the quartz sensor can be measured by recording changes in the dissipation energy (D). By using the Sauerbrey equation it is possible to calculate the change in mass (Δm) using the measured frequency shift:

Equation 18: $\Delta m = - \frac{\Delta F}{n} C$

where C is the mass sensitivity constant at 5 MHz for a quartz sensor of area $A = 0.75 \text{ cm}^2$ and n is the number of the harmonics.

3. Materials

| Material | Source | Purity (%) |
|--|----------------------------|------------|
| Solvent | | |
| Chloroform | VWR International GmbH | ≥ 99.5 |
| Methanol | VWR International GmbH | ≥ 99.9 |
| Water (resistivity 18 MΩ·cm at 25°C) | Synergy ® Millipore device | - |
| Salts | | |
| NaCl | VWR International | ≥ 99.9 |
| ZnCl | DON'T KNOW | ≥ 99.9 |
| EDTA | BASF | ≥ 99.5 |
| PBS | Sigma Aldrich GmbH | |
| TRIS | VWR International | ≥ 99.5 |
| Lipids | | |
| [NP] C18; N-(Stearoyl)-phytosphingosine | Synthesis ¹ | ≥ 95 |
| [NP] C24; N-(Tetracosanoyl)-phytosphingosine | Synthesis ¹ | ≥ 95 |
| D-[AP]C18; N-(D-α-Hydroxysteroyl)-phytosphingosine | Synthesis ¹ | ≥ 95 |
| D-[AP]C24; N-(D-α-Hydroxytetracosanoyl)-phytosphingosine | Synthesis ² | ≥ 95 |
| L-[AP]C18; N-(D-α-Hydroxysteroyl)-phytosphingosine | Synthesis ¹ | ≥ 95 |
| L-[AP]C24; N-(D-α-Hydroxytetracosanoyl)-phytosphingosine | Synthesis ² | ≥ 95 |
| Cholesterol | Sigma Aldrich GmbH | ≥ 95 |
| Stearic Acid | Sigma Aldrich GmbH | ≥ 99.5 |
| Lignoceric Acid | Sigma Aldrich GmbH | ≥ 99.9 |
| P100-3 | Lipoid GmbH | - |
| S75-3 | Lipoid GmbH | - |
| H100 | Lipoid GmbH | - |
| H90 | Lipoid GmbH | - |
| H80 | Lipoid GmbH | - |
| Dipalmitoylphosphatidylcholine | Lipoid GmbH | ≥ 99.9 |
| Rhodamine–DHPE | Sigma Aldrich GmbH | ≥ 99 |
| Surfactants | | |

| | |
|------------------------|--------------------------------|
| Polysorbate 80 | Sigma Aldrich GmbH |
| Sucrose Laurate | Glycon |
| Other | |
| dichlorodimethylsilane | Sigma Aldrich GmbH ≥ 99.5 |

*1, gently provided by the group of Prof. Bodo Dobner from the department of Biochemical Pharmacy of the MLUHalle-Wittenberg which purified them from technical grade mixtures from EVONIK GmbH

*2, gently provided by the group of Dr. Lukas Opalka from the Department of Organic and Bioorganic Chemistry, Faculty of Pharmacy in Hradec Králové, Charles University which synthesized and purified them.

4. Cumulative part

The following section contains three publications which were published as research articles in international journals following the peer-review procedure. These articles constitute the basis of this work and summarize the experimental results. Each one represents a chapter of this work and the order in which they are presented is based on the temporal factor of acceptance. In publication I, a quaternary SC model was for the first time developed and used to investigate the effects of non-ionic surfactants (NIS) in order to analyse their potential use as penetration enhancers for dermal and transdermal drug delivery. The surfactants selected were polysorbate 80 (PL 80), a well-known and frequently used surfactant for cosmetic and pharmaceutical purposes, and sucrose monolaurate (SL) a relatively new surfactant mainly used in food technology. Main findings were that both surfactants were able to disorder the monolayer by fluidizing the lipids of the system.

In publication II, CER[AP] a fundamental CER class of the SC, was characterized by means of X-ray scattering and IR spectroscopy. CER[AP] in the skin is present in its D(2R)- form while synthetically the diastereomers mixture can be produced. Since in SC *in-vitro* model system CER[AP] is often used in its diastereomer mixture and not in its natural form, in this work we focused on the characterization of the single diastereomers and of the 1:1 mixture, both with symmetric (18:0, 18:0) and asymmetric (24:0, 18:0) chains. Main finding was that D-CER[AP] was able to create a strong intermolecular HbN while L-CER[AP] does not. Moreover, in the 1:1 mixture a complete immiscibility of the D-form was observed while the L-form in its lattice was able to accommodate some molecules of the D-form.

In publication III, SC liposomes i.e. cerosomes have been formulated, characterized and studied in contact with the SC monolayer. The cerosomes are known to be promising repairing agents for pathological skin diseases associated with SC barrier disruption. In this work, monolayers at the air-water interface and at the solid-liquid interface have been used to study the mode of action by which these cerosomes interact with the SC itself. Main finding is that a strong interaction between the two systems was observed due to the creation of HbN between the CERs headgroups, although both systems are negatively charged and should repel each other.

4.1 Itemization of own contribution

Table 1. Specification of the percentage of own contribution to the publications. The own contribution is made up as follows:

A: own contribution to the planning, the execution, the analysis of the experiments and the preparation of the corresponding illustration

B: own contribution to the preparation of the manuscript

| | |
|-----------------|--|
| Publication I | <p>Non-ionic surfactants as innovative skin penetration enhancers: insight in the mechanism of interaction with simple 2D stratum corneum model system</p> <p>Fabio Strati, Reinhard Neubert, Lukas Opalka, Andreas Kerth, Gerald Brezesinski</p> <p>Eur. J. Pharm. Sci, 157 (2021), 105620</p> <p>A:70 % B:80 %</p> |
| Publication II | <p>2D and 3D physical-chemical characterization of CER[AP]. A study of stereochemistry and chain symmetry</p> <p>Fabio Strati, Joana S.L. Oliveira, Tetiana Muhkina, Bodo Dobner, Reinhard H. H. Neubert, Gerald Brezesinski</p> <p>J. Phys. Chem, 125 (2021), 9960-9969</p> <p>A: 70 % B:70%</p> |
| Publication III | <p>Cerosomes as skin repairing agent: Mode of action studies with a model stratum corneum layer at liquid/air and liquid/solid interfaces</p> <p>Fabio Strati, Tetiana Muhkina, Reinhard H. H. Neubert, Lukas Opalka, Gerd Hause, Christian Schmelzer, Matthias Menzel, Gerald Brezesinski</p> <p>Bbadva, (2021), 100039</p> <p>A:70 % B:70 %</p> |

4.2 Publication I

Non-ionic surfactants as innovative skin penetration enhancers: insight in the mechanism of interaction with simple 2D stratum corneum model system

Link Publication:

<https://www.sciencedirect.com/science/article/abs/pii/S0928098720304085>

Cite: European Journal of Pharmaceutical Sciences, Volume 157, 2021, 105620

4.3 Publication II

2D and 3D physical-chemical characterization of CER[AP]. A study of stereochemistry and chain symmetry

Link Publication:

<https://pubs.acs.org/doi/full/10.1021/acs.jpcb.1c05572>

Link Supporting Information:

<https://pubs.acs.org/doi/10.1021/acs.jpcb.1c05572>

Cite: *The Journal of Physical Chemistry B*, 2021 125 (35), 9960-9969

4.4 Publication III

Cerosomes as skin repairing agent: Mode of action studies with a model stratum corneum layer at liquid/air and liquid/solid interfaces

Link Publication:

<https://www.sciencedirect.com/science/article/pii/S2667160321000387>

Cite: BBA Advances, Volume 2, 2022, 100039

5. General discussion and future perspectives

As reported by pubmed, in only the last 3 years more than 1500 scientific papers have been published concerning SC research showing the importance and popularity of the topic. This work gives a fundamental contribution to the SC research by elucidating the properties of CER[AP] diastereomers, by developing a reliable *in-vitro* SC model and by unveiling the mode of actions by which different excipients and formulations interact with the SC lipid matrix. For this purpose, highly sophisticated biophysical methods applied mainly on monolayer model systems have been deployed. In the next sections, the main findings of this work are discussed in the context of achieved advancements in skin research in comparison to other relevant works.

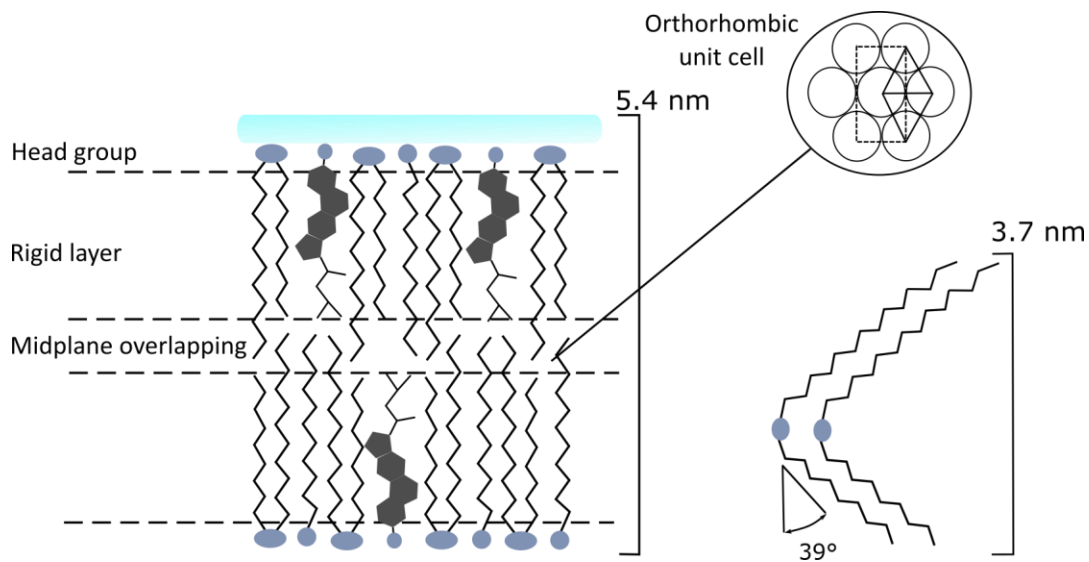


Figure 39. Left: structure of the proposed quaternary model bilayer with lipids arranging in an orthorhombic lattice, the CERs arranged in a hairpin configuration with chains overlapping in the midplane. Right: proposed arrangement of CER[NP] in a V-shape configuration with 39° chain tilt in accordance to Dahlen and Pascher [53].

5.1 Quaternary SC model characterization

First step of this work was the development of a SC lipid matrix model taking in consideration the need of a cheap and reproducible system, which uses a reduced number of lipid species and low amounts of raw material. In publication I, a quaternary SC model composed of CER[NP] (24:0, 18:0), D-CER[AP] (24:0, 18:0), Chol and LA (0.66:0:33:1:0.7 mole fractions) was for the first time studied via Langmuir monolayers. The use of CERs with C24 fatty acid moiety and C18 sphingosine moiety is important considering that most CERs in the LM presents asymmetric chains which are reported to overlap in the lamellar midplane [50]. CER[NP] and D-CER[AP] were selected since these are two of the most abundant CERs in

the skin (~22% and ~8.8% by weight) [20] thus can be expected to play substantial roles for the overall structural arrangement of the LM itself. FTIR studies of ternary SC mixtures based on CER[NP] and D/L-CER[AP] (18:0, 18:0) as model CERs [186] showed that these were able to form homogenous mixtures in comparison to models based on sphingosine which showed phase separation of the CER in their mixture, proving the suitability of phytosphingosines for our model.

Monolayer studies of our quaternary mixture indicated that the lipids organization and behavior closely resembled the native SC lipid matrix. Isotherm studies (publication I) evidenced the presence of a stiff and condensed monolayer (Figure 17) with lipids arranging in two distinct orthorhombic lattices as observed in GIXD experiments (Figure 33). One orthorhombic lattice (defined in publication III as phase 2) arranged in a structure which closely mimicked the organization of native SC while the second orthorhombic lattice (indicated as phase I in publication III) displayed the formation of a badly ordered monolayer filled with packing defects as indicated by the low value of the correlation length L_{xy} . A similar study performed via GIXD of a monolayer composed of a ternary mixture composed of D/L-CER[AP] (18:0, 18:0), SA and Chol, evidenced the formation of a monolayer organized in a hexagonal phase with high value of the correlation length L_{xy} indicating the presence of marginal defects in the monolayer [225] similarly to phase I.

Further indication of phase-separated domains came from AFM experiments of the SC monolayer transferred onto solid support (publication III). Results indicated that two domains with different heights were present (Figure 38). As in GIXD, one domain could be connected to the typical SC organization, which presented a height of 2.4 - 2.6 nm, the second domain with a height of 1.2 – 1.4 nm was of unclear origin since in similar AFM experiments with SC monolayers such heights were never reported.

In parallel to monolayers, dispersions in bulk of our quaternary SC model were analyzed by means of SAXS and WAXS (publication III, supporting information). SAXS results (Figure S7) evidenced the co-existence of two lamellar phases, one with a d-spacing of 54 Å and the second of 37 Å. In addition, phase separated Chol (d-spacing of 34 Å) was observed. The d-spacing of 54 Å featured the presence of CERs in a hairpin configuration with chains overlapped in the midplane and adjacent layers separated by a layer of water (Figure 39). The d-spacing of this lamellar phase was comparable to the SPP of native SC [44]. Similarly to AFM results, the origin of the lamellar phase with d-spacing of 37 Å was not easily predictable. Since this d-spacing was similar to the one of Chol, a phase mainly constituted of Chol mixed with a second lipid could be assumed, however, as proven by Ekelund et al. [226] Chol and LA are not able to mix leaving as option the mixing of Chol with one of the two CERs. SAXS and WAXS experiments of a 7:3 mixture of CER[NP] (24:0, 18:0) and Chol showed two phases with d-spacing of 37 Å and 34 Å (Figure A1a) suggesting the phase separation between the

two compounds. Nevertheless, this experiment clearly indicated the origin of the unknown lamellar phase, which was again confirmed by SAXS analysis of the single CER[NP] (24:0, 18:0) (Figure A1b) which reported a single lamellar phase with d-spacing of 37 Å. Such value is in agreement with that found by Dahlen and Pascher [53] who reported an X-ray powder diffraction (XRD) study of CER[NP] (24:0,18:0) with six polymorphic forms of CER[NP]. Five of these polymorphs arranged in a V-shape configuration and one in a hairpin configuration. A V-shape configuration with a small tilt (calculated to be 39°) and length of 37 Å was observed, thus confirming the composition of the second lamellar phase of our SC model in SAXS experiments. The phase separated CER[NP] in a V-shape could also justify the GIXD results regarding the observed phase I in publication III and therefore, justifying the presence of a monolayer with defected and poorly packed regions as indicated by the calculated correlation lengths. The GIXD profile of CER[NP] (24:0, 18:0) monolayer was studied (Figure S5c), however, the precise peak positions could not be determined. Even though the phase I of our SC model presents well defined peaks (Table 4), it cannot be excluded that a polymorph of CER[NP] was actually responsible for the formation of the observed phase.

Phase separated CER[NP] was also observed in the work of Kindlova [207], using different SC models with different compositions studied by means of XRD and IR spectroscopy. All the models, in which CER[NP] (24:0, 18) was used alone or together with other CERs, presented phase separation of this component due to preferential formation of HbN within its own crystal structure. Furthermore, studies with ternary mixtures composed of CER[NP] (18:0, 18:0), SA and Chol analyzed by Small angle neutron scattering showed how CER[NP] phase separated from the rest of the mixture forming a second lamellar phase with the lipids organized in a V-shape configuration [54]. To conclude, WAXS analysis of the SC mixture (Figure S7) showed the presence of only two peaks with centres at 1.51 and 1.67 Å⁻¹ (orthorhombic unit cell) connected to the 54 Å lamellar phase. Since CER[NP] is very tightly packed, one could expect to see phase-separated CER[NP] also in the WAXS profile. One possible explanation to justify the absence of these peaks is that the signal that this generated is not intense enough to be visualized.

5.2 Hydrogen bonding network and CERs polymorphism

It is well known, and impressively demonstrated in this dissertation, that CERs are able to generate intermolecular HbN. Considering that 18 classes of CERs have been confirmed in the human LM, the selection of the correct CERs for the development of SC *in-vitro* model systems is fundamental. Sphingosine and phytosphingosine, two of the main CERs classes, have been both reported to establish HbN within the SC. In the work from Badhe et al. [227], MD simulations of simple bilayers composed of individual CER subclasses were investigated.

It was found that CER [NP] and [AP] formed at least 30% more HbN in comparison to other classes such as CER[NS] or CER[AS].

As found in publication II, the D-form of CER[AP] was reported to form a supramolecular lattice (or subgel phase) (Figure 25 and 26), which demonstrated the presence of a strong intermolecular HbN between headgroups. A simple change in configuration from D- to L- of the alpha-hydroxy group led to the disappearance of the subgel phase (Figure 25 and 26) proving that a simple change of the headgroup geometry can disrupt the HbN (Figure 30). Some studies reported the development of SC *in-vitro* models using CER[AP] in its diastereomer mixture [186,225]. This must be avoided since, how demonstrated in publication II, these diastereomers showed in a 1:1 mixture an almost complete immiscibility. Therefore, the use of the single and native D-form should be always preferred.

In the supporting information file of publication III we reported the GIXD study of CER[NP] (24:0, 18:0) which showed an extremely complicated diffraction pattern. From the two wide-angle peaks dominating the in-plane component of the lattice (Figure 5b), a clear structure of the lipid could not be determined. Such complicated lattice might origin from multiple polymorphs of CER[NP] present in the same monolayer. The coexistence of two phases is thermodynamically possible in the case of metastable phases, which are very common due to the ability of CERs to form HbN. Surely, the presence of lipid crystals has been observed in the lattice (peak at 1.69 \AA^{-1}) indicating that the lipids interact strongly after spreading at the air-water interface in the gas-analogous phase. The polymorphism of CER[NP] (24:0, 18:0) was observed in SAXS, and the formation of two lamellar phases with slightly different d-spacings (Figure A1b and A1c) was reported. The WAXS profile of CER[NP] is as well highly complex and not easy to interpret.

Another case study is the one of CER[NS]. GIXD showed that this compound was able to form two separated crystalline structures. In the work of Valknin and Kelley [181] hexagonal and orthorhombic phases were found while in the work of Scheffer et al. [228] oblique and hexagonal phases were observed. Since one source of metastability is the sample handling, in the case of CER[NS] the presence of two different results proved the influence of sample history.

In the present work, experiments with CER[AP] have been conducted and the polymorphism of the diastereomers was analyzed via FTIR and DSC. In FTIR experiments performed at room temperature with dry lipid powders before and after heating to 200 °C, variations in the amide I and II regions (Figure S5b) were observed showing the interplay of HbN necessary to stabilize different polymorphic phases. In the DSC thermograms (Figure A7) was clearly visible that for each studied sample different phase transitions were present, phase transitions that were connected with rearranging of the molecules after the rearrangement of the HbN.

Another important evidence of HbN between CERs was reported in publication III. In this work, cerosomes were investigated in presence of our SC monolayer model to clarify the mode of action by which these vesicles act as skin repairing agents. As observed in subphase injection (Figure 36) and AFM (Figure 38) experiments, the two systems strongly interact. Since both systems possess negative electrostatic charge (Table 5), the attraction between the systems was connected to the ability of CERs to form a HbN. The ability to overcome the electrostatic repulsion by the cerosomes might be connected to local fluctuations of charges in both systems. In the SC monolayer and cerosomes the main lipid, which is responsible for creating the charge, is the FFA, which constitutes 37% in mol of the systems (~23% in the cerosome formulated together with PLs). Depending on the distribution of the FFA in each system, there might be areas with higher or lower charge density which would allow the vesicles to reach a certain distance to the monolayer allowing the establishment of HbN between the headgroups.

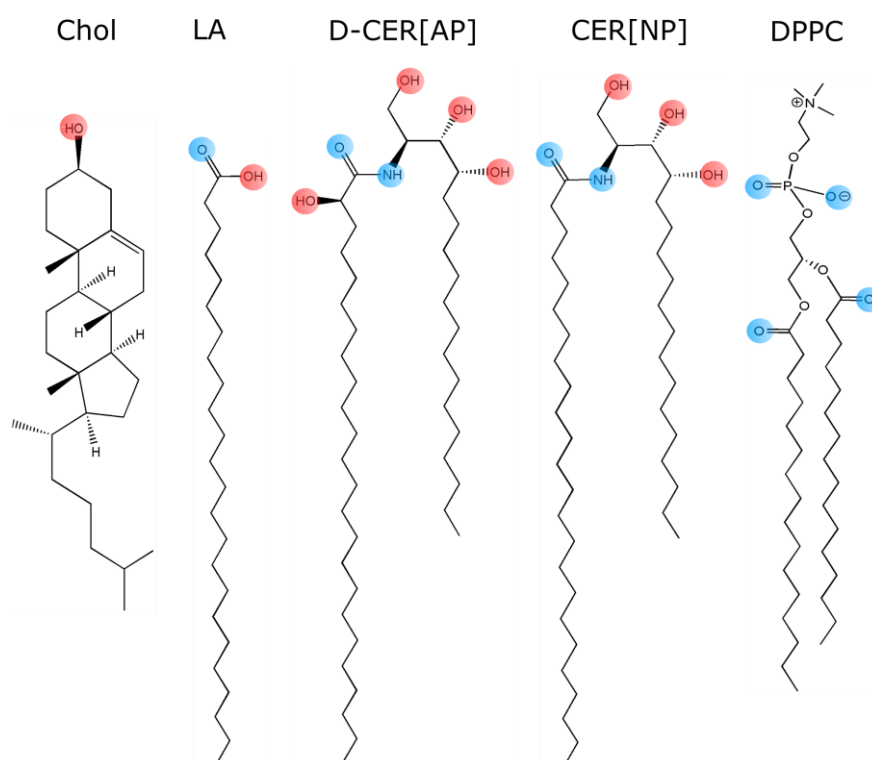


Figure 40. Molecular structures of used lipids in publication III. The hydrogen bond donor groups are marked red and in blue the hydrogen bond acceptor groups.

The same study performed with PLs liposomes pointed out a weaker and less relevant interaction with our SC monolayer model (Figure 36) despite these liposomes were neutral or only slightly negatively charged. PCs headgroups lack of hydrogen bond donor groups presenting only acceptor groups (Figure 40) while CERs headgroup (especially phytosphingosines) present both hydrogen donor and acceptor groups. As reported by Wang and Klauda [229], in MD simulation studies of CER-PC bilayers was shown that these two lipids can form extended HbN which become stronger with relative higher amounts of CERs in

the bilayer. Nevertheless, in subphase injection experiments PCs liposomes interacted markedly less in comparison to the cerosomes showing that the geometry of the PCs headgroups didn't allow to establish strong interaction with the CERs.

5.3 NIS and structure activity relationship for penetration enhancing

Transdermal drug delivery offers numerous advantages over conventional routes of administration. As discussed in section 1.3, the SC can be used as administration site and the penetration of actives can follow different routes, although the most reasonable is the diffusion of actives through the lipophilic LM. Because of this extreme hydrophobicity, only a very limited number of actives have the optimum physical-chemical properties to be able to cross the LM at a constant and satisfactory level to reach their therapeutic concentration. Chemical enhancement is one of the strategies to improve the transport of drugs through the SC itself. In publication I, the mode of action, by which two classes of NIS enact their PE mechanism, was investigated. Polysorbate 80 (PL80) and sucrose monolaurate (SL) have been selected as model surfactants.

An important concept, that is not often discussed regarding the ability of surfactants to enact a chemical enhancement effect, is the one of structure-activity relationship or SAR. Classically, the SAR refers to the chemical structure of a molecule and its biological activity. The same concept can be applied to NIS in order to determine systematically their potential penetration enhancement effect.

SL consist of lauric acid connected via an ester bond to the disaccharide sucrose presenting a medium length alkyl chain (C12:0). PL80 is derived from polyethoxylated sorbitan and oleic acid (C18:1) where the hydrophilic groups consist of polyethers. Directly from their structures is not possible to determine which of these has a bigger potential to enact a PE effect. One easy way to describe surfactants and their physical-chemical properties is by using the concept of C_c which stands for characteristic curvature [230]. This parameter describes the lipophilicity of a surfactant. PL80 possess a C_c value of -3.7 while SL of 1 being the most lipophilic one between the two. The concept of C_c describes better a surfactant than the HLB (hydrophilic lipophilic balance) since this parameter depends on the solubility of surfactants in water [231], being alone not enough descriptive for a surfactant behaviour.

In order to investigate the potential of the selected surfactants as PEs, simple monolayer models were used for screening. This type of experiments is not very common for the study of surfactants as PEs. Some experiments that investigated the influence of surfactants on the order of the SC using monolayers have been performed [124,125]. In these works, the surfactants were directly incorporated in a SC monolayer rather than injected underneath. As already known in literature [119], the use of surfactants above their CMC did not lead to a higher efficacy in its action and as shown in figure 18, at around 80% of each NIS CMCs, a

plateau in the activity was reached. Different articles report that the CMC of the used surfactants changes between producers [232]. Therefore, in figure A1 the CMC has been determined by surface tension measurements. The obtained values are slightly smaller than those reported in literature. As follow, the relative efficacy of the NIS was tested by analysing the so-called MIP (maximal insertion pressure). The concept of MIP was introduced for the first time by Calvez et. al [131] with the intent to study the insertion pressure of proteins and peptides into lipid monolayers after injection underneath the PLs monolayers. The same principal was used to study the ability of surfactants to penetrate our SC monolayer. As demonstrated, SL possessed a higher MIP of 44.9 mN/m than PL80 with 38.6 mN/m. Therefore, SL was able to penetrate the SC monolayer at higher SP than PL80. Since the SC monolayer possessed a lipophilic structure, it might be argued that SL possessing a Cc value higher than PL80 (being more lipophilic), a higher MIP could be expected due its higher lipophilicity. Obviously, to make such assumption on the basis of only two surfactants is insufficient. Therefore, similar experiments performed with different classes of NIS might be useful to confirm or deny such assumption in future.

5.4 Future work

During this work, monolayers have been used as cost-effective models to obtain information regarding the interaction between different systems with our SC model. Considering that the SC consist of a multi-layered matrix with a complex structure, such simplified models are very limited and cannot give information regarding interactions happening in deeper layers. Therefore, first logical step for the future is by translating two-dimensional models in three-dimensional ones.

In publication III, the bulk characterization of the quaternary SC model was performed showing the formation of a system closely mimicking the SC SPP, however, the presence of phase separated CER[NP] was observed. One simple strategy to solve this problem could be by reducing the amount of this lipid until a completely miscible mixture is observed.

A simple way to produce multilayers *in-vitro* models is to use solid supports via different methods (spray-drying, spin coating etc.). Multilayers on solid supports can be studied with many techniques including X-ray and neutron scattering. Neutron scattering in comparison to X-ray scattering has the advantage to distinguish between atoms of hydrogen and deuterium and in multi-layered systems this can be used conveniently. For instance, the experiments performed in publication I could be upscaled with SC multilayers using deuterated NIS and study how deeply these penetrated the model and to observe how its structure is affected. Similarly, liposomal formulations with a deuterated compound could be used to observe how these are able to cross a SC multilayer making easier to predict which formulation can be used for dermal and/or transdermal delivery. However, neutron scattering has some drawbacks.

First, to perform such experiments special facilities are required and its access might be limited to only few days in a year. Second, the synthesis of deuterated or perdeuterated compounds is extremely expensive and needs specialized equipment, and finally, data analysis is complicated, time-consuming and needs trained users.

Another interesting way to take advantage of SC multilayers systems is by using them in permeability membranes such as the PAMPA. The parallel artificial membrane permeability assay (or PAMPA) is a recent procedure developed for a rapid determination of passive transport permeability that is gaining acceptance in pharmaceutical research [233] used as early stage method in drug discovery. PAMPA membranes in comparison to Franz cells allow to measure simultaneously more samples since a 96-well filter plate coated with an artificial membrane is used. Moreover, artificial membranes can be used being more cost-effective and efficient. It consists of two separated compartments, one containing a buffer solution with the formulation to be tested defined as donor well and the other containing an initial fresh buffer solution defined as acceptor well (Figure 41) [234]. With the intent to create quick, reliable and cost-effective permeability models, in the 2012 the so-called skin-PAMPA was produced by Sinko et al. [235] allowing to create a screening system that demonstrated high predictability in comparison with data present into three different databases. Nevertheless, skin-PAMPA is a relatively new method still under development and it's not yet recommended by public authorities for the *in-vitro* permeability studies whilst Franz cells are still the golden standard. Similarly, a PAMPA membrane coated with SC lipid matrix model could be prepared in order to screen the permeability of drugs.

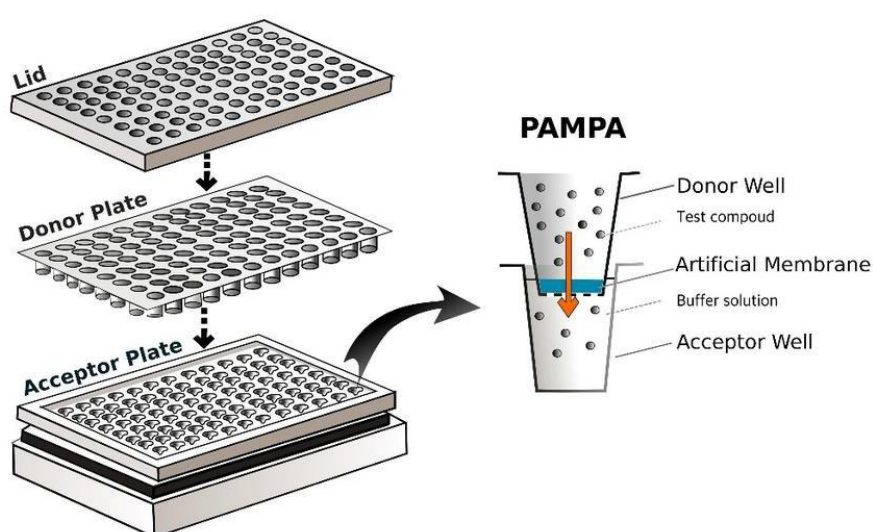


Figure 41. Representation of a PAMPA system taken from [236].

6. Conclusion and final remarks

The major purpose of this thesis was to develop a simplified SC monolayer model and to show that it can be used as a reliable system for predicting the interaction of cosmetic and pharmaceutical formulations with the native SC lipid matrix. In addition, the physical-chemical characterization of CER[AP] was accomplished by studying the structure of its different diastereomer forms.

The selected *in-vitro* SC model was composed of a quaternary mixture made of CER[NP]:D-CER[AP]:Chol:LA (0.66:0.33:0.7:1 molar fractions). The model was thoroughly characterized in mono- and multi-layer systems, however, only monolayers were used for further investigations. The most relevant results are summarised as follows:

In publication I, the SC monolayer model was studied with the Langmuir-Blodgett technique and by epifluorescence microscopy. The selected model was contacted with non-ionic surfactants (NIS) to investigate their use as potential penetration enhancers. Thanks to their low skin toxicity, NIS are proposed to be used as ideal excipients for improving the permeation of hydrophilic drugs through the SC for dermal and transdermal delivery purposes. Polysorbate 80 and sucrose monolaurate were used as model surfactants, and the main objective was to determine for each compound the MIP (maximal insertion pressure). It was found that sucrose monolaurate has a higher insertion capability into the SC lipid layer in comparison to the polysorbate 80.

In publication III, new SC liposomes (i.e. cerosomes) were successfully produced and characterized. Two formulations, one consisting of SC lipids formulated at pH 10 and one with the addition of PLs formulated at pH 7, showed uniform particle distribution and long-term stability. The formulation with the added phospholipids presented some advantages in comparison to the formulation without phospholipids since a buffer at neutral pH was used (more tolerable in case of dermal administration) and presented as well a higher stability. The developed cerosomes were studied together with our stratum corneum model in order to observe for the first time the mode of action by which the cerosomes are able to enact their skin barrier repairing effect. The mechanism behind this repairing effect is based on the establishment of strong interactions between the headgroups of the cerosome to the headgroups of the SC model, and the driving force of this interaction is based on intermolecular HbN between CERs headgroups.

In publication II, CER[AP] diastereomers with symmetric (18:0, 18:0) and asymmetric (24:0, 18:0) chains were studied in detail by X-ray scattering based methods. This CER is reported to exist in the D(2R)-form in the SC. Since CER[AP] is often used for the development of *in-vitro* SC models in its D/L diastereomer mixture, in this publication it was impressively demonstrate that considerable differences exist in the packing and organization of the two diastereomers. The main finding was that D-CER[AP] formed both in mono- and multi-layer

systems a highly ordered subgel phase which is an indicator for strong intermolecular HbN. In contrast, L-CER[AP] formed only an oblique chain lattice in both mono- and multi-layers. The disappearance of the subgel phase proved the absence of the HbN. A consequence of the establishment of the subgel phase is reflected in the arrangement of the lipids in multilayer systems. As proved in SAXS experiments, the D-form arranged in hairpin or FE configurations while the L-form arranged in V-shape. The diastereomer mixture was as well analysed and main findings were that in both mono- and multi-layers two lattices were observed. One lattice consisted of the pure D-form while the second lattice consisted of the L-form which accommodated some molecules of the D-form. To conclude, with and without chain symmetry no relevant differences have been observed.

In summary, with this work we showed that by using simplified SC models and the sophisticated biophysical techniques, is possible to obtain relevant information regarding the molecular background, the strength of interaction and the mode of action by which complex systems interact with monolayers. Of course such methodologies and models present as well disadvantages: a single layer is not representative of more complex structures such as the LM, only four lipids species for the development of the SC model are not representative of the manifoldness of lipids present in the *in-vivo* skin, and the local variability can never be reproduced in *in-vitro* systems. The final message is that the experiments here described represent useful methods to study the molecular background behind the SC organization and as well to characterize the interaction of these lipids with systems of different chemical nature.

7. Appendices

Appendix A, surfactants CMC estimation and effect of SL on SC monolayer

The CMCs of the non-ionic surfactants used in publication I were determined by surface tension experiments. By measuring the SP at different surfactant concentrations, the surface tension of the water can be determined and from it the CMC value extrapolated. The found values were for PS80 (Figure A1a) $\sim 9 \mu\text{M}$ and for SL $\sim 260 \mu\text{M}$. These values are slightly smaller than the literature references.

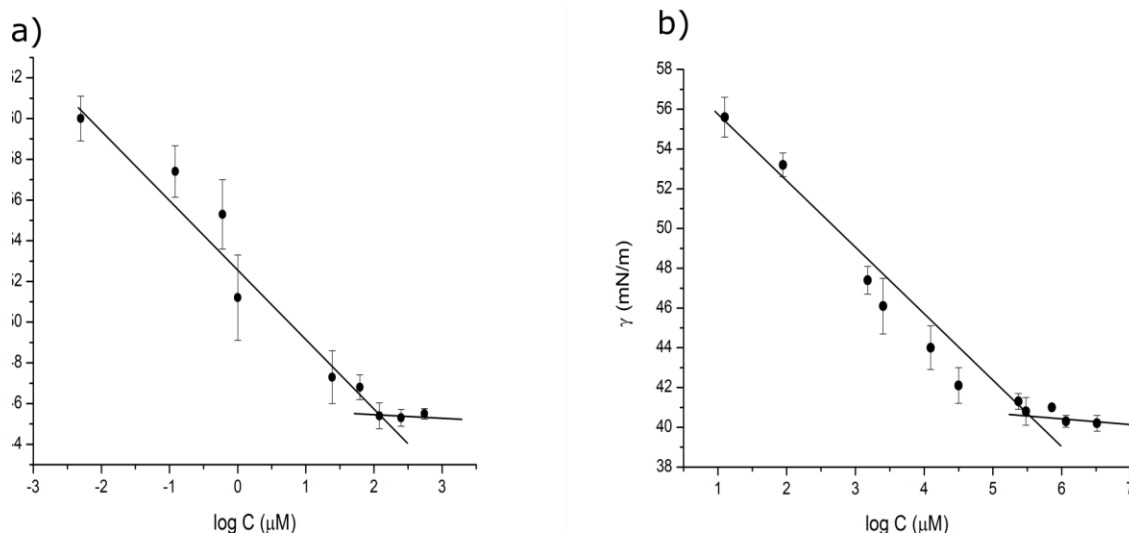


Figure A1. Plot of surface tension (γ) versus natural logarithm of surfactant concentration of a) polysorbate 80 and b) sucrose monolaurate.

Appendix B, CER[NP] (24:0, 18:0) SAXS/WAXS profiles and effect of cholesterol addition on CER[NP]

CER[NP] (24:0, 18:0) was tested via SAXS/WAXS with and without the presence of Chol. As seen in figure A2, it was possible to observe that CER[NP] presents different polymorphic forms. In figure A2a) a d-spacing of 43.3 \AA was observed while in figure A2b) of 37.4 \AA . These values were in agreement with those found by Dahlen and Pascher [53]. In figure A2c, the 7:3 CER[NP]:Chol mixture was studied showing a clear phase separation of the compounds.

In figure A3, the GIXD study of 7:3 mixtures of CER[NP]:Chol was performed. As can be observed, in comparison to the lattice of pure CER[NP] (Figure S5b) a different lattice with clear and defined peaks was originated.

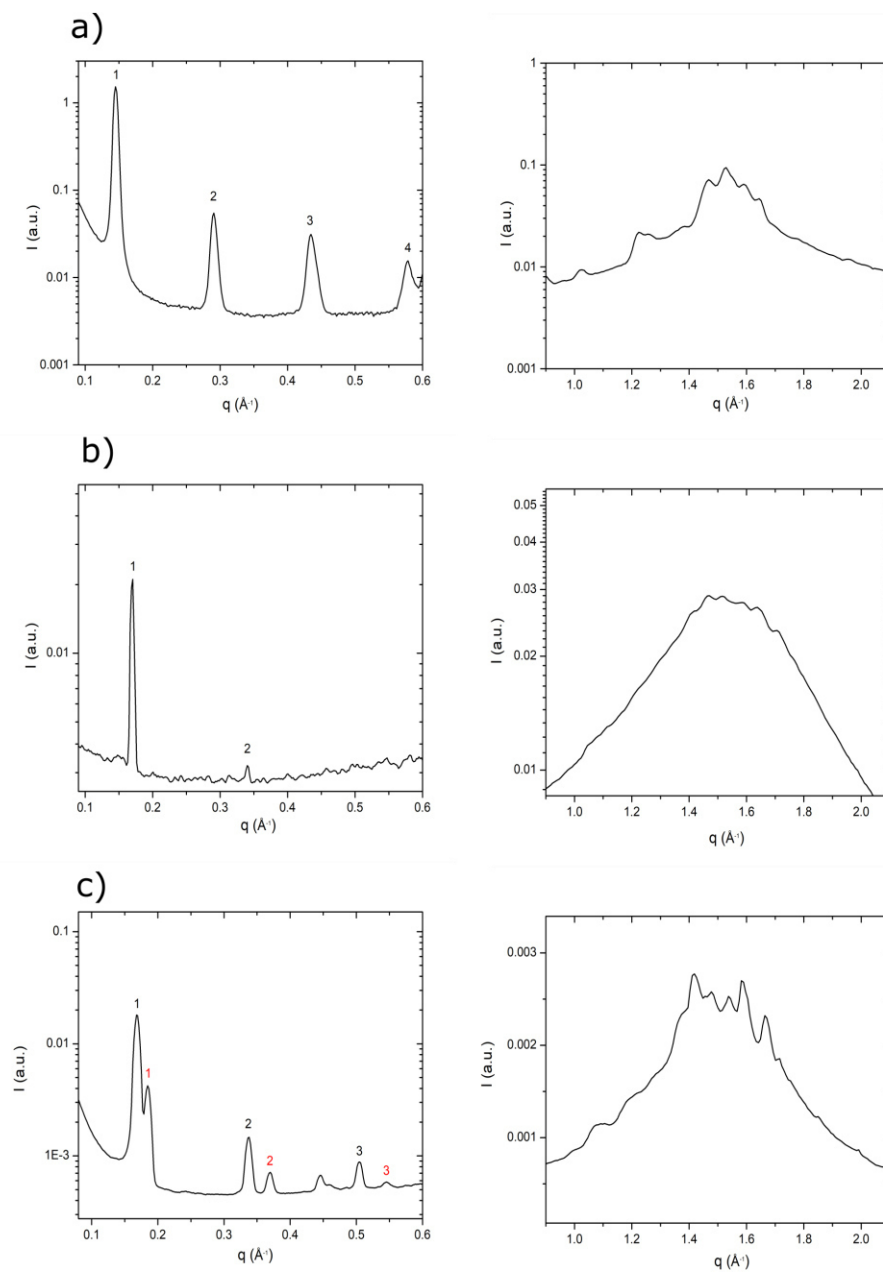


Figure A2. SAXS and WAXS profile of CER[NP] (24:0, 18:0) a) polymorph with d-spacing of 43.3 \AA and b) polymorph with d-spacing of 37.4 \AA , c) SAXS and WAXS profile of 7:3 CER[NP]:Chol mixture with clear phase separation of the CER[NP] from the Chol.

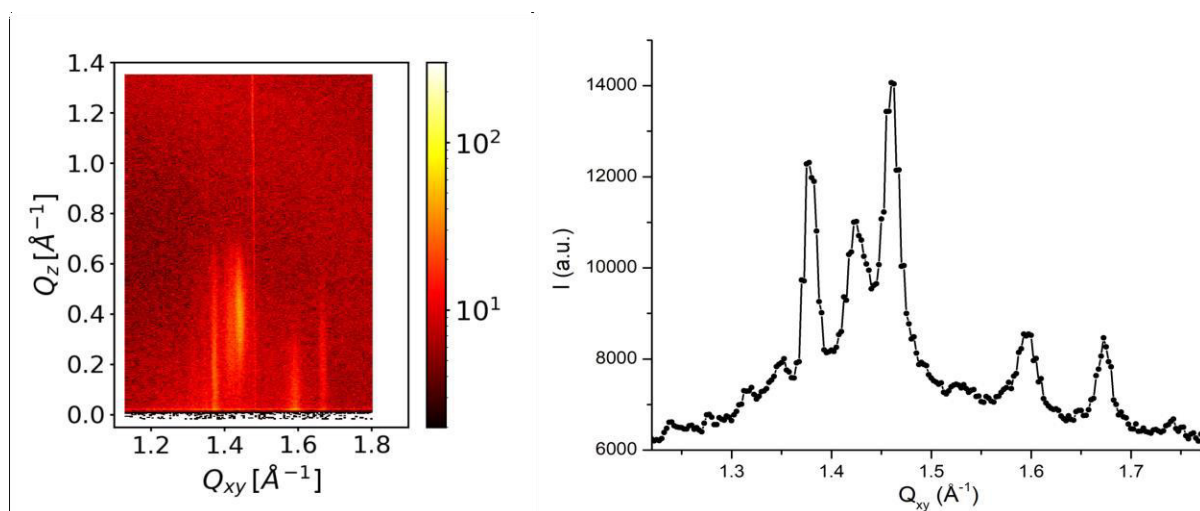


Figure A3. Lattice and in-plane component of 7:3 mixture of CER[NP]:Chol. In comparison to the lattice of pure CER[NP] in figure S5b, the lattice presents more defined peaks.

Appendix C, Lecithin phospholipids characterization

The phospholipids, P100-3 and S75-3, used in publication III for the formulation of the cerosome and for the production of liposomes were characterized in detail via DSC in bulk dispersion, via SAXS in bulk dispersion and via GIXD in monolayers. In each mixture, the number indicates the w% of PC while the -3 indicates hydrogenated chains.

Both P100-3 and S75-3 exhibited in monolayers (at all measured SP) an orthorhombic lattice (Figure A6) with parameters shown in table 1a. SAXS results (Figure A5) indicated that P100-3 formed a lamellar phase with d-spacing of 68.4 Å while S75-3 formed positionally uncorrelated bilayers. Finally, DSC showed that P100-3 (Figure A4a) presented a pre-phase transition at 45.3 °C and a main phase transition at 51.9 °C. Since P100-3 consists mainly of a mixture of DPPC and DSPC such found value is justified. S75-3 presented a main phase transition at 53.2 °C (Figure A4b) with additional peaks at higher temperatures indicating phase separated lipids in the mixture. The precise composition of the mixture is not known, therefore, could not be determined which lipids caused the phase separation.

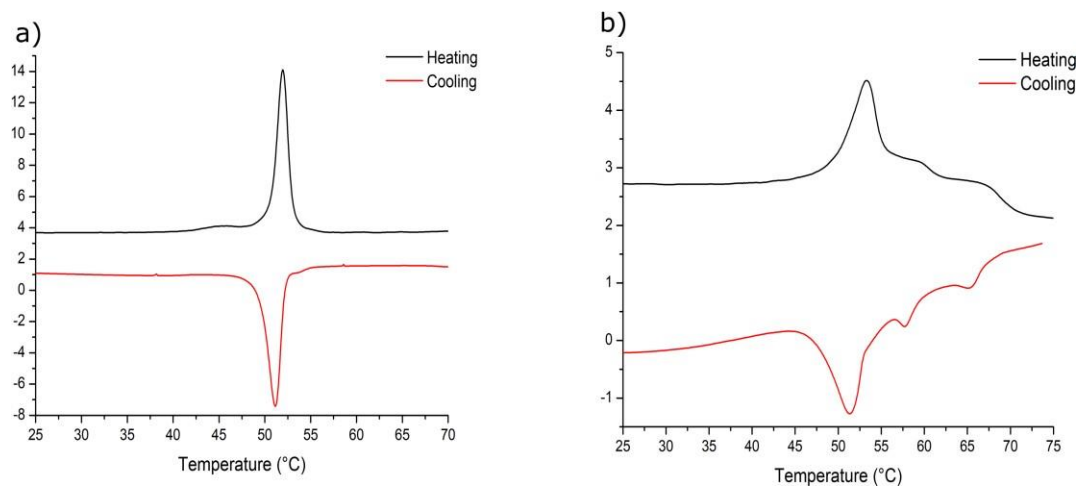


Figure A4. Heating and cooling DSC scans of aqueous dispersions a) P100-3 / sharp main phase transition at 51.9 °C and a pre-transition at 45.3 °C and b) S75-3 (main phase transition at 53.2 °C followed by smaller peaks due to phase separation of components in the mixture).

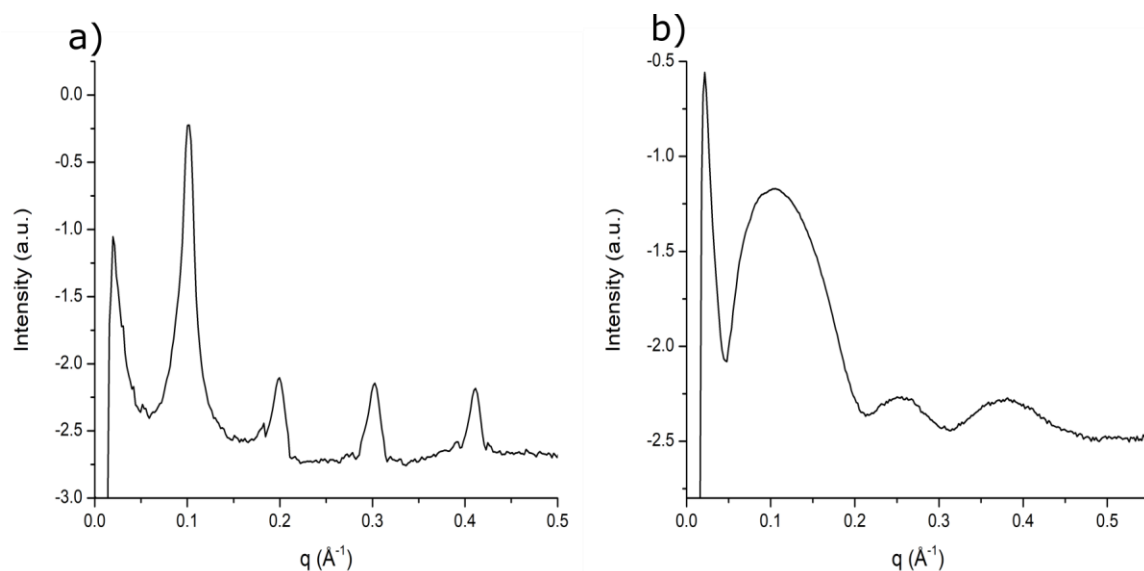


Figure A5. a) SAXS profile of P100-3, a single lamellar phase with d-spacing of 68.4 Å and 4 orders of reflection was observed, b) SAXS profile of S75-3, the presence of positionally uncorrelated bilayers was observed.

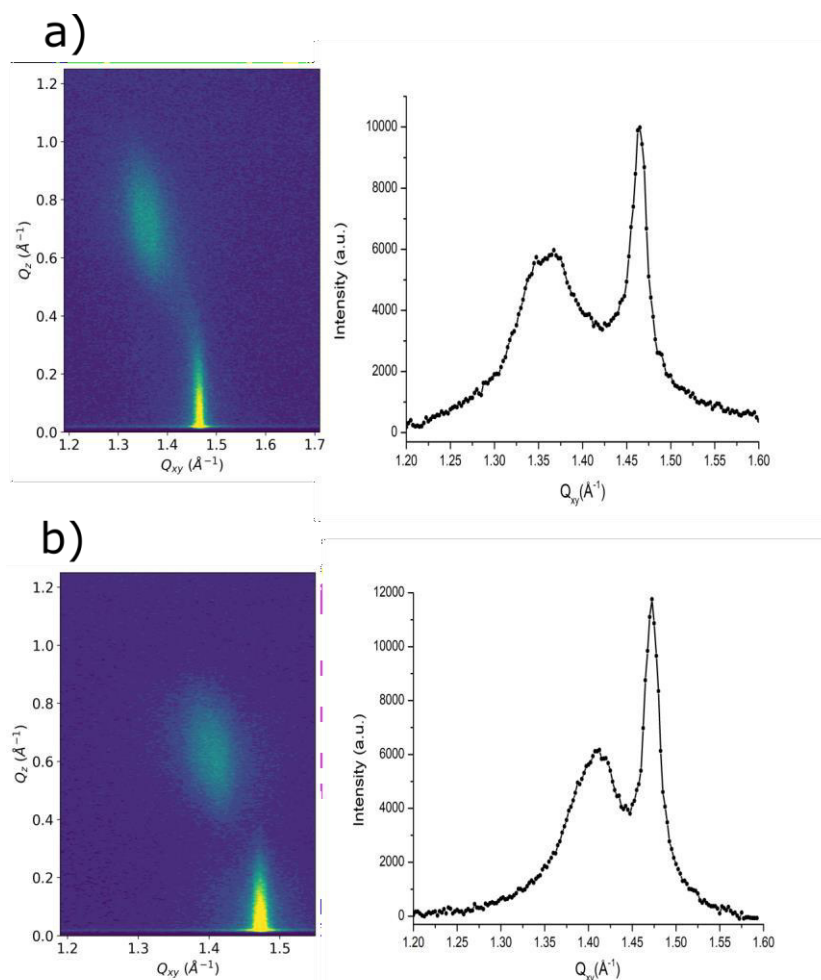


Figure A6. Diffraction patterns and in-plane component analysis of a) P100-3 and b) S75-3 measured at 30 mN/m. Both monolayers presented a lattice with an orthorhombic unit cell but slightly different packing parameters. P100-3 chains had a tilt of 31.6° while S75-3 chains of 27.2° .

Table A1. Peak positions (Q_{xy} and Q_z), with full-width at half-maximum ($fwhm$) of the respective rods, lattice parameters of the unit cell (a , b and c), tilt angle (t), cross-sectional area (A_o) and in-plane chain area (A_{xy}) extracted from GIXD data of the different lecithins on CaBr_2 solution at 20°C measured at 30 mN/m.

| | a | b | α | β | t | fwh | d | A_{xy} | A_o | Q_{xy1} | Q_{xy2} | Q_{z1} | Q_{z2} |
|---------------|--------------|--------------|----------|----------|----------|-------|------|----------------|----------------|-------------------|-------------------|-------------------|-------------------|
| | \AA | \AA | $^\circ$ | $^\circ$ | $^\circ$ | m | | \AA^2 | \AA^2 | \AA^{-1} | \AA^{-1} | \AA^{-1} | \AA^{-1} |
| P100-3 | 5.45 | 5.08 | 115 | 122 | 31.6 | 0.31 | 0.09 | 23.4 | 19.9 | 1.36 | 1.46 | 0.71 | 0 |
| S75-3 | 5.24 | 5.00 | 116 | 121 | 27.2 | 0.32 | 0.06 | 22.4 | 19.9 | 1.41 | 1.47 | 0.62 | 0 |

Appendix D, calorimetry analysis of CER[AP] and of SC mixtures

D- and L-CER[AP] diastereomers with symmetric (18:0,18:0) and asymmetric (24:0, 18:0) chains and the diastereomer mixtures were analysed by means of DSC on dry powder since the temperature limit for DSC analysis in bulk dispersion is 95°C . As can be observed in figure

A7, each profile presented between two to four peaks. The last peaks represented the effective phase transition from solid to liquid phase while the precedents could be connected to transition in new metastable phases due to structure rearrangement.

The dry powders of the SC mixtures with C24 and C18 chains were as well tested with DSC. The SC mixture with C24 chains presented a main phase transition at 77.3 °C (Figure A8a) followed by a wider peak due to same phase separated component. The SC mixture with C18 chains presented a phase transition at 66.2 °C (Figure A8b).

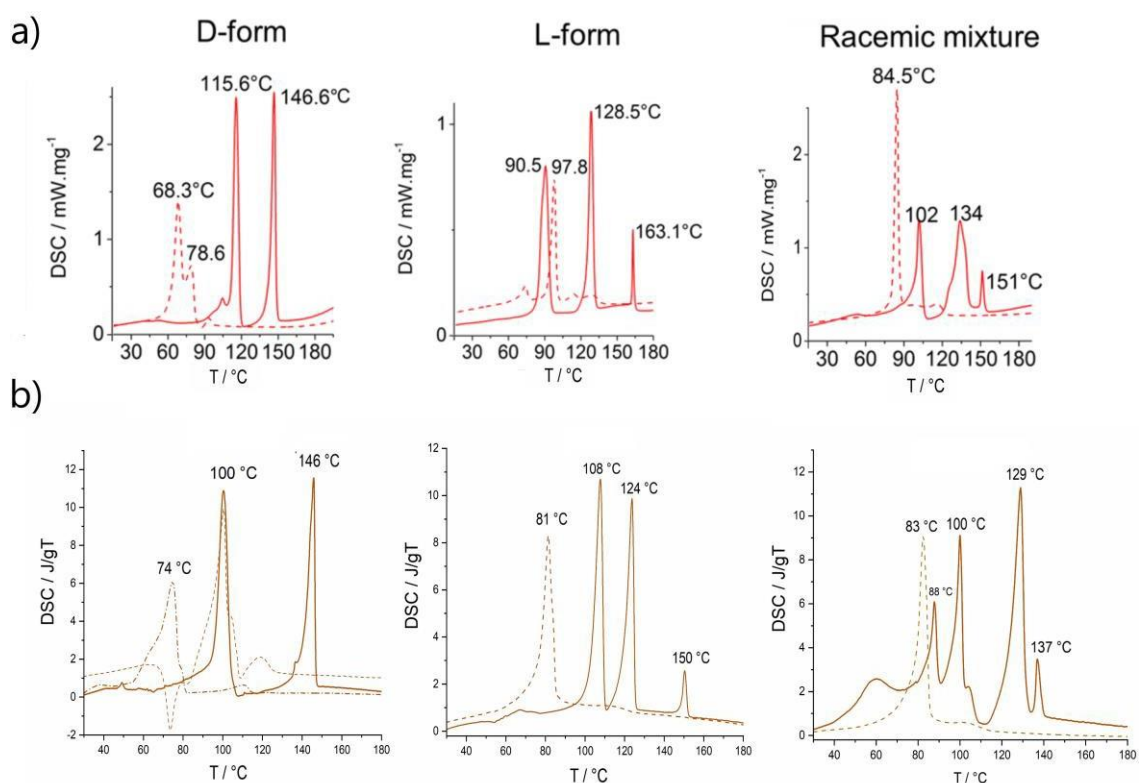


Figure A7. DSC curves of a) symmetric (18:0, 18:0) and b) asymmetric (24:0, 18:0) CER[AP]. Three heating/cooling cycles (full line – 1th scan, dashed line – 2nd scan, dotted-dashed line 3rd scan) were applied using dry powders. The heating scan rate was 10 K/minute.

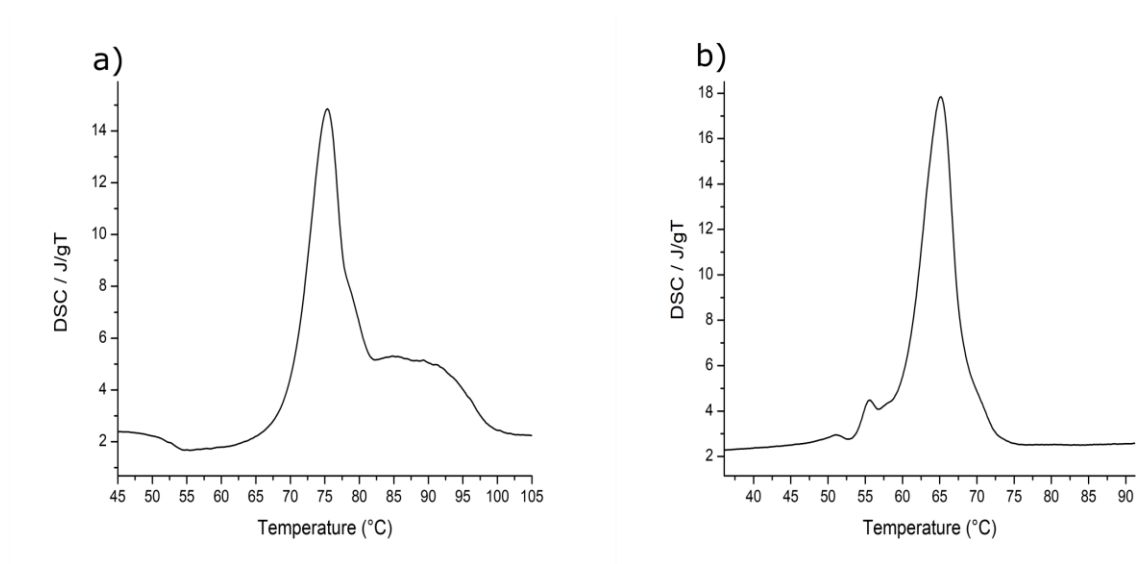


Figure A8. DSC curves of a) dried powder of the SC model with C24 alkyl chains, one main phase transition can be observed at ~ 75 °C and consequent presence of a broader peak at higher temperature due to phase transition and b) dried powder of the SC model with C18 alkyl chains, the main phase transition is observed at ~ 65 °C.

8. Bibliography

- [1] R.D. Mosteller, Simplified calculation of body-surface area., *N. Engl. J. Med.* 317 (1987) 1098. <https://doi.org/10.1056/NEJM198710223171717>.
- [2] G. Grubauer, P.M. Elias, K.R. Feingold, Transepidermal water loss: The signal for recovery of barrier structure and function, *J. Lipid Res.* 30 (1989) 323–333. [https://doi.org/10.1016/s0022-2275\(20\)38361-9](https://doi.org/10.1016/s0022-2275(20)38361-9).
- [3] F.M. Watt, Mammalian skin cell biology: At the interface between laboratory and clinic, *J. Invest. Dermatol.* 124 (2014) 937–940.
- [4] A.C. Kendall, A. Nicolaou, Bioactive lipid mediators in skin inflammation and immunity, *Prog. Lipid Res.* 52 (2013) 141–164. <https://doi.org/10.1016/j.plipres.2012.10.003>.
- [5] L. Eckhart, S. Lippens, E. Tschachler, W. Declercq, Cell death by cornification, *Biochim. Biophys. Acta - Mol. Cell Res.* 1833 (2013) 3471–3480. <https://doi.org/10.1016/j.bbamcr.2013.06.010>.
- [6] G. Denecker, P. Ovaere, P. Vandenabeele, W. Declercq, Caspase-14 reveals its secrets, *J. Cell Biol.* 180 (2008) 451–458. <https://doi.org/10.1083/jcb.200709098>.
- [7] O. Simonetti, A.J. Hoogstraate, W. Bialik, J.A. Kempenaar, A.H. Schrijvers, H.E. Boddé, M. Ponc, Visualization of diffusion pathways across the stratum corneum of native and in-vitro-reconstructed epidermis by confocal laser scanning microscopy., *Arch. Dermatol. Res.* 287 (1995) 465–473. <https://doi.org/10.1007/BF00373430>.
- [8] E. Christophers, A.M. Klingan, Visualization of the Cell Layers of the Stratum Corneum., *J. Invest. Dermatol.* 42 (1964) 407–409. <https://doi.org/10.1038/jid.1964.88>.
- [9] J. Van Smeden, M. Janssens, G.S. Gooris, J.A. Bouwstra, The important role of stratum corneum lipids for the cutaneous barrier function, *Biochim. Biophys. Acta - Mol. Cell Biol. Lipids.* 1841 (2014) 295–313. <https://doi.org/10.1016/j.bbalip.2013.11.00>.
- [10] M. Ponc, A. Weerheim, P. Lankhorst, P. Wertz, New acylceramide in native and reconstructed epidermis, *J. Invest. Dermatol.* 120 (2003) 581–588. <https://doi.org/10.1046/j.1523-1747.2003.12103.x>.
- [11] A.M. Goldstein, W. Abramovits, Ceramides and the stratum corneum: Structure, function, and new methods to promote repair, *Int. J. Dermatol.* 42 (2003) 256–259. <https://doi.org/10.1046/j.1365-4362.2003.01507.x>.
- [12] Y. Masukawa, H. Narita, E. Shimizu, N. Kondo, Y. Sugai, T. Oba, R. Homma, J. Ishikawa, Y. Takagi, T. Kitahara, Y. Takema, K. Kita, Characterization of overall ceramide species in human stratum corneum, *J. Lipid Res.* 49 (2008) 1466–1476. <https://doi.org/10.1194/jlr.m800014-jlr200>.
- [13] P.W. Wertz, M.C. Miethke, S.A. Long, J.S. Strauss, D.T. Downing, The Composition of the Ceramides from Human Stratum Corneum and from Comedones, *J. Invest. Dermatol.* 84 (1985) 410–412. <https://doi.org/10.1111/1523-1747.ep12265510>.
- [14] A. Weerheim, M. Ponc, Determination of stratum corneum lipid profile by tape stripping in combination with high-performance thin-layer chromatography, *Arch. Dermatol. Res.* 293 (2001) 191–199.
- [15] K.C. Madison, Barrier function of the skin: “La Raison d’Être” of the epidermis, *J. Invest. Dermatol.* 121 (2003) 231–241. <https://doi.org/10.1046/j.1523-1747.2003.12359.x>.
- [16] J.A. Bouwstra, P.L. Honeywell-nguyen, G.S. Gooris, Structure of the skin barrier and its modulation by vesicular formulations, *Prog. Lipid Res.* 42 (2003) 1–36.

- [17] N.Y. Schurer, P.M. Elias, *The Biochemistry and Function of Stratum Corneum Lipids*, Second Edi, Academic Press Inc., 1991. <https://doi.org/10.1016/B978-0-12-024924-4.50006-7>.
- [18] M. Janssens, J. Van Smeden, G.S. Gooris, W. Bras, G. Portale, P.J. Caspers, R.J. Vreeken, T. Hankemeier, S. Kezic, R. Wolterbeek, A.P. Lavrijsen, J.A. Bouwstra, Increase in short-chain ceramides correlates with an altered lipid organization and decreased barrier function in atopic eczema patients, *J. Lipid Res.* 53 (2012) 2755–2766. <https://doi.org/10.1194/jlr.P030338>.
- [19] A. Weerheim, M. Ponc, Determination of stratum corneum lipid profile by tape stripping in combination with high-performance thin-layer chromatography, *Arab. J. Chem.* 293 (2001) 191–199.
- [20] R. Kindt, L. Jorge, E. Dumont, P. Couturon, F. David, P. Sandra, K. Sandra, Profiling and Characterizing Skin Ceramides Using Reversed-Phase Liquid Chromatography – Quadrupole Time-of-Flight Mass Spectrometry, *Anal. Chem.* 84 (2011) 403–411. <https://doi.org/10.1021/ac202646v>.
- [21] A. V. Rawlings, I.R. Scott, C.R. Harding, P.A. Bowser, Stratum corneum moisturization at the molecular level, *J. Invest. Dermatol.* 103 (1994) 731–740. <https://doi.org/10.1111/1523-1747.ep12398620>.
- [22] L. Norlén, Skin Barrier Structure and Function: The Single Gel Phase Model, *J. Invest. Dermatol.* 117 (2001) 830–836. <https://doi.org/10.1038/jid.2001.1>.
- [23] R. Gupta, B. Rai, Molecular Dynamics Simulation Study of Skin Lipids: Effects of the Molar Ratio of Individual Components over a Wide Temperature Range, *J. Phys. Chem. B.* 119 (2015) 11643–11655. <https://doi.org/10.1021/acs.jpcc.5b02093>.
- [24] J.A. Bouwstra, G.S. Gooris, F.E.R. Dubbelaar, M. Ponc, Cholesterol sulfate and calcium affect stratum corneum lipid organization over a wide temperature range, *J. Lipid Res.* 40 (1999) 2303–2312. [https://doi.org/10.1016/s0022-2275\(20\)32105-2](https://doi.org/10.1016/s0022-2275(20)32105-2).
- [25] K.R. Elias, Peter M. Feingold, Epidermis as a dynamic interface, in: Old Herborn University Foundation (Ed.), 2015: pp. 1–17.
- [26] P.W. Wertz, The nature of the epidermal barrier: Biochemical Aspects, *Adv. Drug Deliv. Rev.* (1996) 283–294.
- [27] J. Wohlrab, A. Gabel, M. Wolfram, I. Grosse, R.H.H. Neubert, S.C. Steinbach, Age- and diabetes-related changes in the free fatty acid composition of the human stratum corneum, *Skin Pharmacol. Physiol.* 31 (2018) 283–291. <https://doi.org/10.1159/000490800>.
- [28] M. Mao-qiang, P.M. Elias, K.R. Feingold, Fatty acids are required for epidermal permeability barrier function, *J. Clin. Invest.* 92 (1993) 791–798.
- [29] J.-M. Schröder, *Fatty Acids and Inflammatory Skin Diseases*, Springer Basel AG, 1999.
- [30] B.J. Pettus, C.E. Chalfant, Y.A. Hannun, Ceramide in apoptosis: An overview and current perspectives, *Biochim. Biophys. Acta - Mol. Cell Biol. Lipids.* 1585 (2002) 114–125. [https://doi.org/10.1016/S1388-1981\(02\)00331-1](https://doi.org/10.1016/S1388-1981(02)00331-1).
- [31] J.D. Fishbein, R.T. Dobrowsky, A. Bielawska, S. Garrett, Y.A. Hannun, Ceramide-mediated growth inhibition and CAPP are conserved in *Saccharomyces cerevisiae*, *J. Biol. Chem.* 268 (1993) 9255–9261. [https://doi.org/10.1016/s0021-9258\(18\)98343-2](https://doi.org/10.1016/s0021-9258(18)98343-2).
- [32] Y.A. Hannun, Functions of ceramide in coordinating cellular responses to stress, *Science (80-.)*. 274 (1996) 1855–1859. <https://doi.org/10.1126/science.274.5294.1855>.
- [33] M.E. Venable, L.M. Webb-froehlich, E.F. Sloan, J.E. Thomley, Shift in sphingolipid

- metabolism leads to an accumulation of ceramide in senescence, 127 (2006) 473–480. <https://doi.org/10.1016/j.mad.2006.01.003>.
- [34] S. Motta, M. Monti, S. Sesana, R. Caputo, S. Carelli, R. Ghidoni, Ceramide composition of the psoriatic scale, *BBA - Mol. Basis Dis.* 1182 (1993) 147–151. [https://doi.org/10.1016/0925-4439\(93\)90135-N](https://doi.org/10.1016/0925-4439(93)90135-N).
- [35] K.J. Robson, M.E. Stewart, S. Michelsen, N.D. Lazo, D.T. Downing, 6-Hydroxy-4-sphingenine in human epidermal ceramides, *J. Lipid Res.* 35 (1994) 2060–2068. [https://doi.org/10.1016/s0022-2275\(20\)39952-1](https://doi.org/10.1016/s0022-2275(20)39952-1).
- [36] M. Rabionet, K. Gorgas, R. Sandhoff, Ceramide synthesis in the epidermis, *Biochim. Biophys. Acta - Mol. Cell Biol. Lipids.* 1841 (2014) 422–434. <https://doi.org/10.1016/j.bbalip.2013.08.011>.
- [37] Y. Masukawa, J. Ishikawa, R. Homma, H. Narita, T. Kitahara, A. Naoe, Y. Takagi, H. Sato, T. Oba, N. Kondo, Y. Sugai, Comprehensive quantification of ceramide species in human stratum corneum, *J. Lipid Res.* 50 (2009) 1708–1719. <https://doi.org/10.1194/jlr.d800055-jlr200>.
- [38] M. Rabionet, A. Bayerle, C. Marsching, R. Jennemann, H.J. Gröne, Y. Yildiz, D. Wachten, W. Shaw, J.A. Shayman, R. Sandhoff, 1-O-acylceramides are natural components of human and mouse epidermis, *J. Lipid Res.* 54 (2013) 3312–3321. <https://doi.org/10.1194/jlr.M040097>.
- [39] G.M. Gray, R.J. White, Glycosphingolipids and ceramides in human and pig epidermis, *J. Invest. Dermatol.* 70 (1978) 336–341. <https://doi.org/10.1111/1523-1747.ep12543527>.
- [40] P.W. Wertz, D.C. Swartzendruber, K.C. Madison, D.T. Downing, Composition and morphology of epidermal cyst lipids, *J. Invest. Dermatol.* 89 (1987) 419–425. <https://doi.org/10.1111/1523-1747.ep12471781>.
- [41] J. Van Smeden, W.A. Boiten, T. Hankemeier, R. Rissmann, J.A. Bouwstra, R.J. Vreeken, Combined LC / MS-platform for analysis of all major stratum corneum lipids, and the profiling of skin substitutes, *BBA - Mol. Cell Biol. Lipids.* 1841 (2014) 70–79. <https://doi.org/10.1016/j.bbalip.2013.10.002>.
- [42] L. Norlén, I. Nicander, A. Lundsjö, T. Cronholm, B. Forslind, A new HPLC-based method for the quantitative analysis, *Arch. Dermatol. Res.* 290 (1998) 508–516.
- [43] A. Schroeter, M.A. Kiselev, T. Hauß, S. Dante, R.H.H. Neubert, Evidence of free fatty acid interdigitation in stratum corneum model membranes based on ceramide [AP] by deuterium labelling, *BBA - Biomembr.* 1788 (2009) 2194–2203. <https://doi.org/10.1016/j.bbamem.2009.07.024>.
- [44] J.A. Bouwstra, G.S. Gooris, F.E.R. Dubbelaar, M. Ponc, Phase behavior of lipid mixtures based on human ceramides: Coexistence of crystalline and liquid phases, *J. Lipid Res.* 42 (2001) 1759–1770. [https://doi.org/10.1016/s0022-2275\(20\)31502-9](https://doi.org/10.1016/s0022-2275(20)31502-9).
- [45] F. Damien, M. Boncheva, The extent of orthorhombic lipid phases in the stratum corneum determines the barrier efficiency of human skin in vivo, *J. Invest. Dermatol.* 130 (2010) 611–614. <https://doi.org/10.1038/jid.2009.272>.
- [46] R. Mendelsohn, C.R. Flach, D.J. Moore, Determination of molecular conformation and permeation in skin via IR spectroscopy, microscopy, and imaging, *Biochim. Biophys. Acta - Biomembr.* 1758 (2006) 923–933. <https://doi.org/10.1016/j.bbamem.2006.04.009>.
- [47] S. Stahlberg, B. Školová, P.K. Madhu, A. Vogel, K. Vávrová, D. Huster, Probing the role of the ceramide acyl chain length and sphingosine unsaturation in model skin barrier

- lipid mixtures by ²H solid-state NMR spectroscopy, *Langmuir*. 31 (2015) 4906–4915. <https://doi.org/10.1021/acs.langmuir.5b00751>.
- [48] F.F. Sahle, T. Gebre-Mariam, B. Dobner, J. Wohlrab, R.H.H. Neubert, Skin diseases associated with the depletion of stratum corneum lipids and stratum corneum lipid substitution therapy, *Skin Pharmacol. Physiol.* 28 (2015) 42–55. <https://doi.org/10.1159/000360009>.
- [49] M.E. Rerek, Chen, B. Markovic, D. Van Wyck, P. Garidel, R. Mendelsohn, D.J. Moore, Phytosphingosine and Sphingosine Ceramide Headgroup Hydrogen Bonding: Structural Insights through Thermotropic Hydrogen/Deuterium Exchange, *J. Phys. Chem. B*. 105 (2001) 9355–9362. <https://doi.org/10.1021/jp0118367>.
- [50] D. Groen, G.S. Gooris, D.J. Barlow, M.J. Lawrence, J.B. Van Mechelen, B. Demé, J.A. Bouwstra, Disposition of ceramide in model lipid membranes determined by neutron diffraction, *Biophys. J.* 100 (2011) 1481–1489. <https://doi.org/10.1016/j.bpj.2011.02.001>.
- [51] I. Iwai, H. Han, L. Den Hollander, S. Svensson, L.G. Öfverstedt, J. Anwar, J. Brewer, M. Bloksgaard, A. Laloeuf, D. Nosek, S. Masich, L.A. Bagatolli, U. Skoglund, L. Norlén, The human skin barrier is organized as stacked bilayers of fully extended ceramides with cholesterol molecules associated with the ceramide sphingoid moiety, *J. Invest. Dermatol.* 132 (2012) 2215–2225. <https://doi.org/10.1038/jid.2012.43>.
- [52] S. Wartewig, R.H.H. Neubert, Properties of Ceramides and Their Impact on the Stratum Corneum Structure : A Review, *Skin Pharmacol. Physiol.* 20 (2007) 220–229. <https://doi.org/10.1159/000104420>.
- [53] B. Dahlén, I. Pascher, Molecular arrangements in sphingolipids. Thermotropic phase behaviour of tetracosanoylphytosphingosine, *Chem. Phys. Lipids*. 24 (1979) 119–133. [https://doi.org/10.1016/0009-3084\(79\)90082-3](https://doi.org/10.1016/0009-3084(79)90082-3).
- [54] T.N. Engelbrecht, A. Schroeter, T. Hauß, B. Demé, H.A. Scheidt, D. Huster, R.H.H. Neubert, The impact of ceramides NP and AP on the nanostructure of stratum corneum lipid bilayer. Part I: Neutron diffraction and ²H NMR studies on multilamellar models based on ceramides with symmetric alkyl chain length distribution, *Soft Matter*. 8 (2012) 6599–6607. <https://doi.org/10.1039/c2sm25420d>.
- [55] M.A. Kiselev, N.Y. Ryabova, A.M. Balagurov, S. Dante, T. Hauss, J. Zbytovska, S. Wartewig, R.H.H. Neubert, New insights into the structure and hydration of a stratum corneum lipid model membrane by neutron diffraction, *Eur. Biophys. J.* 34 (2005) 1030–1040. <https://doi.org/10.1007/s00249-005-0488-6>.
- [56] P.M. Elias, D.S. Friend, The Permeability Barrier in Mammalian Epidermis, *J. Cell Biol.* 65 (1975) 180–191.
- [57] K.C. Madison, D.C. Swartzendruber, P.W. Wertz, D.T. Downing, Presence of intact intercellular lipid lamellae in the upper layers of the stratum corneum, *J. Invest. Dermatol.* 88 (1987) 714–718. <https://doi.org/10.1111/1523-1747.ep12470386>.
- [58] D.C. Swartzendruber, P.W. Wertz, D.J. Kitko, K.C. Madison, D.T. Downing, Molecular models of intercellular lipid lamellae in mammalian stratum corneum, *J. Invest. Dermatol.* 92 (1989) 251–257.
- [59] B.O. Forslind, A domain mosaic model of the skin barrier, *Acta Derm. Venereol.* 74 (1994) 1–6. <https://doi.org/10.2340/000155557416>.
- [60] R.O. Potts, M.L. Francoeur, Lipid biophysics of water loss through the skin, *Proc. Natl. Acad. Sci. U. S. A.* 87 (1990) 3871–3873. <https://doi.org/10.1073/pnas.87.10.3871>.
- [61] J.A. Bouwstra, F.E.R. Dubbelaar, G.S. Gooris, M. Ponc, The lipid organisation in the

- skin barrier, *Acta Dermato-Venereologica*, Suppl. (2000) 23–30. <https://doi.org/10.1080/000155500750042826>.
- [62] J.A. Bouwstra, G.S. Gooris, J.A. van der Speck, W. Bras, Structural Investigations of Human Stratum Corneum by Small-Angle X-Ray Scattering, *J. Invest. Dermatol.* 97 (1991) 1005–1012.
- [63] J.A. Bouwstra, G.S. Gooris, M.A.S. de Vries, J.A. van der Spek, W. Bras, Structure of human stratum corneum as a function of temperature and hydration: A wide-angle X-ray diffraction study, *Int. J. Pharm.* 84 (1992) 205–216. [https://doi.org/10.1016/0378-5173\(92\)90158-X](https://doi.org/10.1016/0378-5173(92)90158-X).
- [64] T. Schmitt, H.H. Neubert, State of the Art in Stratum Corneum Research . Part II : Hypothetical Stratum Corneum Lipid Matrix Models, *Skin Pharmacol. Physiol.* (2020) 1–18. <https://doi.org/10.1159/000509019>.
- [65] L. Norlén, Current understanding of skin barrier morphology, *Skin Pharmacol. Physiol.* 26 (2013) 213–216. <https://doi.org/10.1159/000351930>.
- [66] F. Knorr, J. Lademann, A. Patzelt, W. Sterry, U. Blume-Peytavi, A. Vogt, Follicular transport route - Research progress and future perspectives, *Eur. J. Pharm. Biopharm.* 71 (2009) 173–180. <https://doi.org/10.1016/j.ejpb.2008.11.001>.
- [67] B.W. Barry, Novel mechanisms and devices to enable successful transdermal drug delivery, *Eur. J. Pharm. Sci.* 14 (2001) 101–114. [https://doi.org/10.1016/S0928-0987\(01\)00167-1](https://doi.org/10.1016/S0928-0987(01)00167-1).
- [68] M.R. Prausnitz, S. Mitragotri, R. Langer, Current status and future potential of transdermal drug delivery, *Nat. Rev. Drug Discov.* 3 (2004) 115–124. <https://doi.org/10.1038/nrd1304>.
- [69] A. Pouillot, N. Dayan, A.S. Polla, L.L. Polla, B.S. Polla, The stratum corneum: A double paradox, *J. Cosmet. Dermatol.* 7 (2008) 143–148. <https://doi.org/10.1111/j.1473-2165.2008.00379.x>.
- [70] K.S. Paudel, M. Milewski, C.L. Swadley, N.K. Brogden, P. Ghosh, A.L. Stinchcomb, Challenges and opportunities in dermal/transdermal delivery, *Ther. Deliv.* 1 (2010) 109–131. <https://doi.org/10.4155/tde.10.16>.
- [71] M.R. Prausnitz, R. Langer, Transdermal drug delivery, *Nat. Biotechnol.* 26 (2008) 1261–1268. <https://doi.org/10.1038/nbt.1504>.
- [72] A. Herman, A.P. Herman, Essential oils and their constituents as skin penetration enhancer for transdermal drug delivery: A review, *J. Pharm. Pharmacol.* 67 (2015) 473–485. <https://doi.org/10.1111/jphp.12334>.
- [73] A.C. Williams, B.W. Barry, Penetration enhancers, *Adv. Drug Deliv. Rev.* 64 (2012) 128–137. <https://doi.org/10.1016/j.addr.2012.09.032>.
- [74] D. Bucks, H.I. Maibach, Occlusion does not uniformly enhance penetration in vivo, in: M. Dekker (Ed.), R.L. Bronaugh, H.I. Maibach (Eds.), *Percutaneous Absorption; Drugs—Cosmetics—Mechanisms—Methodol.*, 3rd ed., New York, (1999).
- [75] P. Ashton, K.A. Walters, K.R. Brain, J. Hadgraft, Surfactant effects in percutaneous absorption II. Effects on protein and lipid structure of the stratum corneum, *Int. J. Pharm.* 87 (1992) 265–269. [https://doi.org/10.1016/0378-5173\(92\)90252-W](https://doi.org/10.1016/0378-5173(92)90252-W).
- [76] R.A. Tupker, J. Pinnagoda, J.P. Nater, The transient and cumulative effect of sodium lauryl sulphate on the epidermal barrier assessed by transepidermal water loss: inter-individual variation, *Acta Derm. Venereol.* 70 (1990) 1–5. <http://europepmc.org/abstract/MED/1967864>.

- [77] M. Reiger, L. Rhein, *Surfactants in Cosmetics*, in: *Basin Res.*, Marcel Dekker, New York, (1997). <https://doi.org/10.1046/j.1365-2117.2001.00145.x>.
- [78] H.A. Ayala-Bravo, D. Quintanar-Guerrero, A. Naik, Y.N. Kalia, J.M. Cornejo-Bravo, A. Ganem-Quintanar, Effects of sucrose oleate and sucrose laureate on in vivo human stratum corneum permeability, *Pharm. Res.* 20 (2003) 1267–1273. <https://doi.org/10.1023/A:1025013401471>.
- [79] K.P. Ananthapadmanabhan, K.K. Yu, C.L. Meyers, M.P. Aronson, Binding of surfactants to stratum corneum, *J. Cosmet. Sci.* 47 (1996) 185–200.
- [80] D. Jenerowicz, W. Silny, A. Danczac-Pazdrowska, A. Polanska, A. Osmola-Mankowska, K. Olek-Hrab, Environmental factors and allergic diseases, *Nippon Rinsho. Japanese J. Clin. Med.* 19 (2012) 475–481.
- [81] M. Lodén, The skin barrier and use of moisturizers in atopic dermatitis, *Clin. Dermatol.* 21 (2003) 145–157. [https://doi.org/10.1016/S0738-081X\(02\)00373-5](https://doi.org/10.1016/S0738-081X(02)00373-5).
- [82] J.A. Bouwstra, M. Ponc, The skin barrier in healthy and diseased state, *Biochim. Biophys. Acta - Biomembr.* 1758 (2006) 2080–2095. <https://doi.org/10.1016/j.bbamem.2006.06.021>.
- [83] B.L. Lew, Y. Cho, J. Kim, W.Y. Sim, N.I. Kim, Ceramides and cell signaling molecules in psoriatic epidermis: Reduced levels of ceramides, PKC- α , and JNK, *J. Korean Med. Sci.* 21 (2006) 95–99. <https://doi.org/10.3346/jkms.2006.21.1.95>.
- [84] E. Proksch, J.M. Jensen, P.M. Elias, Skin lipids and epidermal differentiation in atopic dermatitis, *Clin. Dermatol.* 21 (2003) 134–144. [https://doi.org/10.1016/S0738-081X\(02\)00370-X](https://doi.org/10.1016/S0738-081X(02)00370-X).
- [85] J. Rogers, C. Harding, A. Mayo, J. Banks, A. Rawlings, Stratum corneum lipids: The effect of ageing and the seasons, *Arch. Dermatol. Res.* 288 (1996) 765–770. <https://doi.org/10.1007/BF02505294>.
- [86] A.W. Armstrong, C. Read, Pathophysiology, Clinical Presentation, and Treatment of Psoriasis: A Review, *JAMA - J. Am. Med. Assoc.* 323 (2020) 1945–1960. <https://doi.org/10.1001/jama.2020.4006>.
- [87] M. Boguniewicz, L. Fonacier, E. Guttman-Yassky, P.Y. Ong, J. Silverberg, J.R. Farrar, Atopic dermatitis yardstick: Practical recommendations for an evolving therapeutic landscape, *Ann. Allergy, Asthma Immunol.* 120 (2018) 10-22.e2. <https://doi.org/10.1016/j.anai.2017.10.039>.
- [88] L. Yang, M. Mao-Qiang, M. Taljebini, P.M. Elias, K.R. Feingold, Topical stratum corneum lipids accelerate barrier repair after tape stripping, solvent treatment and some but not all types of detergent treatment, *Br. J. Dermatol.* 133 (1995) 679–685. <https://doi.org/10.1111/j.1365-2133.1995.tb02738.x>.
- [89] A. Vovesná, A. Zhigunov, M. Balouch, J. Zbytovská, Ceramide liposomes for skin barrier recovery: A novel formulation based on natural skin lipids, *Int. J. Pharm.* 596 (2021). <https://doi.org/10.1016/j.ijpharm.2021.120264>.
- [90] T. Schmitt, S. Lange, B. Dobner, S. Sonnenberger, T. Hauß, R.H.H. Neubert, Investigation of a CER[NP]- and [AP]-Based Stratum Corneum Modeling Membrane System: Using Specifically Deuterated CER Together with a Neutron Diffraction Approach, *Langmuir.* 34 (2018) 1742–1749. <https://doi.org/10.1021/acs.langmuir.7b01848>.
- [91] G. Brezesinski, H. Möhwald, Langmuir monolayers to study interactions at model membrane surfaces, *Adv. Colloid Interface Sci.* 100–102 (2003) 563–584. [https://doi.org/10.1016/S0001-8686\(02\)00071-4](https://doi.org/10.1016/S0001-8686(02)00071-4).

- [92] D. Vollhardt, V.B. Fainerman, Progress in characterization of Langmuir monolayers by consideration of compressibility, *Adv. Colloid Interface Sci.* 127 (2006) 83–97. <https://doi.org/10.1016/j.cis.2006.11.006>.
- [93] K. Gerwert, C. Kötting, Fourier transform infrared (FTIR) spectroscopy, *Encycl. Life Sci.* (2010). <https://doi.org/10.5650/jos1956.32.586>.
- [94] A. Blume, M. Jansen, M. Ghyczy, J. Gareiss, Interaction of phospholipid liposomes with lipid model mixtures for stratum corneum lipids, *Int. J. Pharm.* 99 (1993) 219–228. [https://doi.org/10.1016/0378-5173\(93\)90364-L](https://doi.org/10.1016/0378-5173(93)90364-L).
- [95] R. Mendelsohn, G. Mao, C.R. Flach, Infrared reflection-absorption spectroscopy: Principles and applications to lipid-protein interaction in Langmuir films, *Biochim. Biophys. Acta - Biomembr.* 1798 (2010) 788–800. <https://doi.org/10.1016/j.bbamem.2009.11.024>.
- [96] C.R. Flach, J.W. Brauner, J.W. Taylor, R.C. Baldwin, R. Mendelsohn, External reflection FTIR of peptide monolayer films in situ at the air/water interface: experimental design, spectra-structure correlations, and effects of hydrogen-deuterium exchange, *Biophys. J.* 67 (1994) 402–410. [https://doi.org/10.1016/S0006-3495\(94\)80495-3](https://doi.org/10.1016/S0006-3495(94)80495-3).
- [97] E. Prince, Diffraction: X-ray, neutron and electron, in: *Encycl. Chem. Phys. Phys. Chem.*, Moore, J,H, Bristol, (2001).
- [98] Wim H. De Jeu, *Basic X-ray scattering for soft matter*, Oxford, (2016).
- [99] V.M. Kaganer, H. Möhwald, P. Dutta, Structure and phase transitions in Langmuir monolayers, *Rev. Mod. Phys.* 71 (1999) 779–819.
- [100] C. Stefaniu, G. Brezesinski, X-ray investigation of monolayers formed at the soft air/water interface, *Curr. Opin. Colloid Interface Sci.* 19 (2014) 216–227. <https://doi.org/10.1016/j.cocis.2014.01.004>.
- [101] D. Marsh, Lateral order in gel, subgel and crystalline phases of lipid membranes: Wide-angle X-ray scattering, *Chem. Phys. Lipids.* 165 (2012) 59–76. <https://doi.org/10.1016/j.chemphyslip.2011.11.001>.
- [102] G. PABST, Global Properties of Biomimetic Membranes: Perspectives on Molecular Features, *Biophys. Rev. Lett.* 01 (2006) 57–84. <https://doi.org/10.1142/s1793048006000069>.
- [103] B.L. Stottrup, A.H. Nguyen, E. Tüzel, Taking another look with fluorescence microscopy : Image processing techniques in Langmuir monolayers for the twenty- first century, *BBA - Biomembr.* 1798 (2010) 1289–1300. <https://doi.org/10.1016/j.bbamem.2010.01.003>.
- [104] P. Senthil Kumar, K. Grace Pavithra, M. Naushad, Characterization techniques for nanomaterials, Elsevier Inc., 2019. <https://doi.org/10.1016/B978-0-12-813337-8.00004-7>.
- [105] G.W. Stachowiak, A.W. Batchelor, G.B. Stachowiak, 8 - Surface micrography and analysis, in: *Tribol. Ser.*, (2004): pp. 165–220. [https://doi.org/10.1016/s0167-8922\(04\)80024-5](https://doi.org/10.1016/s0167-8922(04)80024-5).
- [106] R. Pecora, Dynamic Light Scattering Measurement of Nanometer Particles in Liquids, *J. Nanoparticle Res.* 2 (2000) 123–131. <https://doi.org/10.1023/A:1010067107182>.
- [107] S. Bhattacharjee, DLS and zeta potential – What they are and what they are not?, *J. Control. Release.* 235 (2016) 337–351. <https://doi.org/https://doi.org/10.1016/j.jconrel.2016.06.017>.
- [108] R.R.L. De Oliveira, D.A.C. Albuquerque, T.G.S. Cruz, F.M. Yamaji, F.L. Leite,

- Measurement of the Nanoscale Roughness by Atomic Force Microscopy: Basic Principles and Applications, in: InTech, 2012. <https://doi.org/10.5772/37583>.
- [109] L.M. Menon GK, Cleary GW, The structure and function of the stratum corneum., *Int J Pharm.* . 435 (2012) 3–9. <https://doi.org/10.1016/j.ijpharm.2012.06.005>.
- [110] K.A. Walters, M. Dekker, *Dermatological and Transdermal Formulations*, 2002. <https://doi.org/10.1201/9780824743239>.
- [111] K.A. Holbrook, G.F. Odland, Regional differences in the thickness (cell layers) of the human stratum corneum: an ultrastructural analysis, *J. Invest. Dermatol.* 62 (1974) 415–422. <https://doi.org/10.1111/1523-1747.ep12701670>.
- [112] M.A. Lampe, A.L. Burlingame, J. Whitney, M.L. Williams, B.E. Brown, E. Roitman, P.M. Elias, Human stratum corneum lipids: characterization and regional variations., *J. Lipid Res.* 24 (1983) 120–30. <http://www.ncbi.nlm.nih.gov/pubmed/6833889>.
- [113] R. Notman, J. Anwar, Breaching the skin barrier - Insights from molecular simulation of model membranes, *Adv. Drug Deliv. Rev.* 65 (2013) 237–250. <https://doi.org/10.1016/j.addr.2012.02.011>.
- [114] M.N. Pastore, Y.N. Kalia, M. Horstmann, M.S. Roberts, Transdermal patches: History, development and pharmacology, *Br. J. Pharmacol.* 172 (2015) 2179–2209. <https://doi.org/10.1111/bph.13059>.
- [115] T. Marjukka Suhonen, J. A. Bouwstra, A. Urtti, Chemical enhancement of percutaneous absorption in relation to stratum corneum structural alterations, *J. Control. Release.* 59 (1999) 149–161. [https://doi.org/10.1016/S0168-3659\(98\)00187-4](https://doi.org/10.1016/S0168-3659(98)00187-4).
- [116] K. Saroha, S. Nanda, S. Rani, Chemical Penetration Enhancers : a Novel Approach in Transdermal Drug Delivery System, *Int J Curr Pharm Res*, 3 (2011), 5-9.
- [117] G.M.M. El Maghraby, A.C. Williams, B.W. Barry, Interactions of surfactants (edge activators) and skin penetration enhancers with liposomes, *Int. J. Pharm.* 276 (2004) 143–161. <https://doi.org/10.1016/j.ijpharm.2004.02.024>.
- [118] N. Dragicevic, H.I. Maibach, Percutaneous penetration enhancers chemical methods in penetration enhancement: Modification of the stratum corneum, *Percutaneous Penetration Enhanc. Chem. Methods Penetration Enhanc. Modif. Strat. Corneum.* (2015) 1–411. <https://doi.org/10.1007/978-3-662-47039-8>.
- [119] I. Som, K. Bhatia, M. Yasir, Status of surfactants as penetration enhancers in transdermal drug delivery, *J. Pharm. Bioallied Sci.* 4 (2012) 2–9. <https://doi.org/10.4103/0975-7406.92724>.
- [120] F. Cilurzo, G. Vistoli, F. Selmin, C.G.M. Gennari, U.M. Musazzi, S. Franzé, M. Lo Monte, P. Minghetti, An Insight into the Skin Penetration Enhancement Mechanism of N-Methylpyrrolidone, *Mol. Pharm.* 11 (2014) 1014–1021. <https://doi.org/10.1021/mp400675d>.
- [121] H. Trommer, R.H.H. Neubert, Overcoming the Stratum Corneum: The Modulation of Skin Penetration, *Skin Pharmacol. Physiol.* 19 (2006) 106–121. <https://doi.org/10.1159/000091978>.
- [122] B. Sapra, S. Jain, A.K. Tiwary, Percutaneous Permeation Enhancement by Terpenes: Mechanistic View, *AAPS J.* 10 (2008) 120–132. <https://doi.org/10.1208/s12248-008-9012-0>.
- [123] H. Moehwald, G. Brezesinski, From Langmuir Monolayers to Multilayer Films, *Langmuir*, (2016), 10445-10458. <https://doi.org/10.1021/acs.langmuir.6b02518>.
- [124] A. López-Castellano, C. Cortell-Ivars, G. López-Carballo, M. Herráez-Domínguez, The

- influence of Span®20 on stratum corneum lipids in Langmuir monolayers: Comparison with Azone®, *Int. J. Pharm.* 203 (2000) 245–253. [https://doi.org/10.1016/S0378-5173\(00\)00463-4](https://doi.org/10.1016/S0378-5173(00)00463-4).
- [125] M.N. Todosijević, G. Brezesinski, S.D. Savić, R.H.H. Neubert, Sucrose esters as biocompatible surfactants for penetration enhancement: An insight into the mechanism of penetration enhancement studied using stratum corneum model lipids and Langmuir monolayers, *Eur. J. Pharm. Sci.* 99 (2017) 161–172. <https://doi.org/10.1016/j.ejps.2016.12.002>.
- [126] S. Lange, T. Schmitt, R.H.H. Neubert, S. Sonnenberger, B. Dobner, T. Hauß, Investigation of a CER[NP]- and [AP]-Based Stratum Corneum Modeling Membrane System: Using Specifically Deuterated CER Together with a Neutron Diffraction Approach, *Langmuir*. 34 (2017) 1742–1749. <https://doi.org/10.1021/acs.langmuir.7b01848>.
- [127] C. Stefaniu, G. Brezesinski, H. Möhwald, Langmuir monolayers as models to study processes at membrane surfaces, *Adv. Colloid Interface Sci.* 208 (2014) 197–213. <https://doi.org/10.1016/j.cis.2014.02.013>.
- [128] B. Moghaddam, M.H. Ali, J. Wilkhu, D.J. Kirby, A.R. Mohammed, Q. Zheng, Y. Perrie, The application of monolayer studies in the understanding of liposomal formulations, *Int. J. Pharm.* 417 (2011) 235–244. <https://doi.org/10.1016/j.ijpharm.2011.01.020>.
- [129] G. Mao, D. Vanwyck, X. Xiao, M.C. Mack Correa, E. Gunn, C.R. Flach, R. Mendelsohn, R.M. Walters, Oleic acid disorders stratum corneum lipids in langmuir monolayers, *Langmuir*. 29 (2013) 4857–4865. <https://doi.org/10.1021/la4002384>.
- [130] P. Pullmannová, L. Pavlíková, A. Kováčik, M. Sochorová, B. Školová, P. Slepíčka, J. Maixner, J. Zbytovská, K. Vávrová, Permeability and microstructure of model stratum corneum lipid membranes containing ceramides with long (C16) and very long (C24) acyl chains, *Biophys. Chem.* 224 (2017) 20–31. <https://doi.org/https://doi.org/10.1016/j.bpc.2017.03.004>.
- [131] P. Calvez, S. Bussièeres, Éric Demers, C. Salesse, Parameters modulating the maximum insertion pressure of proteins and peptides in lipid monolayers, *Biochimie*. 91 (2009) 718–733. <https://doi.org/10.1016/j.biochi.2009.03.018>.
- [132] W.R. Gombotz, S.C. Pankey, L.S. Bouchard, D.H. Phan, A.P. MacKenzie, Stability, Characterization, Formulation, and Delivery System Development for Transforming Growth Factor-Beta1, in: R. Pearlman, Y.J. Wang (Eds.), *Formul. Charact. Stab. Protein Drugs Case Hist. Case Hist.*, Springer US, Boston, MA, (2002): pp. 219–245. https://doi.org/10.1007/0-306-47452-2_4.
- [133] I. Kralova, J. Sjöblom, Surfactants Used in Food Industry: A Review, *J. Dispers. Sci. Technol.* 30 (2009) 1363–1383. <https://doi.org/10.1080/01932690902735561>.
- [134] K. Hill, C. Ach, Sugar-based surfactants for consumer products and technical applications, *Sugar-Based Surfactants Fundam. Appl.* (2008) 1–20. <https://doi.org/10.1201/9781420051674>.
- [135] T.D. Andreeva, J.G. Petrov, G. Brezesinski, H. Moehwald, Structure of the Langmuir monolayers with fluorinated ethyl amide and ethyl ester polar heads creating dipole potentials of opposite sign, *Langmuir*. 24 (2008) 8001–8007. <https://doi.org/10.1021/la8009282>.
- [136] R.P. Clark, Human Skin Temperature and Its Relevance in Physiology and Clinical Assessment, in: E.F.J. Ring, B. Phillips (Eds.), *Recent Adv. Med. Thermol.*, Springer New York, Boston, MA, (1984): pp. 5–15. https://doi.org/10.1007/978-1-4684-7697-2_2.
- [137] P. Dynarowicz-Łątka, K. Hąc-Wydro, Interactions between phosphatidylcholines and

- cholesterol in monolayers at the air/water interface, *Colloids Surfaces B Biointerfaces*. 37 (2004) 21–25. <https://doi.org/10.1016/j.colsurfb.2004.06.007>.
- [138] M.R. Vidal-Paruta, L.D. King, Critical micelle concentration of nonionic surfactants in water and carbon tetrachloride, *J. Pharm. Sci.* 53 (1964) 1217–1220. <https://doi.org/10.1002/jps.2600531020>.
- [139] A. Jelinek, H. Klocking, In vitro toxicity of surfactants in U937 cells : Cell membrane integrity and mitochondrial function *, 78 (1998). [https://doi.org/10.1016/S0940-2993\(98\)80036-5](https://doi.org/10.1016/S0940-2993(98)80036-5).
- [140] S. Makino, S. Ogimoto, S. Koga, Sucrose monoesters of fatty acids: Their properties and interaction with proteins, *Agric. Biol. Chem.* 47 (1983) 319–326. <https://doi.org/10.1080/00021369.1983.10865614>.
- [141] L.S.C. Wan, P.F.S. Lee, CMC of Polysorbates, *J. Pharm. Sci.* 63 (1974) 136–137. <https://doi.org/https://doi.org/10.1002/jps.2600630136>.
- [142] L. Kiss, É. Hellinger, A. Pilbat, Á. Kittel, Z. Török, A. Füredi, G. Szakács, S. Veszelka, P. Sipos, B. Ózsvári, L.G. Puskás, M. Vastag, P. Szabó-Révész, M.A. Deli, Sucrose Esters Increase Drug Penetration, But Do Not Inhibit P-Glycoprotein in Caco-2 Intestinal Epithelial Cells, *J. Pharm. Sci.* 103 (2014) 3107–3119. <https://doi.org/https://doi.org/10.1002/jps.24085>.
- [143] N. Akhtar, M.U. Rehman, H.M.S. Khan, F. Rasool, T. Saeed, G. Murtaza, Penetration enhancing effect of polysorbate 20 and 80 on the in vitro percutaneous absorption of L-ascorbic acid, *Trop. J. Pharm. Res.* 10 (2011) 281–288. <https://doi.org/10.4314/tjpr.v10i3.1>.
- [144] A. Szuts, P. Szabó-Révész, Sucrose esters as natural surfactants in drug delivery systems - A mini-review, *Int. J. Pharm.* 433 (2012) 1–9. <https://doi.org/10.1016/j.ijpharm.2012.04.076>.
- [145] T.J. Hall-Manning, G.H. Holland, G. Rennie, P. Revell, J. Hines, M.D. Barratt, D.A. Basketter, Skin irritation potential of mixed surfactant systems, *Food Chem. Toxicol.* 36 (1998) 233–238. [https://doi.org/10.1016/S0278-6915\(97\)00144-0](https://doi.org/10.1016/S0278-6915(97)00144-0).
- [146] P.N. Moore, S. Puvvada, D. Blankschtein, Challenging the surfactant monomer skin penetration model: Penetration of sodium dodecyl sulfate micelles into the epidermis, *J. Cosmet. Sci.* 54 (2003) 29–46.
- [147] D. Marsh, Lateral pressure in membranes, *Biochim. Biophys. Acta - Rev. Biomembr.* 1286 (1996) 183–223. [https://doi.org/10.1016/S0304-4157\(96\)00009-3](https://doi.org/10.1016/S0304-4157(96)00009-3).
- [148] R.G. Snyder, H.L. Strauss, C.A. Elliger, Carbon-hydrogen stretching modes and the structure of n-alkyl chains. 1. Long, disordered chains, *J. Phys. Chem.* 86 (1982) 5145–5150. <https://doi.org/10.1021/j100223a018>.
- [149] E. Csányi, S. Berkó, P. Szabó-Révész, O. Berkesi, E. Csizmazia, G. Erős, Ibuprofen penetration enhance by sucrose ester examined by ATR-FTIR in vivo, *Pharm. Dev. Technol.* 17 (2010) 125–128. <https://doi.org/10.3109/10837450.2010.508076>.
- [150] A. Blume, A. Kerth, Peptide and protein binding to lipid monolayers studied by FT-IRRA spectroscopy, *Biochim. Biophys. Acta - Biomembr.* 1828 (2013) 2294–2305. <https://doi.org/10.1016/j.bbamem.2013.04.014>.
- [151] H.M. McConnell, Structures and Transitions in Lipid Monolayers Monola at the Air-Water Interface, *Annu. Rev. Phys. Chem.* (1991) 171–195.
- [152] A. Radhakrishnan, T.G. Anderson, H.M. McConnell, Condensed complexes, rafts, and the chemical activity of cholesterol in membranes, *Proc. Natl. Acad. Sci. U. S. A.* 97

- (2000) 12422–12427. <https://doi.org/10.1073/pnas.220418097>.
- [153] P.M. Elias, The Epidermal Permeability Barrier: From the Early Days at Harvard to Emerging Concepts, *J. Invest. Dermatol.* 122 (2004) xxxvi–xxxix. <https://doi.org/10.1046/j.0022-202x.2004.22233.x>.
- [154] P.M. Elias, Stratum Corneum Defensive Functions : An Integrated View, *J. Invest. Dermatol.* 125 (2005) 183–200. <https://doi.org/10.1111/j.0022-202X.2005.23668.x>.
- [155] B. Skolova, B. Janusova, J. Zbytovska, goori, Ceramides in the Skin Lipid Membranes: Length Matters, *Langmuir.* 29 (2013) 15624–15633. <https://doi.org/dx.doi.org/10.1021/la4037474> | *Langmuir* 2013, 29, 15624–15633.
- [156] A.S. Breathnach, T. Goodman, C. Stolinski, M. Gross, Freeze-fracture replication of cells of stratum corneum of human epidermis, *J. Anat.* 114 (1973) 65–81.
- [157] M.W. De Jager, G.S. Gooris, M. Ponec, J.A. Bouwstra, Lipid mixtures prepared with well-defined synthetic ceramides closely mimic the unique stratum corneum lipid phase behavior, *J. Lipid Res.* 46 (2005) 2649–2656. <https://doi.org/10.1194/jlr.M500221-JLR200>.
- [158] T.J. McIntosh, M.E. Stewart, D.T. Downing, X-ray Diffraction Analysis of Isolated Skin Lipids : Reconstitution of Intercellular, *Biochemistry.* 35 (1996) 3649–3653. <https://doi.org/10.1021/bi952762q>.
- [159] B. Školová, B. Janůšová, K. Vávrová, Ceramides with a pentadecasphingosine chain and short acyls have strong permeabilization effects on skin and model lipid membranes, *Biochim. Biophys. Acta - Biomembr.* 1858 (2016) 220–232. <https://doi.org/10.1016/j.bbamem.2015.11.019>.
- [160] B. Janůšová, J. Zbytovská, P. Lorenc, H. Vavrysová, K. Palát, A. Hrabálek, K. Vávrová, Effect of ceramide acyl chain length on skin permeability and thermotropic phase behavior of model stratum corneum lipid membranes, *Biochim. Biophys. Acta - Mol. Cell Biol. Lipids.* 1811 (2011) 129–137. <https://doi.org/https://doi.org/10.1016/j.bbalip.2010.12.003>.
- [161] X. Li, Li, Tang, K.G. Taylor, D.B. Dupre, M.C. Yappert, Conformational Characterization of Ceramides by Nuclear Magnetic Resonance Spectroscopy, *Biophys. J.* 82 (2002) 2067–2080. [https://doi.org/10.1016/S0006-3495\(02\)75554-9](https://doi.org/10.1016/S0006-3495(02)75554-9).
- [162] F. Strati, R.H.H. Neubert, L. Opálka, A. Kerth, G. Brezesinski, Non-ionic surfactants as innovative skin penetration enhancers : insight in the mechanism of interaction with simple 2D stratum corneum model system, *Eur. J. Pharm. Sci.* 157 (2020). <https://doi.org/10.1016/j.ejps.2020.105620>.
- [163] M.E. Rerek, H. Chen, B. Markovic, D. Van Wyck, P. Garidel, R. Mendelsohn, D.J. Moore, Phytosphingosine and Sphingosine Ceramide Headgroup Hydrogen Bonding : Structural Insights through Thermotropic Hydrogen / Deuterium Exchange, *J. Phys. Chem. B.* 105 (2001) 9355–9362. <https://doi.org/10.1021/jp0118367>.
- [164] L.E. Uche, G.S. Gooris, C.M. Beddoes, J.A. Bouwstra, New insight into phase behavior and permeability of skin lipid models based on sphingosine and phytosphingosine ceramides, *Biochim. Biophys. Acta - Biomembr.* 1861 (2019) 1317–1328. <https://doi.org/10.1016/j.bbamem.2019.04.005>.
- [165] B. Westerlund, P.-M. Grandell, Y.J.E. Isaksson, J.P. Slotte, Ceramide acyl chain length markedly influences miscibility with palmitoyl sphingomyelin in bilayer membranes, *Eur. Biophys. J.* 39 (2010) 1117–1128. <https://doi.org/10.1007/s00249-009-0562-6>.
- [166] J.M. Holopainen, J. Lemmich, F. Richter, O.G. Mouritsen, G. Rapp, P.K.J. Kinnunen, Dimyristoylphosphatidylcholine / C16: 0-Ceramide Binary Liposomes Studied by

- Differential Scanning Calorimetry and Wide- and Small-Angle X-Ray Scattering, *Biophys. J.* 78 (2000) 2459–2469.
- [167] S. Raudenkolb, S. Wartewig, R.H.H. Neubert, Polymorphism of ceramide 6 : a vibrational spectroscopic and X-ray powder diffraction investigation of the diastereomers of N-(α -hydroxyoctadecanoyl)-phytosphingosine, *Chem. Phys. Lipids.* 133 (2005) 89–102. <https://doi.org/10.1016/j.chemphyslip.2004.09.015>.
- [168] K. Kjaer, J. Als-Nielsen, C.A. Helm, L.A. Laxhuber, H. Möhwald, Ordering in lipid monolayers studied by synchrotron x-ray diffraction and fluorescence microscopy, *Phys. Rev. Lett.* 58 (1987) 2224–2227. <https://doi.org/10.1103/PhysRevLett.58.2224>.
- [169] D.J.F. Leveiller, S.P.W.M. Lahav, L.L.K. Kjaer, Crystal Structures of Self-Aggregates of Insoluble Aliphatic Amphiphilic Molecules at the Air-Water Interface . An X-ray Synchrotron Study, *J. Am. Chem. Soc.* 113 (1991) 7684–7691. <https://doi.org/10.1021/ja00020a034>.
- [170] K. Kjaer, Some simple ideas on X-ray reflection and grazing-incidence diffraction from thin surfactant films, *Phys. B Phys. Condens. Matter.* 198 (1994) 100–109. [https://doi.org/10.1016/0921-4526\(94\)90137-6](https://doi.org/10.1016/0921-4526(94)90137-6).
- [171] P. Garidel, Calorimetric and spectroscopic investigations of phytosphingosine ceramide membrane organisation, *Phys. Chem. Chem. Phys.* 4 (2002) 1934–1942. <https://doi.org/10.1039/b108769j>.
- [172] I. Pascher, S. Sundell, Molecular arrangements in sphingolipids : crystal structure of the ceramide, *Chem. Phys. Lipids.* 61 (1992) 79–86.
- [173] E.E. Kooijman, D. Vaknin, W. Bu, L. Joshi, S. Kang, A. Gericke, E.K. Mann, S. Kumar, Structure of Ceramide-1-Phosphate at the Air-Water Solution Interface in the Absence and Presence of Ca²⁺, *Biophys. J.* 96 (2009) 2204–2215. <https://doi.org/10.1016/j.bpj.2008.11.062>.
- [174] C. Stefaniu, I. Vilotijevic, M. Santer, D.V. Silva, G. Brezesinski, P.H. Seeberger, Subgel Phase Structure in Monolayers of Glycosylphosphatidylinositol Glycolipids**, *Angew. Chemie - Int. Ed.* 51 (2012) 12874–12878. <https://doi.org/10.1002/anie.201205825>.
- [175] J.N. Israelachvili, *Intermolecular and Surface Forces*, 3rd ed., (2011). <https://doi.org/https://doi.org/10.1016/C2009-0-21560-1>.
- [176] C. Tanford, *The Hydrophobic Effect: Formation of Micelles and Biological Membranes* (2nd Edition), *Biochem. Soc. Trans.* 9 (1981) 178. <https://doi.org/10.1042/bst0090178>.
- [177] J. Katsaras, J. Raghunathan, V. Dufourc, E.J. Duforcq, Evidence for a Two-Dimensional Molecular Lattice in Subgel Phase DPPC Bilayers, *Biochemistry.* 34 (1995) 4684–4688.
- [178] N. Albon, Transitions and molecular packing in highly purified 1,2-dipalmitoyl-phosphatidyl choline–water phases. II. The structures of DPPC phases with low water content, *J. Chem. Phys.* 79 (1983) 469–476. <https://doi.org/10.1063/1.445545>.
- [179] H. Löfgren, I. Pascher, Molecular arrangements of sphingolipids. The monolayer behaviour of ceramides, *Chem. Phys. Lipids.* 20 (1977) 273–284.
- [180] J.M. Boggs, Lipid intermolecular hydrogen bonding: influence on structural organization and membrane function, *BBA - Rev. Biomembr.* 906 (1987) 353–404. [https://doi.org/10.1016/0304-4157\(87\)90017-7](https://doi.org/10.1016/0304-4157(87)90017-7).
- [181] D. Vaknin, M.S. Kelley, The Structure of D-Erythro-C18 Ceramide at the Air-Water Interface, *Biophys. J.* 79 (2000) 2616–2623. [https://doi.org/10.1016/S0006-3495\(00\)76500-3](https://doi.org/10.1016/S0006-3495(00)76500-3).
- [182] J. Blazek, E.P. Gilbert, Application of small-angle X-ray and neutron scattering

- techniques to the characterisation of starch structure: A review, *Carbohydr. Polym.* 85 (2011) 281–293. <https://doi.org/10.1016/j.carbpol.2011.02.041>.
- [183] M.A. Kiselev, Conformation of ceramide 6 molecules and chain-flip transitions in the lipid matrix of the outermost layer of mammalian skin, the stratum corneum, *Crystallogr. Reports.* 52 (2007) 525–528. <https://doi.org/10.1134/S1063774507030340>.
- [184] Y. Badhe, R. Gupta, B. Rai, Development and application of coarse-grained MARTINI model of skin lipid ceramide [AP], *J. Mol. Model.* 26 (2020). <https://doi.org/10.1007/s00894-020-04435-z>.
- [185] T. Schmitt, S. Lange, S. Sonnenberger, B. Dobner, B. Demé, R.H.H. Neubert, G. Gooris, J.A. Bouwstra, Determination of the influence of C24 D/(2R)- and L/(2S)-isomers of the CER[AP] on the lamellar structure of stratum corneum model systems using neutron diffraction, *Chem. Phys. Lipids.* 209 (2017) 29–36. <https://doi.org/10.1016/j.chemphyslip.2017.11.001>.
- [186] M.E. Rerek, D. Van Wyck, R. Mendelsohn, D.J. Moore, FTIR spectroscopic studies of lipid dynamics in phytosphingosine ceramide models of the stratum corneum lipid matrix, *Chem. Phys. Lipids.* 134 (2005) 51–58. <https://doi.org/10.1016/j.chemphyslip.2004.12.002>.
- [187] R.A. MacPhail, H.L. Strauss, R.G. Snyder, C.A. Eiliger, C-H stretching modes and the structure of n-alkyl chains. 2. Long, all-trans chains, *J. Phys. Chem.* 88 (1984) 334–341. <https://doi.org/10.1021/j150647a002>.
- [188] E. Proksch, J.M. Brandner, J.M. Jensen, The skin: An indispensable barrier, *Exp. Dermatol.* 17 (2008) 1063–1072. <https://doi.org/10.1111/j.1600-0625.2008.00786.x>.
- [189] P.M. Elias, K.R. Feingold, M. Mao-qiang, P.M. Elias, K.R. Feingold, Fatty acids are required for epidermal permeability barrier function . Fatty Acids Are Required for Epidermal Permeability Barrier Function, *J. Clin. Invest.* 92 (1993) 791–798.
- [190] A. Imokawa, G. Abe, A. Jin, K. Higaki, Y. Kawashima, M. Hidano, Decreased level of Ceramides in Stratum Corneum of Atopic Dermatitis: An Etiologic Factor in Atopic Dry Skin?, *J. Invest. Dermatol.* 96 (1991) 523–526.
- [191] F.F. Sahle, J. Wohlrab, R.H.H. Neubert, Controlled penetration of ceramides into and across the stratum corneum using various types of microemulsions and formulation associated toxicity studies, *Eur. J. Pharm. Biopharm.* 86 (2014) 244–250. <https://doi.org/10.1016/j.ejpb.2013.07.011>.
- [192] F.F. Sahle, H. Metz, J. Wohlrab, R.H.H. Neubert, Lecithin-based microemulsions for targeted delivery of Ceramide AP into the stratum corneum: Formulation, characterizations, and in vitro release and penetration studies, *Pharm. Res.* 30 (2013) 538–551. <https://doi.org/10.1007/s11095-012-0899-x>.
- [193] S. Heuschkel, A. Goebel, R.H.H. Neubert, Microemulsions—Modern Colloidal Carrier for Dermal and Transdermal Drug Delivery, *J. Pharm. Sci.* 97 (2008) 603–631. <https://doi.org/https://doi.org/10.1002/jps.20995>.
- [194] R. Abdelgawad, M. Nasr, N.H. Moftah, M.Y. Hamza, Phospholipid membrane tubulation using ceramide doping “Cerosomes”: Characterization and clinical application in psoriasis treatment, *Eur. J. Pharm. Sci.* 101 (2017) 258–268. <https://doi.org/10.1016/j.ejps.2017.02.030>.
- [195] V. V. Kumar, Complementary molecular shapes and additivity of the packing parameter of lipids, *Proc. Natl. Acad. Sci. USA.* 88 (1991) 444–448. <https://doi.org/10.1073/pnas.88.2.444>.
- [196] E. Khazanov, A. Prieve, J.P. Shillemans, Y. Barenholz, Physicochemical and biological

- characterization of ceramide-containing liposomes: Paving the way to ceramide therapeutic application, *Langmuir*. 24 (2008) 6965–6980. <https://doi.org/10.1021/la800207z>.
- [197] J. Mueller, J.S.L. Oliveira, R. Barker, M. Trapp, A. Schroeter, G. Brezesinski, R.H.H. Neubert, The effect of urea and taurine as hydrophilic penetration enhancers on stratum corneum lipid models, *Biochim. Biophys. Acta - Biomembr.* 1858 (2016) 2006–2018. <https://doi.org/10.1016/j.bbamem.2016.05.010>.
- [198] A. Fathi-Azarbayjani, K.X. Ng, Y.W. Chan, S.Y. Chan, Lipid Vesicles for the Skin Delivery of Diclofenac: Cerosomes vs. Other Lipid Suspensions, *Adv. Pharm. Bull.* 5 (2015) 25–33. <https://doi.org/10.5681/apb.2015.004>.
- [199] J.E. Chang, H.J. Cho, E. Yi, D.D. Kim, S. Jheon, Hypocrellin B and paclitaxel-encapsulated hyaluronic acid-ceramide nanoparticles for targeted photodynamic therapy in lung cancer, *J. Photochem. Photobiol. B Biol.* 158 (2016) 113–121. <https://doi.org/10.1016/j.jphotobiol.2016.02.035>.
- [200] S.M. Jung, G.H. Yoon, H.C. Lee, M.H. Jung, S. Il Yu, S.J. Yeon, S.K. Min, Y.S. Kwon, J.H. Hwang, H.S. Shin, Thermodynamic Insights and Conceptual Design of Skin-Sensitive Chitosan Coated Ceramide/PLGA Nanodrug for Regeneration of Stratum Corneum on Atopic Dermatitis, *Sci. Rep.* 5 (2015) 1–12. <https://doi.org/10.1038/srep18089>.
- [201] G.Y. Noh, J.Y. Suh, S.N. Park, Ceramide-based nanostructured lipid carriers for transdermal delivery of isoliquiritigenin: Development, physicochemical characterization, and in vitro skin permeation studies, *Korean J. Chem. Eng.* 34 (2017) 400–406. <https://doi.org/10.1007/s11814-016-0267-3>.
- [202] A.D. Bangham, M.M. Standish, J.C. Watkins, Diffusion of univalent ions across the lamellae of swollen phospholipids, *J. Mol. Biol.* 13 (1965) 238–252. [https://doi.org/10.1016/S0022-2836\(65\)80093-6](https://doi.org/10.1016/S0022-2836(65)80093-6).
- [203] C.H. Tian, G. Zorinants, R. Gronheid, M. Van Der Auweraer, F.C. De Schryver, Confocal fluorescence microscopy and AFM of thiocyanine J aggregates in Langmuir-Schaefer monolayers, *Langmuir*. 19 (2003) 9831–9840. <https://doi.org/10.1021/la034817s>.
- [204] D. Kessner, A. Ruettinger, M.A. Kiselev, S. Wartewig, R.H.H. Neubert, Properties of ceramides and their impact on the stratum corneum structure: A review - Part 2: Stratum corneum lipid model systems, *Skin Pharmacol. Physiol.* 21 (2008) 58–74. <https://doi.org/10.1159/000112956>.
- [205] C. Das, P.D. Olmsted, The physics of stratum corneum lipid membranes, *Philos. Trans. R. Soc. A Math. Phys. Eng. Sci.* 374 (2016). <https://doi.org/10.1098/rsta.2015.0126>.
- [206] G. Brezesinski, E. Schneck, Investigating Ions at Amphiphilic Monolayers with X-ray Fluorescence, *Langmuir*. 35 (2019) 8531–8542. <https://doi.org/10.1021/acs.langmuir.9b00191>.
- [207] B.A. Čuríková-Kindlová, O. Diat, F. Štěpánek, K. Vávrová, J. Zbytovská, Probing the interactions among sphingosine and phytosphingosine ceramides with non- and alpha-hydroxylated acyl chains in skin lipid model membranes, *Int. J. Pharm.* 563 (2019) 384–394. <https://doi.org/10.1016/j.ijpharm.2019.04.010>.
- [208] J. Zbytovská, M.A. Kiselev, S.S. Funari, V.M. Garamus, S. Wartewig, K. Palát, R. Neubert, Aspects Influence of cholesterol on the structure of stratum corneum lipid model membrane, *Colloids Surf. A Physicochem. Eng. Asp.* 328 (2008) 90–99. <https://doi.org/10.1016/j.colsurfa.2008.06.032>.
- [209] F. Arends, H. Chaudhary, P. Janmey, M.M.A.E. Claessens, O. Lieleg, Lipid Head Group

- Charge and Fatty Acid Configuration Dictate Liposome Mobility in Neurofilament Networks, *Macromol. Biosci.* 17 (2017) 1600229. <https://doi.org/10.1002/mabi.201600229>.
- [210] P. Dreher, F. Walde, P. Luisi, P.L. Elsner, Human skin irritation studies of a lecithin microemulsion gel and of lecithin liposomes, *Ski. Pharmacol.* 9 (1996) 124–126.
- [211] B. Heurtault, P. Saulnier, B. Pech, J.E. Proust, J.P. Benoit, Physico-chemical stability of colloidal lipid particles, *Biomaterials.* 24 (2003) 4283–4300. [https://doi.org/10.1016/S0142-9612\(03\)00331-4](https://doi.org/10.1016/S0142-9612(03)00331-4).
- [212] P.J. Kadu, S.S. Kushare, D.D. Thacker, S.G. Gattani, Enhancement of oral bioavailability of atorvastatin calcium by self-emulsifying drug delivery systems (SEDDS), *Pharm. Dev. Technol.* 16 (2011) 65–74. <https://doi.org/10.3109/10837450903499333>.
- [213] H. Lambers, S. Piessens, A. Bloem, H. Pronk, P. Finkel, Natural skin surface pH is on average below 5, which is beneficial for its resident flora, *Int. J. Cosmet. Sci.* 28 (2006) 359–370. <https://doi.org/10.1111/j.1467-2494.2006.00344.x>.
- [214] J. Blaak, P. Staib, The Relation of pH and Skin Cleansing, *Curr. Probl. Dermatology.* 54 (2018) 132–142. <https://doi.org/10.1159/000489527>.
- [215] A. Blume, A. Kerth, Peptide and protein binding to lipid monolayers studied by FT-IRRA spectroscopy, *Biochim. Biophys. Acta - Biomembr.* 1828 (2013) 2294–2305. <https://doi.org/10.1016/j.bbmem.2013.04.014>.
- [216] A. Schlaich, A.P. Dos Santos, R.R. Netz, Simulations of Nanoseparated Charged Surfaces Reveal Charge-Induced Water Reorientation and Nonadditivity of Hydration and Mean-Field Electrostatic Repulsion, *Langmuir.* 35 (2019) 551–560. <https://doi.org/10.1021/acs.langmuir.8b03474>.
- [217] L. Fumagalli, A. Esfandiari, R. Fabregas, S. Hu, P. Ares, A. Janardanan, Q. Yang, B. Radha, T. Taniguchi, K. Watanabe, G. Gomila, K.S. Novoselov, A.K. Geim, Anomalously low dielectric constant of confined water, *Science (80-.)*. 360 (2018) 1339–1342. <https://doi.org/10.1126/science.aat4191>.
- [218] T. Mukhina, A. Hemmerle, V. Rondelli, Y. Gerelli, G. Fragneto, J. Daillant, T. Charitat, Attractive Interaction between Fully Charged Lipid Bilayers in a Strongly Confined Geometry, *J. Phys. Chem. Lett.* 10 (2019) 7195–7199. <https://doi.org/10.1021/acs.jpcllett.9b02804>.
- [219] V.M. Latza, B. Demé, E. Schneck, Membrane Adhesion via Glycolipids Occurs for Abundant Saccharide Chemistries, *Biophys. J.* 118 (2020) 1602–1611. <https://doi.org/10.1016/j.bpj.2020.02.003>.
- [220] T.J. McIntosh, A.D. Magid, S.A. Simon, Cholesterol Modifies the Short-Range Repulsive Interactions between Phosphatidylcholine Membranes, *Biochemistry.* 28 (1989) 17–25. <https://doi.org/10.1021/bi00427a004>.
- [221] B. Skolova, B. Janusova, J. Zbytovska, G. Gooris, J.A. Bouwstra, P. Slepíčka, P. Berka, J. Roh, K. Palát, A. Hrabálek, K. Vavrova, Ceramides in the Skin Lipid Membranes: Length Matters, *Langmuir.* 29 (2013) 15624–15633.
- [222] A. Ivankin, I. Kuzmenko, D. Gidalevitz, Cholesterol-Phospholipid Interactions: New Insights from Surface X-Ray Scattering Data, *Phys. Rev. Lett.* 104 (2010) 108101. <https://doi.org/10.1103/PhysRevLett.104.108101>.
- [223] F. Strati, J.S.L. Oliveira, L. Opalka, T. Mukhina, B. Dobner, R.H.H. Neubert, G. Brezesinski, 2D and 3D Physical-Chemical Characterization of CER[AP]: A Study of Stereochemistry and Chain Symmetry, *J. Phys. Chem. B.* 125 (2021) 9960–9969.

- [224] C.A. Keller, B. Kasemo, Surface specific kinetics of lipid vesicle adsorption measured with a quartz crystal microbalance, *Biophys. J.* 75 (1998) 1397–1402. [https://doi.org/10.1016/S0006-3495\(98\)74057-3](https://doi.org/10.1016/S0006-3495(98)74057-3).
- [225] J.S.L. Oliveira, S. Lange, B. Dobner, G. Brezesinski, The effect of non-deuterated and deuterated isopropyl myristate on the thermodynamical and structural behavior of a 2D Stratum Corneum model with Ceramide [AP], *Chem. Phys. Lipids.* 204 (2017) 1–9. <https://doi.org/10.1016/j.chemphyslip.2017.02.002>.
- [226] K. Ekelund, E. Sparr, J. Engblom, H. Wennerstrom, S. Engstrom, The effect of cholesterol on fatty acid monolayers, *Proc. Control. Release Soc.* (1999) 403–404.
- [227] Y. Badhe, R. Gupta, B. Rai, Structural and barrier properties of the skin ceramide lipid bilayer: a molecular dynamics simulation study, *J. Mol. Model.* 25 (2019). <https://doi.org/10.1007/s00894-019-4008-5>.
- [228] L. Scheffer, I. Solomonov, M.J. Weygand, K. Kjaer, L. Leiserowitz, L. Addadi, Structure of cholesterol/ceramide monolayer mixtures: Implications to the molecular organization of lipid rafts, *Biophys. J.* 88 (2005) 3381–3391. <https://doi.org/10.1529/biophysj.104.051870>.
- [229] E. Wang, J.B. Klauda, Molecular Dynamics Simulations of Ceramide and Ceramide-Phosphatidylcholine Bilayers, *J. Phys. Chem. B.* 121 (2017) 10091–10104. <https://doi.org/10.1021/acs.jpcc.7b08967>.
- [230] S. Abbott, *Surfactant Science: Principles & Practice*, (2017) 249.
- [231] J. Boyd, C. Parkinson, P. Sherman, Factors affecting emulsion stability, and the HLB concept, *J. Colloid Interface Sci.* 41 (1972) 359–370. [https://doi.org/https://doi.org/10.1016/0021-9797\(72\)90122-1](https://doi.org/https://doi.org/10.1016/0021-9797(72)90122-1).
- [232] N. Scholz, T. Behnke, U. Resch-Genger, Determination of the Critical Micelle Concentration of Neutral and Ionic Surfactants with Fluorometry, Conductometry, and Surface Tension—A Method Comparison, *J. Fluoresc.* 28 (2018) 465–476. <https://doi.org/10.1007/s10895-018-2209-4>.
- [233] A. Avdeef, The rise of PAMPA, *Expert Opin. Drug Metab. Toxicol.* 1 (2005) 325–342. <https://doi.org/10.1517/17425255.1.2.325>.
- [234] G. Ottaviani, S. Martel, P.A. Carrupt, Parallel artificial membrane permeability assay: A new membrane for the fast prediction of passive human skin permeability, *J. Med. Chem.* 49 (2006) 3948–3954. <https://doi.org/10.1021/jm060230+>.
- [235] B. Sinkó, T.M. Garrigues, G.T. Balogh, Z.K. Nagy, O. Tsinman, A. Avdeef, K. Takács-Novák, Skin-PAMPA: A new method for fast prediction of skin penetration, *Eur. J. Pharm. Sci.* 45 (2012) 698–707. <https://doi.org/10.1016/j.ejps.2012.01.011>.
- [236] J. Ponmozhi, S. Dhinakaran, Z. Varga-medveczky, K. Fónagy, L.A. Bors, K. Iván, F. Erdő, Development of skin-on-a-chip platforms for different utilizations: Factors to be considered, *Micromachines.* 12 (2021) 1–25. <https://doi.org/10.3390/mi12030294>.

CURRICULUM VITAE FABIO STRATI

Education

PhD candidate at IADP – Institute for Applied Dermatopharmacy – Martin-Luther-University Halle-Wittenberg

11/2018 – Current

Supervisors: Prof. Dr. Gerald Brezesinski, Prof. Dr. Reinhard Neubert

Research topic: I am currently studying the interaction between different pharmaceutical formulations and monolayer models of stratum corneum lipid matrix

Martin-Luther-University Halle-Wittenberg

10/2017 – 07/2018

Research period in biopharmacy department (Prof. Dr. Lee Ann Dailey's group) via Erasmus+ program

Research topic: I studied the kinetics and mode of interaction between anionic antimicrobial peptides and membrane models of *Staphylococcus aureus*

Farmacia 'Bottego'

03/2016 – 11/2016

Pharmacist trainee at 'Bottego' pharmacy in the city of Parma

University of Parma

09/2012 – 10/2018

Master in Chemistry and Pharmaceutical Technology, Final Vote 110/110 cum Laude.

Thesis title: The kinetics of antimicrobial peptide action against model of *Staphylococcus aureus* membrane

Supervisors: Prof. Dr. Fabio Sonvico, Dr. Richard Harvey

List of publications

- Wölk, C., Nawaz, H. A., Maqsood, I., **Strati, F.**, Brezesinski, G., Hause, G., Schulz-Siegmund, M., Hacker, M. C.
Amphiphilic Functionalized Oligomers: A Promising Strategy for the Postfabrication Functionalization of Liposomes. *Adv. Mater. Interfaces* 2020, 7, 2001168.
<https://doi.org/10.1002/admi.202001168>

- **Fabio Strati**, Reinhard H.H. Neubert, Lukáš Opálka, Andreas Kerth, Gerald Brezesinski.
Non-ionic surfactants as innovative skin penetration enhancers: insight in the mechanism of interaction with simple 2D stratum corneum model system, *European Journal of Pharmaceutical Sciences*, 2020.
<https://doi.org/10.1016/j.ejps.2020.105620>

- G. Brezesinski, **F. Strati**, R. Rudert, D. Vollhardt
Influence of chirality on the monolayer characteristics of N-alkanoyl substituted threonine and serine amphiphiles at the air-water interface, *Langmuir*, 2021, 37, 9069-9097.
[10.1021/acs.langmuir.1c01108](https://doi.org/10.1021/acs.langmuir.1c01108)

- **F. Strati**, J. S. L. Oliveira, T. Muhkina, B. Dobner, L. Opalka, R. H. H. Neubert, G. Brezesinski.
2D and 3D physical-chemical characterization of CER[AP]. A study of stereochemistry and chain symmetry, *J. Phys. Chem. B*, 125 (2021), 9960-9969
<https://doi.org/10.1021/acs.jpcc.1c05572>

- **Fabio Strati**, Tetiana Muhkina, Reinhard H. H. Neubert, Lukas Opalka, Gerd Hause, Christian Schmelzer, Matthias Menzel, Gerald Brezesinski
Cerosomes as skin repairing agent: Mode of action studies with a model stratum corneum layer at liquid/air and liquid/solid interfaces
Bbadva, (2021), 100039
[10.1016/j.bbadva.2021.100039](https://doi.org/10.1016/j.bbadva.2021.100039)

Oral Conference Presentations

- *Characterization of plant-based hydrogenated phospholipid mixtures and interaction with Stratum Corneum model*, Researcher's Day, Phospholipid Research Centre
- *Stratum Corneum vesicles as promising strategy to treat skin diseases*, European Joint Theoretical/Experimental Meeting on Membranes (EJTEMM)

Acknowledgments

To begin I would like to thank Prof. Neubert who gave me the opportunity to pursue my studies in IADP and to guide me in these years.

Special thanks to Prof. Gerald Brezesinski that from the beginning to the end mentored and motivated me in my studies. You never pretended anything from my work, you slowly allowed me to adapt and grow in my path making me (hopefully) the good scientist I am now. You are not only a great scientist but as well a great human being.

Thanks to my colleagues in IADP that created a relaxed and welcoming environment, that allowed me to find all the necessary tools for my research and thanks for helping me improve my spoken German skills.

Thanks to Dr. Christian Wölk and Dr. Richard Harvey that since my first day involved me in some of their scientific works, inviting me to my very first scientific trip in Soleil (Paris), a trip that I will not easily forget. Thanks as well for the good time shared together and the mentoring.

Thanks to Prof. Lea Ann Dailey that allowed me to access to many of her equipment and thanks to her group members and friend Moritz Schuller and Robert Neumann for the nice time spent inside and outside the office.

Thanks to Tetiana Mukhina, to the long whatsapp conversations, to the time spent together in Petra III and for performing important experiments part of my dissertation. I hope in the future we will be still collaborating.

Thanks to the group of Prof. Thurn-Albrecht Petzold which granted me the access to the Microfocus device which was often used in this work.

Thanks to Dr. Huse which performed the TEM experiments and for the patience with my small imprecisions.

Thanks to Admassu Assen which for short time worked in IADP, you are a good friend and I pray that peace and prosperity comes for you and for Ethiopia.

Thanks to Frau Rudolph which performed FTIR experiments and for the conversations over relatives and Valentino Rossi during the time I performed IRRAS experiments.

Thanks to all my friends that in these years in Halle have filled my life with good memories and great time, Antonis, Michael, Nicholas, Muhsin, Moritz and many others.

Thanks to my parents and family that always took care of me, even if more than 2000 km is separating us. I wish we could spend more time together and hope the future will allow it.

Special thanks to my girlfriend, Isabel, that was always there helping me to slowly get out from a bad time and for making me a better person.